Universiteit Twente

faculteit der
werktuigbouwkunde

Two-Dimensional Potential Flow Through a Centrifugal Impeller

THERMISCHE WERKTUIGBOUWKUNDE

by F.C. Visser

may 1991

TWO-DIMENSIONAL POTENTIAL FLOW THROUGH A CENTRIFUGAL IMPELLER

by

F.C. Visser

M.Sc. Thesis

Board of Examiners:

Prof. dr. ir. J.J.H. Brouwers
Prof. dr. ir. L. van Wijngaarden
Dr. ir. J.B. Jonker (tutor)
Ir. R. Badie (mentor)

University of Twente
Faculty of Mechanical Engineering
Chair of Thermal Engineering
Enschede
The Netherlands

may 1991

I don't know what I may seem to the world, but, as to myself, I seem to have been only like a boy playing on the seashore, and diverting myself in now and then finding a smoother pebble or a prettier shell than ordinary, whilst the great ocean of truth lay all undiscovered before me.

Sir Isaac Newton
(1642–1727)

To my beloved parents

ABSTRACT

Using the theory of functions of a complex variable, where in particular the method of conformal mapping, the two–dimensional irrotational solenoidal flow through both pump and turbine centrifugal impellers is analyzed on the basis of two representative models; viz. the impeller fitted with straight radial blades, and the impeller fitted with so–called logarithmic spiral blades. The fluid velocity – and consequently the pressure distribution – along a straight radial blade is solved analytically and expressed as a Fourier sine series, with the Fourier coefficients given by the hypergeomeric series. The solutions for logarithmic spiral blades are formulated analytically and then treated both numerically and asymptotically; comparison with finite element solutions showed an excellent agreement. Based on the obtained results a general discussion on the two–dimensional flow through centrifugal impellers is given. Interesting features of both pump and turbine impellers are discussed, as for instance: slip factor(s), shockless entry, and head or work reduction, which are all related to the limited number of blades. Practical solutions (improving the one–dimensional theory) are given, based on the assumption of a respectable number of blades and/or a low inlet–to–outlet radius ratio for the impeller. All results show excellent agreement with the works of various authors that have explored this field of fluid dynamics, and, moreover, they add substantially to these works.

PREFACE

Computing the two–dimensional potential flow through centrifugal impellers, by using the theory of functions of a complex variable is not a recent development but has been practiced by a number of notable authors since the early years of this century. It was Kucharski (1918) who pioneered this field of fluid dynamics, by examining the flow field of an impeller fitted with straight radial blades with the inner tips placed at the center of the impeller. Spannhake (1925) then improved on this matter by taking a more realistic inlet–to–outlet ratio for the impeller, and introduced the method of conformal presentation to solve the flow problem. Next Sörensen (1927), Busemann (1928), and Schulz (1928) treated the impeller fitted with so–called logarithmic spiral blades, where the latter developed, and subsequently used, a rather dubious alternative mapping whereas the former two (correctly) based their study on the work of König (1922). Uchimaru and Kito (1931) next applied the (questionable) results obtained by Schulz to compute slip coefficients. Then after a few years Acosta (1954) rephrased the work of Busemann, extended this by computing the pressure distribution along the blades, and compared the results with experiment. Thereupon Ayyubi and Rao (1971), and Mohann Kumar and Rao (1977) took Acosta's work as a reference and treated the same by using a distribution of singularities on the blade surface(s).

The above–mentioned authors all contributed significantly to (the solution of) the problem of two–dimensional flow through a centrifugal impeller, but none of them obtained arithmetical solutions; eventually they all used a numerical treatment to compute their respective results. This hiatus has recently been taken up by Badie (1989) and Van Essen (1989), who developed solutions – expressed by a Fourier series – for the impeller fitted with straight radial blades, with the inner tip placed at the center of the impeller (like Kucharski first started). Adopting their ideas, the solutions for a more realistic inlet–to–outlet ratio are now also obtained. Following the works of Busemann and Acosta it was intended to do the same for the impeller fitted with logarithmic spiral blades. This, however, has not been fully completed yet; though interesting results have been obtained already, as for instance arithmetical expressions for so–called slip factors that fully comply with the numerically obtained results of Busemann.

In the first instance the work(s) of Schulz (and Uchimaru and Kito) were followed. Comparing the thus obtained results with finite element solutions, however, indicated severe deficiencies. These were probably due to the fact that the nature of singularities is affected by Schulz' mapping (sources transferring to vortex–sources), so the necessary imposition of boundary conditions is incorrectly done in the image plane. The next employed, and in this work described, König transformation (also used by Sörensen, Busemann, and Acosta) does not embody such deficiencies.

The discussions given in this work are rather extensive. This is done intentionally, so that the well–grounded reader should experience no (severe) difficulties to comprehend and check the writings; though there may always be some imperfections that were not foreseen. To obtain a thorough understanding it is convenient to have some knowledge of complex analysis and the applications to fluid dynamics, as well as being acquainted with integral calculus, Fourier analysis, and special functions.

ACKNOWLEDGEMENTS

There are a few persons that have been of great importance to me during the preparation of this work. They all kindly provided valuable comments, and enabled me to see things more clearly. Especially I thank my mentor ir. R. Badie for his outstanding (mathematical) support, and ir. T.G. van Essen for helping me to get acquainted with the finite element package SEPRAN and serving in this context as a trouble shooter; both also provided the preliminaries that I gratefully put to use. I am also grateful to prof. J.J.H. Brouwers, prof. L. van Wijngaarden, and dr. F. Twilt, who all willingly advised me, and consequently provided me with some useful ideas. Next I am indebted to ir. K. Spijker, H. Rave, and J.J. de Wilde, who all kindly checked and commented the concept. Then I would like to mention my roommates, in chronological order: ir. B.J.W. ter Weeme, ir. R. Gort, D.F. de Lange, A.J.W. Voorthuis, and H.H.L.M. Witz, whose company was both pleasant and studious. Last but certainly not least I want to thank dr. J.B. Jonker for his enthusiastic support and constructive advices.

F.C.V.

Enschede, the Netherlands
May 1991

CONTENTS

NOMENCLATURE

The below–listed notations and conventions, symbols, subscripts, and superscripts, have been adopted from what is generally accepted in the fields of fluid dynamics, turbomachinery, and mathematics. Dimensions are given in terms of mass (M), length (L), and time (t). Symbols, signs, and operators that appear infrequently or in one section only are not listed.

Notations and Conventions

s	= scalar or complex (lightface italic or greek)
v	= vector (boldface italic or greek)
$\|v\|$, $\|s\|$	= modulus or absolute value
$\cdot$	= dot product
$\times$	= cross product
∇	= nabla operator
∇^2	= Laplace operator
$\left[\frac{\partial}{\partial s}\right], \frac{d}{ds}$	= (partial) derivative
$\bar{z} = x - iy$	= complex conjugate of $z = x + iy$
$arg(z)$	= argument of z
$k!$	= $1{\cdot}2{\cdot}3 \ldots k$, $0! = 1$
$\sum_{k=n}^{m} u_k$	= $u_n + u_{n+1} + u_{n+2} + \ldots + u_m$
$\prod_{k=n}^{m} u_k$	= $u_n{\cdot}u_{n+1}{\cdot}u_{n+2} \cdot \ldots u_m$
$\int_a^b$	= line integral; path of integration from a to b
$\oint_a^b$	= line integral; Cauchy's principal value
$\sqrt{z}$, $\sqrt{z}$	= square root of z (principal value)
e^z	= exponential of z (principal value)
$ln\, z$	= natural logarithm of z (principal value)
$sin\, z$, $cos\, z$, $tan\, z$	= trigonometric functions

$\mathbf{N}$	= set of natural numbers
$\mathbf{Z}$	= set of whole numbers
$[M]$	= unit of mass, e.g. (kg)
$[L]$	= unit of length, e.g. (m)
$[t]$	= unit of time, e.g. (s)
$[-]$	= dimensionless

Symbols

A_k , a_k	= Fourier coefficients	$[-]$
a	= modulus of ζ_0	$[-]$
$B(z,w)$	= beta function	$[-]$
c , c	= absolute fluid velocity	$^{\Delta}[Lt^{-1}], [L^2t^{-1}]$
$F(a,b;c;z)$	= hypergeometric function or hypergeometric series	$[-]$
f , $f(z)$, $f(\zeta)$	= complex potential	$[L^2t^{-1}]$
f_1 , f_2	= degenerated work reduction factors	$[-]$
g	= acceleration due to gravity	$[Lt^{-2}]$
H_{Eu}	= Eulerian head	$[L]$
H_{th}	= theoretical head	$[L]$
HRF	= head reduction factor	$[-]$
I_0 , I_1	= integrals related to straight radial blades	$[-]$
$I(\theta)$	= integral function (straight radial blades)	$[-]$
i	= imaginary unit ($i^2 = -1$)	$[-]$
J_0 , J_0^* , J_1	= integrals related to logarithmic spiral blades	$[L^2t^{-1}]$
j	= blade index	$[-]$
K	= (scale) constant	$[L^2t^{-1}]$
k	= index number $\in \mathbf{Z}$	$[-]$
$\boldsymbol{n}$	= (outward directed) unit normal	$[-]$
n	= number of blades	$[-]$
$P_\alpha(\xi)$, $P_\nu(\xi)$	= Legendre functions of the first kind	$[-]$
$P_\nu^k(\xi)$	= associated Legendre functions of the first kind	$[-]$
p	= thermodynamic pressure	$[ML^{-1}t^{-2}]$
Q	= fluid flux or source strength	$[L^2t^{-1}]$
$\boldsymbol{r}$	= position vector	$[L]$
r	= radial variable in physical plane	$[L]$
s	= blade coordinate	$[L]$
$\boldsymbol{w}$, w	= relative fluid velocity (in physical plane)	$[Lt^{-1}]$
WRF	= work reduction factor	$[-]$

$^{\Delta}$ In physical plane $[Lt^{-1}]$, in mapped plane $[L^2t^{-1}]$.

x	= cartesian x–coordinate	$[L]$
y	= cartesian y–coordinate	$[L]$
z	= complex variable ($z = x + iy$)	$[L]$
α_v	= volute angle	[–]
β	= blade angle	[–]
Γ	= circulation or vortex strength	$[L^2t^{-1}]$
$\Gamma(z)$	= (complete) gamma function	[–]
δ	= argument of ζ_0	[–]
ε	= mapping constant ($\ll 1$)	[–]
$Z(z)$	= conformal transformation $Z : z \rightarrow \zeta$	[–]
ζ	= complex variable (mapped plane)	[–]
ζ_0	= map of origin of physical plane	[–]
θ	= argument of ζ	[–]
$\boldsymbol{\kappa}$, κ	= relative stream function	$[L^2t^{-1}]$
λ	= (dummy) argument of ζ, integration variable	[–]
μ	= geometry parameter $(r_1/r_2)^n$	[–]
π	= the number π (= 3.14159...)	[–]
ρ	= fluid density	$[ML^{-3}]$
σ_p	= slip factor pump situation	[–]
σ_t	= slip factor turbine situation	[–]
τ_p	= prerotation factor pump situation	[–]
τ_t	= prerotation factor turbine situation	[–]
Υ_1 , Υ_2	= vortex coefficients	[–]
Φ	= flow coefficient	[–]
ϕ	= angular variable in physical plane	[–]
φ	= velocity potential	$[L^2t^{-1}]$
Ψ	= head coefficient	[–]
$\boldsymbol{\psi}$, ψ	= absolute stream function	$[L^2t^{-1}]$
$\boldsymbol{\Omega}$, Ω	= angular speed	$[t^{-1}]$

Subscripts

0	= origin or zero prerotation
1	= inner (tip)
2	= outer (tip)
B	= blade (points)
D	= displacement flow
Eu	= Eulerian
K	= Kutta condition

n	= (outward) normal
o	= offset
Q	= source flow
r	= radial
s	= tangent
SL	= shockless
t	= tangential (counter clock wise)
th	= theoretical
x	= coordinate direction
y	= coordinate direction
z	= physical plane
Γ	= vortex flow
ζ	= mapped plane

Superscripts

D	= displacement flow
K	= Kutta condition
Q	= source flow
Γ	= vortex flow
*	= adjusted/modified to fulfill boundary condition
+	= pressure side
-	= suction side

1

INTRODUCTION

The one dimensional (Eulerian) flow theory of turbomachinery is momentarily still indispensable for the general engineering practice, regarding the determination of main dimensions, blade angle(s), and operating conditions, such as: prerotation, angular speed, optimum through flow, developed head (pump), and delivered work (turbine). To improve this one–dimensional approach numerous experimental investigations and theoretical analyses have been performed in the past. The latter will also be done in the present work, so that we may obtain a clear understanding of the flow process, which is necessary to establish a proper rationale for design. To that end we will confine ourselves to single stage centrifugal machines, though multistage machines are a common practice nowadays.

Roughly a single stage centrifugal machine may be considered to be composed of three main parts: a stationary inlet or guidance system, the runner or impeller, and an outlet or collecting device. Since the impeller is responsible for the energy transfer, and thus highly determines the performance of the machine, it seems clear that this component should be the item of our first interest. Thus confining ourselves to the flow as that it manifests itself in the (isolated) impeller, it would be highly desirable to be able to predict the developed head (pump) or delivered work (turbine), and to determine both the velocity and pressure distribution along the blades of the impeller (friction losses, blade loading). This is however, in general, unfeasible due to the behaviour of real fluids, and the complex geometries of impellers found in practice. Therefore the flow problem has to be simplified, as far as strictly necessary, leaving the essentials intact, so that practical and useful solutions can be obtained.

The first assumption reasonably to be made, simplifying the (flow) problem considerably, is that the fluid is inviscous and incompressible. The second assumption, usually implicitly made, is that the flow enters the impeller free from vorticity, so the flow field may mathematically be characterized as irrotational and solenoidal, counting the first assumption. The third and

conclusive assumption is that the flow field may be considered two–dimensional, that is, the flow is restricted to depend on radial and angular coordinates only. The above–mentioned assumptions make it possible to use two–dimensional methods of potential flow theory, in particular the theory of functions of a complex variable, to compute the flow through the impeller. For the sake of analysis we additionally adopt so–called logarithmic spiral blades, that is, blades having a constant angle between radius and tangent; this obviously also includes the radially bladed impeller. These logarithmic spiral or equiangular blades are not only mathematically convenient but also highly representative, since most blade designs in practice are closely represented by such spirals.

The line of thought followed in this work is not new, but basically follows the ideas earlier outlined by Spannhake (1925), Busemann (1928), Acosta (1954), Badi (1989), and Van Essen (1989). Their results are, more or less, again obtained and partially improved, that is, where they used a numerical treatment and/or employed asymptotic solutions, (better) arithmetical solutions have now been obtained. Our discussion starts with a short mathematical description of the used two–dimensional models for the radially bladed and logarithmically spiraled centrifugal impeller (chapter 2), followed by a brief discussion of the essentials of using the complex potential for irrotational solenoidal flows in two dimensions, and employing the principle of superposition to solve the flow problem (chapter 3). Next the fundamentals of this work, viz. the method of analytical solution, that is, the conformal mapping of the impeller blades (chapter 4), and solving the flow problem in general (chapter 5), are discussed. Thereupon the solutions for both straight radial blades and logarithmic spiral blades are treated (chapter 6 and chapter 7 respectively); this mainly concerns computing velocity and pressure distributions along the blades, with some circumstantialities like shockless entry, blade circulation, and slip factor(s), being treated as well. Then we briefly discuss the finite element solution of the flow through the impeller fitted with logarithmic spiral blades, and compare the results with the analytical solution (chapter 8). Finally we discuss the analytically obtained two–dimensional results, by applying them in comparison with one–dimensional flow theory (chapter 9), and draw some conclusions and give a few recommendations for future work (chapter 10).

2

MODELLING THE IMPELLER

In order to be able to examine the flow through the impeller analytically we first of all need to have a mathematically convenient and also representative model of the impeller. Confining ourselves strictly to two–dimensional motion we have two such mathematically convenient models, which will be outlined in this chapter. Distinctively we will discuss the impeller fitted with straight radial blades and the impeller fitted with logarithmic spiral blades; the former being deductible from the latter, though.

2.1 Straight Radial Blades

The simplest two–dimensional model for a centrifugal impeller, say with inner radius r_1 and outer radius r_2, consists of a finite number of equally spaced straight radial blades (see figure 2.1). The blades of this type of impeller are simply characterized by a constant pole angle or zero blade angle. A mathematically consistent description of this type of impeller will be given in the next paragraph; there we will regard straight radial blades as a special case of logarithmic spiral blades.

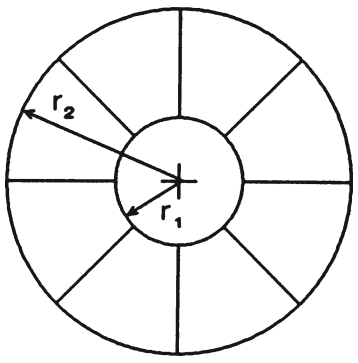

figure 2.1 *impeller with* (8) *straight radial blades*

2.2 Logarithmic Spiral Blades

A more sophisticated model for a centrifugal impeller, than the previous one described, consists of a finite number equally spaced logarithmic spiral blades (see figure 2.2). The blades of this type of impeller are characterized by a constant blade angle, i.e.

$$r \frac{d\phi}{dr} = \tan\beta \ (= \textit{constant}) \tag{2.1}$$

where

r = radial variable
ϕ = angular variable
β = blade angle

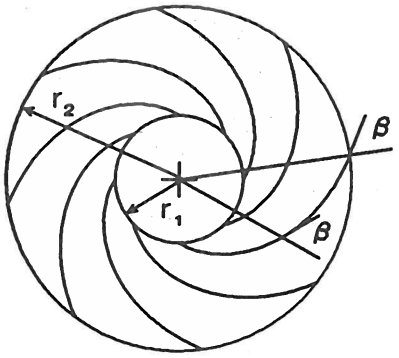

figure 2.2 impeller with (8) logarithmic spiral blades

By integration of equation (2.1) it follows that each individual blade of the impeller is described by

$$\phi^{j}(r) = \phi_o + \frac{2\pi(j-1)}{n} + \tan\beta \ ln\left[\frac{r}{r_1}\right] \tag{2.2}$$

or

$$r^j(\phi) = r_1 \, e^{\frac{\phi-\phi_o}{\tan \beta}} \, e^{-\frac{2\pi(j-1)}{n \tan \beta}} \tag{2.3}$$

where

$$r_1 \leq r \leq r_2$$

and

n = number of blades
j = blade index, $\{j \in \mathbb{N} | 1 \leq j \leq n\}$
ϕ_o = offset angle, $\{\phi_o = \phi^1(r_1)\}$
r_1 = inner tip radius
r_2 = outer tip radius

Putting $\beta = 0$ we readily obtain from equation (2.2) that the impeller fitted with straight radial blades (figure 2.1) is characterized mathematically by

$$\phi^j = \phi_o + \frac{2\pi(j-1)}{n} \tag{2.4}$$

3

MATHEMATICAL APPROACH OF THE FLOW FIELD

In this chapter we briefly consider two mathematically important properties of the flow field. These form the bases in solving the potential flow through the impeller. First the use of the complex potential for two–dimensional irrotational solenoidal flow is discussed, and secondly the superposition of (sub) flows will be outlined. For references on these subjects (and related aspects) any (decent) textbook will suffice, as for instance Bachelor, Lamb, or Milne–Thomson.

3.1 Using the Complex Potential for Irrotational Solenoidal Flow in Two Dimensions

From basic fluid dynamics we know that, in general, an irrotational solenoidal flow is characterized (mathematically) by

$$\nabla \times \boldsymbol{c} = \boldsymbol{0} \tag{3.1}$$

$$\nabla \cdot \boldsymbol{c} = 0 \tag{3.2}$$

where $\boldsymbol{c}$ is the absolute velocity vector.

For two dimensional flows, equations (3.1) and (3.2) become when referring to Cartesian (x,y)–coordinates

$$\frac{\partial c_y}{\partial x} - \frac{\partial c_x}{\partial y} = 0 \tag{3.3}$$

$$\frac{\partial c_x}{\partial x} + \frac{\partial c_y}{\partial y} = 0 \tag{3.4}$$

where c_x and c_y are the velocity components in x and y direction respectively.

Equations (3.3) and (3.4) guarantee the existence of a velocity potential φ

and a stream function ψ, both satisfying the Laplace equation, i.e.

$$\nabla^2\varphi = 0 \tag{3.5}$$

$$\nabla^2\psi = 0 \tag{3.6}$$

and determining the fluid velocity by

$$c_x = \frac{\partial\varphi}{\partial x} = \frac{\partial\psi}{\partial y} \tag{3.7}$$

$$c_y = \frac{\partial\varphi}{\partial y} = -\frac{\partial\psi}{\partial x} \tag{3.8}$$

Equations (3.7) and (3.8) state the so–called Cauchy–Riemann conditions for an analytical function $f(z)$ with real part $\varphi(x,y)$ and imaginary part $\psi(x,y)$, i.e.

$$f(z) = \varphi(x,y) + i\psi(x,y) \tag{3.9}$$

where

$$z = x + iy \tag{3.10}$$

The function $f = \varphi + i\psi$ is called the complex potential; the real functions φ and ψ being conjugate functions. From this complex potential we obtain the fluid velocity by taking the derivative with respect to z, i.e.

$$\frac{df}{dz} = c_x - ic_y \tag{3.11}$$

The great advantage of using a complex potential to determine the flow through the impeller lies in the direct use of the theory of functions of a complex variable, as will be discussed throughout chapters 4, 5, and 6.

3.2 Superposition of Flows

To solve the potential flow through the impeller we will employ the principle of superposition, which is permissible by the linearity of the Laplace operator. We distinguish the following 4 (sub) potentials:

1 – A potential due to the rotation of the impeller. This flow will be referred to as the displacement flow.

2 – A potential connected with a source flow originating from the origin of the physical plane, in case of a turbine this source will be negative (a sink).

3 – A potential due to a vortex placed in the origin of the physical plane. This vortex either represents a prerotation, by which we can impose a shockless entry when acting as a pump, or merely the circulation of the flow leaving the impeller in case of a turbine situation.

4 – A potential due to the imposition of the Kutta condition or Joukowski's hypothesis. This condition expresses the physical fact that there is a smooth flow off both surfaces of the impeller blades at the trailing edge.

The above–mentioned subdivision of potentials, which are to be discussed (mathematically) in chapter 5, may be summarized by

$$f = f_D + f_Q^* + f_\Gamma^* + f_K \tag{3.12}$$

where the potentials denote

f_D = displacement flow

f_Q^* = source flow

f_Γ^* = vortex flow

f_K = Kutta condition

and where the asterisk (*) indicates that these potentials are adjusted so that the boundary condition is satisfied, as will be discussed in chapter 5. The potentials representing the displacement flow and Kutta condition are given without an asterisk because these potentials already satisfy the boundary condition (chapter 5).

4

METHOD OF ANALYTICAL SOLUTION

To solve the flow through the impeller analytically we employ a conformal transformation which maps the impeller on the unit circle. In this circle plane we can easily determine the previously mentioned (sub) flows by using the theory of functions of a complex variable.

In this chapter we will discuss the mapping of the impeller on the unit circle in general, and we will specify the mapping function for both straight radial blades and logarithmic spiral blades. The actual solving of the flow(s) will be treated in the following chapters.

4.1 Mapping the Impeller on a Circle

The mapping function that we employ is originally credited to König, and originates from the transformation of a plane source–vortex flow to a source–vortex flow in a circle plane (see appendix A). Denoting the physical plane by z and the mapped plane by ζ the transformation $Z : z \longrightarrow \zeta$, which maps the impeller conformally on the unit circle, is given by

$$\left[\frac{z}{z_2}\right]^n = \left[\frac{\zeta - \zeta_0}{\zeta_2 - \zeta_0}\right] \left[\frac{\frac{1}{\zeta} - \bar{\zeta}_0}{\frac{1}{\zeta_2} - \bar{\zeta}_0}\right]^{e^{2i\beta}} \tag{4.1}$$

where

$$\zeta_0 = Z(z=0) \tag{4.2}$$

$$\zeta_2 = Z(z_2) \tag{4.3}$$

with z_2 being the complex representation of the outer blade tip in the physical plane and the over bar denoting a complex conjugate.

Because of the periodicity of the flow(s) through the impeller we only have to

consider a periodical section containing just one blade. The mapping (4.1) therefore embodies a so–called Schwartz–Christoffel transformation which maps n blades on just one blade. Properly speaking the impeller is mapped on n Riemann surfaces from which we take only the first one, which is permissible by the just mentioned periodicity of the flow(s). For a discussion on Schwartz–Christoffel transformations (and related aspects) see for instance Henrici or Dettman.

Mapping the impeller according to transformation (4.1) we still have a degree of freedom left, namely the exact location of the image ζ_0 of the origin ($z=0$) of the physical plane. This image ζ_0 may either be chosen freely or derived from a chosen image ζ_2. The latter will be done for both straight radial blades and logarithmic spiral blades (paragraphs 4.2 and 4.3 respectively).

To illustrate the mapping of an impeller according to transformation (4.1) we have mapped in figure 4.1 an impeller with 8 blades and a 60 degree blade angle. A detailed description of this mapping will be given in section 4.3.

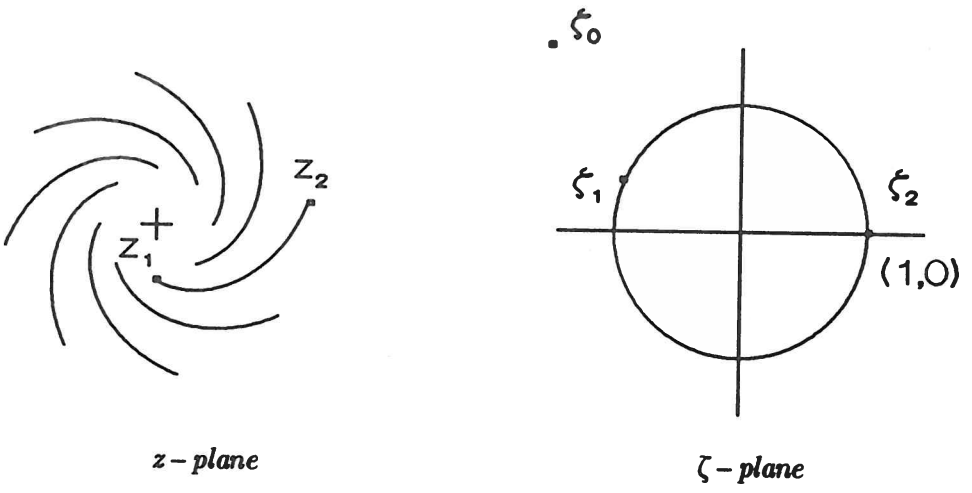

figure 4.1 *illustrative example of an impeller being mapped on the unit circle*

4.2 Mapping Function for Straight Radial Blades

In case of straight radial blades ($\beta = 0$) the transformation (4.1) simply becomes

$$\left[\frac{z}{z_2}\right]^n = \left[\frac{\zeta - \zeta_0}{\zeta_2 - \zeta_0}\right]\left[\frac{\frac{1}{\zeta} - \bar{\zeta}_0}{\frac{1}{\zeta_2} - \bar{\zeta}_0}\right] \tag{4.4}$$

In order to embed this mapping of the impeller we will examine the transformation (4.4) somewhat closer.

First of all we recall that the blade tips are so–called branch points of the transformation, in which the derivative vanishes or tends to infinity, i.e.[1]

$$\left|\frac{dz}{d\zeta}\right|_{\zeta_1,\zeta_2} = 0 \tag{4.5}$$

$$\left|\frac{d\zeta}{dz}\right|_{z_1,z_2} \longrightarrow \infty \tag{4.6}$$

where the subscripts 1 and 2 refer to the inner and outer blade tips respectively. Based on equations (4.5) and (4.6) we may now exactly specify the mapping function.

Putting

$$\zeta_B = e^{i\theta} \tag{4.7}$$

$$\zeta_0 = ae^{i\delta} \tag{4.8}$$

where ζ_B denotes an image (of a blade point) on the unit circle, we obtain by taking the derivative of equation (4.4)

$$\left[\frac{dz}{d\zeta}\right]_B = \frac{iz_B}{ne^{i\theta}} \frac{2a\sin(\delta-\theta)}{1 + a^2 - 2a\cos(\theta-\delta)} \tag{4.9}$$

where the subscript B is used to indicate that we are looking at points on a blade.

According to equation (4.5) it then follows from equation (4.9) that

[1] The fat vertical bars $|\ |$ denote the absolute value (or modulus) of a vector or (complex) number.

$$\delta - \theta_{1,2} = k_{1,2}\,\pi \tag{4.10}$$

where $k_{1,2} \in \mathbb{Z}$, and the subscripts 1 and 2 again referring to the blade tips.

Next choosing the image of the outer blade tip in $\zeta_2 = 1$ ($\theta_2 = 0$) it follows from equation (4.10) that

$$\delta = \pi \tag{4.11}$$

$$\theta_1 = \pi \tag{4.12}$$

where we have taken into account that the inner tip is mapped near ζ_0, and that the arguments (δ,θ_1) have to be in the interval $<-\pi,\pi]$.

The inner tip is thus mapped in $\zeta_1 = -1$ and the image of the origin lies somewhere on the negative real axis, i.e. $\zeta_0 = -a$. Substituting this result in equation (4.4) we obtain

$$\left[\frac{z_1}{z_2}\right]^n = \left[\frac{1 - a}{1 + a}\right]^2 \tag{4.13}$$

Then defining

$$\mu = \left[\frac{r_1}{r_2}\right]^n \tag{4.14}$$

while knowing that $arg(z_1) = arg(z_2)$ for straight radial blades, and that the origin is mapped outside the unit circle, so $a > 1$ (see appendix A), we obtain from equation (4.13)

$$a = \frac{1 + \sqrt{\mu}}{1 - \sqrt{\mu}} \tag{4.15}$$

Conclusively the mapping function for straight radial blades can be written as

$$\left[\frac{z}{z_2}\right]^n = \left[\frac{\zeta + a}{1 + a}\right]\left[\frac{\frac{1}{\zeta} + a}{1 + a}\right] \tag{4.16}$$

with a according to equation (4.15).

Restricting ourselves further to points on a blade, i.e. $\zeta = \zeta_B$ and $z = z_B$ where $arg(z_B) = arg(z_2)$ for straight radial blades, the mapping function (4.16) becomes, using equation (4.7)

$$\left[\frac{r_B}{r_2}\right]^n = \left[\frac{e^{i\theta} + a}{1 + a}\right]\left[\frac{e^{-i\theta} + a}{1 + a}\right] \tag{4.17}$$

where

$$r_B = |z_B| \tag{4.18}$$

$$r_2 = |z_2| \tag{4.19}$$

Substituting equation (4.15) and using Euler's well-known exponential theorem, $cos\,\theta + i\,sin\,\theta = e^{i\theta}$, we obtain for the transformation (4.17) of blade located points

$$\left[\frac{r_B}{r_2}\right]^n = \frac{1+\mu}{2}\left[1 + \frac{1-\mu}{1+\mu}\,cos\,\theta\right] \tag{4.20}$$

The above-discussed mapping of an impeller with straight radial blades is illustrated graphically in figure 4.2.

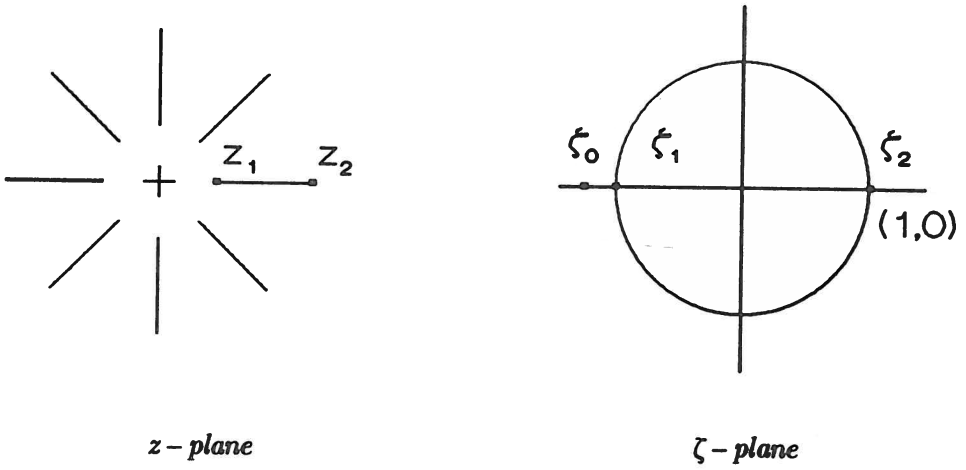

figure 4.2 *mapping of an impeller with* (8) *straight radial blades*

4.3 Mapping Function for Logarithmic Spiral Blades

The specification of the mapping function for logarithmic spiral blades (section 4.3.1) will be done in a way similar to the one for straight radial blades, as was described in the previous paragraph. Having specified the mapping function we will also discuss a first order approximation of the mapping constants (section 4.3.2), which will be shown to be extremely useful.

4.3.1 Specifying the mapping

Recalling transformation (4.1) we obtain by taking the derivative, using equations (4.7) and (4.8)

$$\left[\frac{dz}{d\zeta}\right]_B = \frac{2iz_B e^{i\beta}}{ne^{i\theta}} \frac{a\,sin(\delta+\beta-\theta) - sin\,\beta}{1 + a^2 - 2a\,cos(\delta-\theta)} \tag{4.21}$$

From equations (4.5) and (4.21) it then follows that

$$a\,sin(\delta+\beta-\theta_{1,2}) = sin\,\beta \tag{4.22}$$

Again choosing the image of the outer tip in $\zeta_2 = 1$ ($\theta_2 = 0$) we derive from equation (4.22)

$$a = \frac{sin\ \beta}{sin(\delta+\beta)} \tag{4.23}$$

Equation (4.23) states a simple relation between the modulus (a) and the argument (δ) of the image (ζ_0) of the origin.

Before dealing with the second requisite relation that fully determines the mapping, we first take a closer look at equations (4.22) and (4.23).

From equations (4.22) and (4.23) it follows that, since $\theta_2 = 0$

$$sin(\delta+\beta-\theta_1) = sin(\delta+\beta) \tag{4.24}$$

So the inner tip is located at

$$\theta_1 = 2\delta + 2\beta - \pi \tag{4.25}$$

where we have used the fact that $0 < \delta+\beta < \pi$, as can be seen from equation (4.23) since this equation may be regarded as an expression of the sine rule. Consequently we may next put

$$\gamma = \pi - \delta - \beta \tag{4.26}$$

where $0 < \gamma < \pi$.

Substituting equation (4.26) in equation (4.25) we obtain for the argument of the inner tip

$$\theta_1 = \pi - 2\gamma \tag{4.27}$$

The (effects of the) above–discussed relations are illustrated in figure 4.3. This figure will show to be very useful in specifying the second relation that determines the mapping.

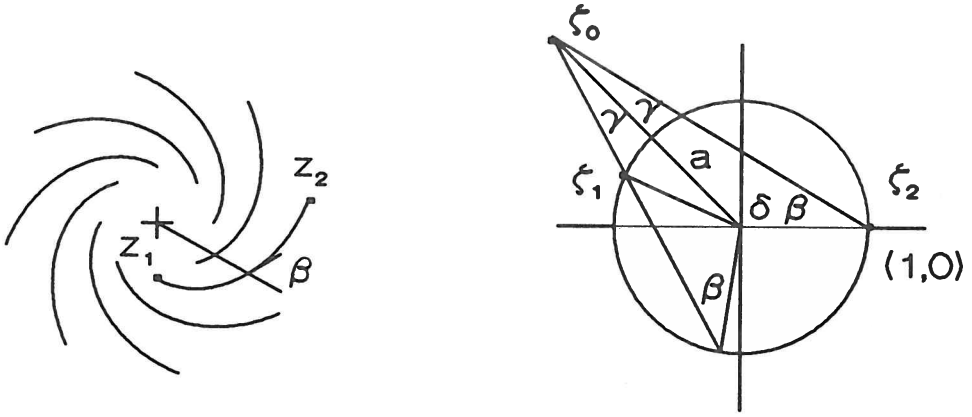

figure 4.3 *graphical illustration of the transformation for logarithmic spiral blades*

The second relation, now required, to embed the transformation follows from the mapping of the inner tip. Substituting equation (4.6) in equation (4.1) we obtain

$$\left[\frac{z_1}{z_2}\right]^n = \left[\frac{e^{i\theta_1} - ae^{i\delta}}{1 - ae^{i\delta}}\right]\left[\frac{e^{-i\theta_1} - ae^{-i\delta}}{1 - ae^{-i\delta}}\right]^{e^{2i\beta}} \tag{4.28}$$

which may also be written as

$$\left[\frac{z_1}{z_2}\right]^{ne^{-i\beta}} = \left|\left[\frac{e^{i\theta_1} - ae^{i\delta}}{1 - ae^{i\delta}}\right]^{e^{-i\beta}}\right|^2 \tag{4.29}$$

Next – referring to equation (2.2) – we have as a possible complex representation to describe the blades of the impeller (fitted with logarithmic spiral blades)

$$z_B^j = r_B\, e^{i\left\{\phi_o + \frac{2\pi(j-1)}{n} + \tan\beta\, \ln(r_B/r_2)\right\}} \tag{4.30}$$

where the subscript B is added for clarity of the remainder.

From equation (4.30) we readily obtain

$$\frac{z_1}{z_2} = \frac{r_1}{r_2}\, e^{i\, \tan\beta\, \ln(r_1/r_2)} \tag{4.31}$$

or

$$\frac{z_1}{z_2} = \left[\frac{r_1}{r_2}\right]^{1 + i\tan\beta} = \left[\frac{r_1}{r_2}\right]^{\frac{e^{i\beta}}{\cos\beta}} \tag{4.32}$$

where the blade index (j) has been omitted for convenience.

Then substituting equation (4.32) in equation (4.29) we get

$$\left[\frac{r_1}{r_2}\right]^{\frac{n}{\cos\beta}} = \left|\left[\frac{e^{i\theta_1} - ae^{i\delta}}{1 - ae^{i\delta}}\right]^{e^{-i\beta}}\right|^2 \tag{4.33}$$

Putting further

$$l_1 = |\zeta_1 - \zeta_0| = |e^{i\theta_1} - ae^{i\delta}| \tag{4.34}$$

$$l_2 = |\zeta_2 - \zeta_0| = |1 - ae^{i\delta}| \tag{4.35}$$

and using

$$arg\left(\zeta_1 - \zeta_0\right) = arg\left(e^{i\theta_1} - ae^{i\delta}\right) = -(\beta+2\gamma) \tag{4.36}$$

$$arg\left(\zeta_2 - \zeta_0\right) = arg\left(1 - ae^{i\delta}\right) = -\beta \tag{4.35}$$

the latter following from figure 4.3, equation (4.33) becomes

$$\left(\frac{r_1}{r_2}\right)^{\frac{n}{\cos\beta}} = \left| \left(\left(\frac{l_1}{l_2}\right) e^{-2i\gamma} \right)^{e^{-i\beta}} \right|^2 \tag{4.38}$$

or

$$\left(\frac{r_1}{r_2}\right)^{\frac{n}{\cos\beta}} = \left(\left(\frac{l_1}{l_2}\right)^{\cos\beta} e^{-2\gamma\sin\beta} \right)^2 \tag{4.39}$$

From figure 4.3 we next obtain by applying the sine rule

$$\frac{l_1}{\sin(\pi-\delta-2\gamma)} = \frac{1}{\sin\gamma} \tag{4.40}$$

$$\frac{l_2}{\sin\delta} = \frac{1}{\sin\gamma} \tag{4.41}$$

Substituting equations (4.40) and (4.41) in equation (4.39), and using equations (4.14) and (4.26), we finally obtain

$$\mu = \left(\frac{\sin(2\beta+\delta)}{\sin\delta}\right)^{2\cos^2\beta} e^{-2(\pi-\beta-\delta)\sin 2\beta} \tag{4.42}$$

Equations (4.23) and (4.42) together determine the mapping function (4.1) for

logarithmic spiral blades, with the outer tip being mapped in $\zeta_2 = 1$.

Finally for points located on a blade we state the transformation (4.1) alternatively as, using equation (4.30)[2]

$$\left[\frac{r_B}{r_2}\right]^{\frac{n}{\cos\beta}} = \omega\bar{\omega} = |\omega|^2 \tag{4.43}$$

where

$$\omega = \omega(\theta) = \left[\frac{\zeta_B - \zeta_0}{1 - \zeta_0}\right]^{e^{-i\beta}} = \left[\frac{e^{i\theta} - ae^{i\delta}}{1 - ae^{i\delta}}\right]^{e^{-i\beta}} \tag{4.44}$$

4.3.2 First order approximation of mapping constants

In case $\mu \ll 1$ we may employ a simple first order approximation for the mapping constants a and δ. This approximation will be shown to be very useful to obtain the mapping constants numerically.

For $\mu \ll 1$ it follows from equation (4.42) that δ will be in the vicinity of $\pi - 2\beta$; we therefore put

$$\delta = \pi - 2\beta + \varepsilon \tag{4.45}$$

where we will assume

$$|\varepsilon| \ll 1 \tag{4.46}$$

Substitution of equation (4.45) in equation (4.23) then gives

$$a = \frac{\sin\beta}{\sin(\beta - \varepsilon)} = \frac{1}{\cos\varepsilon - \sin\varepsilon\,\cotan\beta} \tag{4.47}$$

2 Analogous to equation (4.32) we have $\frac{z_B}{z_2} = \left[\frac{r_B}{r_2}\right]^{1 + i\tan\beta} = \left[\frac{r_B}{r_2}\right]^{\frac{e^{i\beta}}{\cos\beta}}$

or by equation (4.46)

$$a \approx \frac{1}{1 - \varepsilon \, cotan \, \beta} \tag{4.48}$$

which may even be further approximated by

$$a \approx 1 + \varepsilon \, cotan \, \beta \tag{4.49}$$

with the latter being valid if

$$| \varepsilon \, cotan \, \beta | \ll 1 \tag{4.50}$$

The final step in our approximation of the mapping constants is now to obtain a suitable expression for ε. Substituting equation (4.45) in equation (4.42) we get

$$\left[\frac{r_1}{r_2}\right]^n = \left[\frac{sin \ \varepsilon}{sin(2\beta - \varepsilon)}\right]^{2cos^2\beta} e^{-2(\beta-\varepsilon)sin\,2\beta} \tag{4.51}$$

Imposing further

$$| \varepsilon | \ll | \beta | \tag{4.52}$$

which will be valid for most practical cases, we finally obtain from equation (4.51), using equation (4.46)

$$\varepsilon \approx \left[\frac{r_1}{r_2}\right]^{\frac{n}{2cos^2\beta}} e^{2\beta \, tan \, \beta} \, sin \, 2\beta \tag{4.53}$$

Employing equation (4.53), the mapping constants as given by equations (4.45) and (4.48) are easy to determine; though one should reckon with the restrictions of the approximation. From equations (4.45) and (4.25) we conclusively notice that the inner tip is located at

$$\theta_1 = \pi - 2\beta + 2\varepsilon \tag{4.54}$$

or

$$\theta_1 = \delta + \varepsilon \tag{4.55}$$

5

SOLVING THE FLOW FIELD

As was pointed out in paragraph 3.2 we employ the superposition of sub flows to solve the potential flow through the impeller. In this chapter we will further discuss these sub flows, and derive the necessary equations that describe the flow field mathematically.

5.1 Displacement Flow

The first sub flow that we will treat is the displacement flow due to the rotation of the impeller. The potential of this flow (and subsequently the fluid velocity) is easily derived from the flow in the circle–plane or ζ–plane, using the theory of functions of a complex variable.

From complex analysis we have by Cauchy's theorem[3]

$$f(\zeta_B) = \frac{1}{\pi i} \oint_C \frac{df}{d\zeta} \ln \frac{1}{\zeta - \zeta_B} d\zeta \tag{5.1}$$

and

$$f(\zeta_P) = \frac{1}{2\pi i} \oint_C \frac{df}{d\zeta} \ln \frac{1}{\zeta - \zeta_P} d\zeta \tag{5.2}$$

where $f(\zeta)$ is an analytic function, in our case the complex potential, in a simply connected domain bounded by a simple closed contour C, with $\zeta_B \in C$ and $\zeta_P \in INT\{C\}$.

Since we are primarily interested in the fluid velocity in the vicinity of the

[3] The integral symbol $\oint$ denotes Cauchy's principal value.

blades (that is, mathematically speaking at the blades) we will base our analysis on equation (5.1). The domain of our concern being the ζ–plane outside the unit circle. The contour C to be chosen to consist of the unit circle, a circle at infinity, and an arbitrary path (traversed twice) connecting the unit circle with the circle at infinity.

Then with the imposed restriction that the fluid is at rest at infinity, i.e.

$$\left[\frac{df}{d\zeta}\right]_{|\zeta|\to\infty} = 0 \tag{5.3}$$

and putting

$$\zeta = e^{i\lambda} \tag{5.4}$$

for points on the unit circle, so that the derivative of the potential $f(\zeta)$ on the unit circle may be written as (see chapter 3)

$$\left[\frac{df}{d\zeta}\right]_{|\zeta|=1} = c_{x\zeta}(\lambda) - ic_{y\zeta}(\lambda) = e^{-i\lambda}\left(c_{n\zeta}(\lambda) - ic_{t\zeta}(\lambda)\right) \tag{5.5}$$

with the (absolute) fluid velocities as shown in figure 5.1, we obtain from equation (5.1) by taking the contour of integration as mentioned

$$f(\zeta_B) = \frac{1}{\pi}\oint_{-\pi}^{\pi}\left(c_{n\zeta}(\lambda) - ic_{t\zeta}(\lambda)\right)\, ln(e^{i\lambda}-\zeta_B)\, d\lambda \tag{5.6}$$

where the subscripts n and t denote the normal and tangential parts, and the subscript ζ refers to the ζ–plane.

Next taking the derivative of equation (5.6) with respect to ζ_B we obtain for the fluid velocity on the unit circle

$$f'(\zeta_B) = \frac{1}{\pi}\oint_{-\pi}^{\pi}\left(c_{n\zeta}(\lambda) - ic_{t\zeta}(\lambda)\right)\, \frac{1}{\zeta_B - e^{i\lambda}}\, d\lambda \tag{5.7}$$

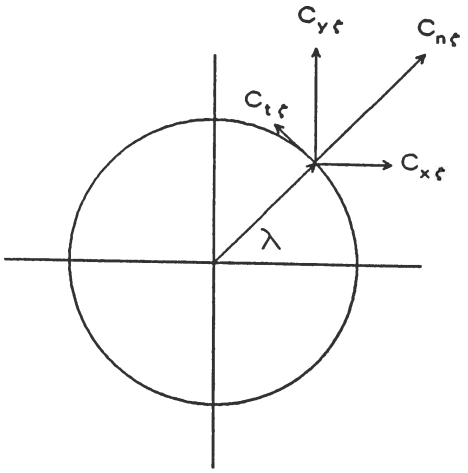

figure 5.1 *fluid velocities along the unit circle in the* $\zeta-$*plane*

From equation (5.5) it further readily follows that the fluid velocity on the unit circle also obeys

$$f'(\zeta_B) = e^{-i\theta}\,\left(c_{n\zeta}(\theta) - ic_{t\zeta}(\theta)\right) \tag{5.8}$$

Then combining equations (5.7) and (5.8) we obtain

$$c_{n\zeta}(\theta) - ic_{t\zeta}(\theta) = \frac{1}{\pi}\fint_{-\pi}^{\pi}\left(c_{n\zeta}(\lambda) - ic_{t\zeta}(\lambda)\right)\frac{e^{i\,\theta}}{e^{i\theta}-e^{i\lambda}}\,d\lambda \tag{5.9}$$

Finally using the identity

$$\frac{2\,e^{i\theta}}{e^{i\theta}-\,e^{i\lambda}} = 1 + i\,cotan\left[\frac{\lambda-\theta}{2}\right] \tag{5.10}$$

we obtain from equation (5.9), separating real and imaginary parts

$$c_{n\zeta}(\theta) = \frac{1}{2\pi}\fint_{-\pi}^{\pi} c_{t\zeta}(\lambda)\;cotan\left[\frac{\lambda-\theta}{2}\right]\,d\lambda + \frac{1}{2\pi}\int_{-\pi}^{\pi} c_{n\zeta}(\lambda)\,d\lambda \tag{5.11}$$

$$c_{t\zeta}(\theta) = -\frac{1}{2\pi}\oint_{-\pi}^{\pi} c_{n\zeta}(\lambda)\ cotan\left[\frac{\lambda-\theta}{2}\right]\ d\lambda + \frac{1}{2\pi}\int_{-\pi}^{\pi} c_{t\zeta}(\lambda)\ d\lambda \qquad (5.12)$$

Equations (5.11) and (5.12) are generally know as Poisson's integrals. These integrals relate, in the present case, the normal and the tangential component of an analytic function on the unit circle. The integral equation (5.12) will serve as a basis to determine the fluid motion due to the rotation of the impeller; but to do so we will first alter it to some extent.

From general potential flow theory we know that the circulation around a body that is placed in a two–dimensional potential flow field equals zero, that is, the flow is free from circulation. Thus, since the second integral in equation (5.12) represents the circulation (Γ) around the unit circle[4], i.e.

$$\Gamma = \int_{-\pi}^{\pi} c_{t\zeta}(\lambda)\ d\lambda \qquad (5.13)$$

we may put

$$c^{D}_{t\zeta}(\theta) = \frac{1}{2\pi}\oint_{-\pi}^{\pi} c^{D}_{n\zeta}(\lambda)\ cotan\left[\frac{\theta-\lambda}{2}\right]\ d\lambda \qquad (5.14)$$

where the superscript D is added to denote the displacement flow.

Equation (5.14), however, gives us a relation for the fluid velocity in the ζ–plane while we are interested in the fluid velocity in the physical or z–plane. Applying a simple transformation this inconvenience may be eliminated as follows.

From complex analysis we know, when mapping an analytical function conformally (say $Z : z \rightarrow \zeta$), that the normal and tangential parts in the respective planes are related by

$$c_{t\zeta}(\varrho,\lambda)\ |d\zeta| = c_{tz}(r,\phi)\ |dz| \qquad (5.15)$$

[4] In a similar way the second integral in equation (5.11) represents the fluid flux (Q).

and

$$c_{n\zeta}(\varrho,\lambda)\ |d\zeta| \ = \ c_{nz}(r,\phi)\ |dz| \tag{5.16}$$

where

$$\zeta \ = \ \varrho e^{i\lambda} \tag{5.17}$$

$$z \ = \ re^{i\phi} \tag{5.18}$$

and the normal and tangential parts (being real functions) are as indicated in figure 5.2.

z – plane *ζ – plane*

figure 5.2 *conformal transformation of an analytical function*

Equations (5.15) and (5.16) basically state the conservation of fluid flux and fluid circulation when transforming a flow field from the z–plane to the ζ–plane, and vice versa. From these equations it readily follows that the fluid velocities at the blades in the respective planes are related by

$$c_{t\zeta} \ = \ c_{tz} \left| \frac{dz}{d\zeta} \right|_B \tag{5.19}$$

$$c_{n\zeta} \ = \ c_{nz} \left| \frac{dz}{d\zeta} \right|_B \tag{5.20}$$

with the corresponding blade points ($z_B \longleftrightarrow \zeta_B$) being determined by the

mapping employed.

So to obtain the fluid velocity (tangentially directed) along a blade due to the rotation of the impeller, we need to know the normal velocity (c_{nz}^{D}) on the blade. This velocity may simply be derived from the physical condition that, at the blades, the relative fluid velocity normal to the blades equals zero. By this boundary condition we have

$$c_{nz}^{D} = (\Omega \times \mathbf{r}_B) \cdot \mathbf{n} \tag{5.21}$$

where

Ω = angular speed of the impeller
$\mathbf{r}_B$= position vector for a blade point
$\mathbf{n}$ = outward directed unit normal on the blade

In two dimensions and for logarithmic spiral blades, or taking $\beta = 0$ for straight radial blades, equation (5.21) simply becomes

$$c_{nz}^{D} = \begin{bmatrix} + \\ - \end{bmatrix} \Omega r_B \cos\beta \tag{5.22}$$

where

$$\Omega = |\Omega| \tag{5.23}$$

$$r_B = |\mathbf{r}_B| \tag{5.24}$$

and the sign $\begin{bmatrix} + \\ - \end{bmatrix}$ depending on the side of the blade, that is $(+)$ for pressure side and $(-)$ for suction side, due to the changing of $\mathbf{n}$.

Furthermore we may write the derivative of the mapping, for points that are located on either straight radial blades ($\beta = 0$) or logarithmic spiral blades, as

$$\left| \frac{dz}{d\zeta} \right|_B = \frac{|dz|_B}{|d\zeta|_B} = \begin{bmatrix} - \\ + \end{bmatrix} \frac{1}{\cos\beta} \frac{dr_B}{d\theta} \tag{5.25}$$

Again the sign $\begin{bmatrix} - \\ + \end{bmatrix}$ depending on the side of the blade.

Substitution of equations (5.22) and (5.25) in equation (5.20) next gives for

the normal velocity in the ζ–plane, due to the rotation of the impeller

$$c^{D}_{n\zeta}(\lambda) = -\Omega r_B(\lambda) \frac{dr_B}{d\lambda} \tag{5.26}$$

where we have used the argument λ to avoid confusion when using equations (5.26) with equation (5.14); the relation $r_B(\lambda)$ in equation (5.26) being further determined by the mapping.

The above allows us to determine the fluid motion (in the vicinity of a blade) due to the rotation of the impeller, as will be demonstrated in the chapters 6 and 7 for straight radial blades and logarithmic spiral blades respectively.

5.2 Source Flow

The potential and accompanying velocity distribution due to the source flow originate from a fluid source at the origin of the z–plane, and are simply obtained from the flow in the ζ–plane.

Placing a fluid source with strength Q in the origin of the z–plane, the potential would be

$$f_Q(z) = \frac{Q}{2\pi} \ln z \tag{5.27}$$

Substitution of transformation (4.1) in equation (5.27) would then give for the potential in the ζ–plane

$$f_Q(\zeta) = \frac{Q}{2\pi n} \ln\left[\frac{\zeta - \zeta_0}{\zeta_2 - \zeta_0}\right] + \frac{Qe^{2i\beta}}{2\pi n} \ln\left[\frac{\frac{1}{\zeta} - \bar{\zeta}_0}{\frac{1}{\zeta_2} - \bar{\zeta}_0}\right] + \frac{1}{2\pi} \ln z_2 \tag{5.28}$$

However, since we are only interested in the fluid velocity, i.e. the derivative of the potential, we may skip those terms in equation (5.28) that occur as constants. Furthermore, with respect to imposing the boundary condition, we only have to consider the contribution of image points outside the unit circle. For the inside of the unit circle has no counterpart in the physical plane.

Equation (5.28) may thus be simplified to

$$f_Q(\zeta) = \frac{Q}{2\pi n} ln(\zeta - \zeta_0) \tag{5.29}$$

Then applying the circle theorem (Milne–Thomson, 1958, pp. 84–85) on equation (5.29), we impose the boundary condition (in the ζ–plane) and obtain

$$f_Q^*(\zeta) = \frac{Q}{2\pi n} \left[ln(\zeta - \zeta_0) + ln(\frac{1}{\zeta} - \bar{\zeta}_0) \right] \tag{5.30}$$

where the asterisk (*) indicates that the potential (5.30) satisfies the boundary condition, that is, the fluid velocity normal to the blades equals zero.

Next taking the derivative of equation (5.30) with respect to ζ, we obtain for the fluid velocity on the unit circle

$$\left[\frac{df_Q^*}{d\zeta} \right]_B = \frac{Q}{2\pi n} \left[\frac{1}{\zeta_B - \zeta_0} - \frac{\zeta_B^{-2}}{\frac{1}{\zeta_B} - \bar{\zeta}_0} \right] \tag{5.31}$$

Substitution of equations (4.7) and (4.8) in equation (5.31) then gives

$$\left[\frac{df_Q^*}{d\zeta} \right]_B = \frac{Qi}{\pi n e^{i\theta}} \frac{a\, sin(\theta-\delta)}{1 + a^2 - 2a\, cos(\theta-\delta)} \tag{5.32}$$

By equation (5.8) we then obtain from equation (5.32) for the fluid velocity on the unit circle in the ζ–plane

$$c_{n\zeta}^Q(\theta) = 0 \tag{5.33}$$

$$c_{t\zeta}^Q(\theta) = \frac{Q}{\pi n} \frac{a\, sin(\theta-\delta)}{1 + a^2 - 2a\, cos(\theta-\delta)} \tag{5.34}$$

where the superscript Q denotes the source flow. Equation (5.33) clearly shows that the boundary condition is properly imposed, with respect to the source flow.

Finally substituting equation (5.34) in equation (5.19), and using the derivative of the mapping as given by equation (4.21), i.e.

$$\left|\frac{dz}{d\zeta}\right|_B = \frac{2r}{n}\left|\frac{a\,sin(\delta+\beta-\theta) - sin\ \beta}{1 + a^2 - 2a\,cos(\delta-\theta)}\right| \tag{5.35}$$

we obtain for the fluid velocity along a blade (in the z–plane) due to the source flow

$$c^Q_{tz} = \frac{Q}{2\pi r}\,\frac{a\,sin(\theta-\delta)}{|a sin(\delta+\beta-\theta) - sin\ \beta|} \tag{5.36}$$

When applying equation (5.36) one should bear in mind that this velocity is directed tangentially in a mathematically positive sense, that is, counter clock wise.

For straight radial blades ($\beta = 0$) equation (5.36) reduces to the well known expression

$$c^Q_{tz} = \begin{bmatrix}+\\-\end{bmatrix}\frac{Q}{2\pi r} \tag{5.37}$$

with the sign $\begin{bmatrix}+\\-\end{bmatrix}$ depending on the side of the blades as mentioned previously.

5.3 Vortex Flow

Since vortices and sources are singularities that only differ by their nature we may treat the vortex flow analogously to the source flow, as just described; likewise we now have a fluid flow that originates from a (point rectilinear) vortex with strength Γ_1 located at the origin of the z–plane, whose potential would be

$$f_\Gamma(z) = \frac{\Gamma_1}{2\pi i}\,ln\,z \tag{5.38}$$

Again only the relevant contribution to the potential in the ζ–plane has to be considered, which leads to

$$f_\Gamma(\zeta) = \frac{\Gamma_1}{2\pi n i}\,ln(\zeta - \zeta_0) \tag{5.39}$$

Then applying the circle theorem to equation (5.39) we obtain

$$f^*_\Gamma(\zeta) = \frac{\Gamma_1}{2\pi n i}\left[ln(\zeta - \zeta_0) - ln(\tfrac{1}{\bar{\zeta}} - \bar{\zeta}_0)\right] \tag{5.40}$$

Next taking the derivative of equation (5.40) with respect to ζ, we obtain for the fluid velocity on the unit circle in the ζ–plane

$$\left[\frac{df^*_\Gamma}{d\zeta}\right]_B = \frac{\Gamma_1}{2\pi n i}\left[\frac{1}{\zeta_B - \zeta_0} + \frac{\zeta_B^{-2}}{\frac{1}{\zeta_B} - \bar{\zeta}_0}\right] \tag{5.41}$$

Substitution of equations (4.7) and (4.8) in equation (5.41) and using equation (5.8) then gives for the fluid velocity (in the ζ–plane) due to the vortex

$$c^\Gamma_{n\zeta} = 0 \tag{5.42}$$

$$c^\Gamma_{t\zeta}(\theta) = \frac{\Gamma_1}{\pi n}\,\frac{1 - a\cos(\theta-\delta)}{1 + a^2 - 2a\cos(\theta-\delta)} \tag{5.43}$$

where the superscript Γ is used to denote the vortex flow. Equation (5.42) again shows that the boundary condition has been properly imposed.

Finally substituting equations (5.43) and (5.35) in (5.19) we obtain for the fluid velocity along a blade (in the z–plane) due to the vortex flow

$$c^\Gamma_{tz} = \frac{\Gamma_1}{2\pi r}\,\frac{1 - a\cos(\theta-\delta)}{|a\sin(\delta+\beta-\theta) - \sin\beta|} \tag{5.44}$$

5.4 Kutta's Condition or Joukowski's Hypothesis

The last sub flow or potential to be discussed is due to the Kutta condition or Joukowski's hypothesis[5], which impose a smooth flow off both surfaces of the impeller blades at the trailing edge. This smooth flow off implies elimination of the singularity at the trailing edge of a blade.

The smoothing of the flow (in the z–plane) near the trailing edge is done by superposing a vortex flow (in the ζ–plane) originating from the origin of the

[5] Joukowski's hypothesis states that the circulation around an aerofoil always adjusts itself so that there is a stagnation point at the trailing edge, and the velocity being finite at that point (Milne-Thomson, 1958, pp. 112-113).

ζ–plane. This additional flow both satisfies the potential equation and the boundary conditions; its potential is given by

$$f_K(\zeta) = \frac{\Gamma_B}{2\pi} \ln \zeta \tag{5.45}$$

where Γ_B is the strength of the superposed vortex – the so–called blade circulation – which is (to be) determined by the Kutta condition.

From equation (5.45) we obtain for the fluid velocity on the unit circle, using equation (5.8)

$$c^K_{t\zeta} = \left[\frac{df_K}{d\zeta}\right]_B e^{i\theta} = \frac{\Gamma_B}{2\pi} \tag{5.46}$$

$$c^K_{n\zeta} = 0 \tag{5.47}$$

where the superscript K denotes that the velocities are related to the Kutta condition, and where we have omitted the argument (θ) since the the velocities are constant along the unit circle.

Now by simply requiring a zero (overall) fluid velocity at the trailing edge in the ζ–plane we impose the Kutta condition; this method will be valid as long as the decrease of the fluid velocity exceeds the increase of the derivative $(\frac{d\zeta}{dz})$ of the mapping near the trailing edge. Imposing the Kutta condition accordingly we have to distinguish the pump and the turbine since the trailing edge of the blade of a pump impeller lies at the outer tip, while in case of a turbine the trailing edge lies at the inner tip. In the following we will first consider the impeller acting as a pump rotor, and secondly we will outline the case of a turbine.

5.4.1 Impeller acting as pump rotor

Imposing the Kutta condition for the pump impeller, i.e. outer tip ($\theta = 0$) as trailing edge, gives the relation

$$c^D_{t\zeta}(0) + c^Q_{t\zeta}(0) + c^\Gamma_{t\zeta}(0) + c^K_{t\zeta} = 0 \tag{5.48}$$

Substitution of equation (5.46) in equation (5.48) next gives for the

circulation around each blade of a pump impeller

$$\Gamma_B = -2\pi\left[c^D_{t\zeta}(0) + c^Q_{t\zeta}(0) + c^\Gamma_{t\zeta}(0)\right] \tag{5.49}$$

5.4.2 Impeller acting as turbine rotor

Imposing the Kutta condition for the turbine impeller, i.e. inner tip ($\theta = \theta_1$) as trailing edge, gives the relation

$$c^D_{t\zeta}(\theta_1) + c^Q_{t\zeta}(\theta_1) + c^\Gamma_{t\zeta}(\theta_1) + c^K_{t\zeta} = 0 \tag{5.50}$$

Substitution of equation (5.46) in equation (5.50) next gives for the blade circulation in case of a turbine

$$\Gamma_B = -2\pi\left[c^D_{t\zeta}(\theta_1) + c^Q_{t\zeta}(\theta_1) + c^\Gamma_{t\zeta}(\theta_1)\right] \tag{5.51}$$

Although equation (5.51) strongly resembles equation (5.49), one should bear in mind that in case of a turbine the circulation Γ_1 is not predetermined, as by a pump, but instead the circulation Γ_2 around the impeller is predetermined; both circulations are simply related by

$$\Gamma_2 = \Gamma_1 + \sum_{j=1}^{n} \Gamma_B \tag{5.52}$$

or since all blade circulations are equal by the periodicity of the flow

$$\Gamma_2 = \Gamma_1 + n\Gamma_B \tag{5.53}$$

5.5 Condition of Shockless Entry

After imposing the Kutta condition still an other singularity remains, viz. the one at the leading edge of the blades. In the remaining paragraph of this chapter we will discuss how this singularity may be eliminated, which is generally known as (imposing) the condition of shockless entry. This condition of shockless entry determines the requisite prerotation of the flow entering the impeller, which will give a so–called shockless operation. Perhaps needless to say that the condition of shockless entry is an operating

condition while the Kutta condition embodies a physical fact, that is, the Kutta condition determines the circulation around the blades whereas the condition of shockless entry gives the prerotation to impose a shockless operation. From a mathematical point of view, however, both conditions are alike. Discussing the condition of shockless entry a distinction will be made between the pump and turbine, as has been done for the Kutta condition.

5.5.1 Pump impeller

Imposing the condition of shockless entry for the pump impeller, i.e. the inner tip ($\theta = \theta_1$) as leading edge, gives the relation

$$c^{\mathrm{D}}_{t\zeta}(\theta_1) + c^{\mathrm{Q}}_{t\zeta}(\theta_1) + c^{\Gamma}_{t\zeta}(\theta_1) + c^{\mathrm{K}}_{t\zeta} = 0 \qquad (5.54)$$

Substitution of equation (5.46) in equation (5.54) and taking the blade circulation according to equation (5.49) next gives

$$c^{\mathrm{D}}_{t\zeta}(\theta_1) - c^{\mathrm{D}}_{t\zeta}(0) + c^{\mathrm{Q}}_{t\zeta}(\theta_1) - c^{\mathrm{Q}}_{t\zeta}(0) + c^{\Gamma}_{t\zeta}(\theta_1) - c^{\Gamma}_{t\zeta}(0) = 0 \qquad (5.55)$$

Equation (5.55) fully determines the prerotation ($\Gamma_{1,\mathrm{SL}}$) of the flow entering the pump impeller, such that a shockless operation is obtained.

5.5.2 Turbine impeller

Imposing the condition of shockless entry for the turbine impeller, i.e. the outer tip ($\theta = 0$) as leading edge, gives the relation

$$c^{\mathrm{D}}_{t\zeta}(0) + c^{\mathrm{Q}}_{t\zeta}(0) + c^{\Gamma}_{t\zeta}(0) + c^{\mathrm{K}}_{t\zeta} = 0 \qquad (5.56)$$

Substitution of equation (5.46) in equation (5.56) and taking the blade circulation as given by equation (5.51) next gives

$$c^{\mathrm{D}}_{t\zeta}(0) - c^{\mathrm{D}}_{t\zeta}(\theta_1) + c^{\mathrm{Q}}_{t\zeta}(0) - c^{\mathrm{Q}}_{t\zeta}(\theta_1) + c^{\Gamma}_{t\zeta}(0) - c^{\Gamma}_{t\zeta}(\theta_1) = 0 \qquad (5.57)$$

From equation (5.57) we indirectly derive the prerotation of the flow entering the turbine impeller, such that a shockless operation is obtained. Having solved Γ_1 from equation (5.57) the prerotation (Γ_2) is next readily given by equation (5.53).

6

SOLUTIONS FOR STRAIGHT RADIAL BLADES

In this chapter we will derive the (analytical) solution of the flow field for the impeller fitted with straight radial blades, as we have generally described in the previous chapter. Both the pump and turbine will be considered, where we will discuss the pump rather extensively (paragraph 6.1) while the turbine will merely be considered with regard to the blade circulation and the condition of shockless entry (paragraph 6.2).

6.1 Pump Impeller

Discussing the case of a pump we will first determine the blade circulation, as imposed by the Kutta condition, and the prerotation required for a shockless operation. Using these results we will then derive the velocity distribution in the ζ–plane due to the displacement flow, as well as the velocity distributions (also in the ζ–plane) due to the source and vortex flow. Then we will give the resulting velocity distribution in the z–plane, and as a simple application we will finally discuss the pressure distribution along a blade.

6.1.1 Blade circulation

For simplicity we employ the following subdivision of the blade circulation

$$\Gamma_B = \Gamma_B^D + \Gamma_B^Q + \Gamma_B^\Gamma \tag{6.1}$$

where each superscript denotes the origin of the respective sub circulations.

By equation (5.49) it next follows that

$$\Gamma_B^D = -2\pi c_{t\zeta}^D(0) \tag{6.2}$$

$$\Gamma_B^Q = -2\pi c_{t\zeta}^Q(0) \tag{6.3}$$

$$\Gamma_B^\Gamma = -2\pi c_{t\zeta}^\Gamma(0) \tag{6.4}$$

The latter contributions, due to the source (Q) and the vortex (Γ), are readily to be obtained from the foregoing. From equations (5.34) and (5.43) it follows that, putting $\delta = \pi$, $\theta = 0$ and using equation (4.15)

$$c_{t\zeta}^Q(0) = 0 \tag{6.5}$$

$$c_{t\zeta}^\Gamma(0) = (1 - \sqrt{\mu})\,\frac{\Gamma_1}{2\pi n} \tag{6.6}$$

So the contributions given by equations (6.3) and (6.4) simply become

$$\Gamma_B^Q = 0 \tag{6.7}$$

$$\Gamma_B^\Gamma = -\frac{1-\sqrt{\mu}}{n}\,\Gamma_1 \tag{6.8}$$

The result of equation (6.7) being trivial since the source flow already satisfies the Kutta condition in case of straight radial blades.

Having determined the contributions due to the source and the vortex we now focus our attention on the still remaining contribution due to the displacement flow.

From equation (5.26) we first derive, substituting equation (4.20)

$$c_{n\zeta}^D(\lambda) = \frac{\Omega r_2^2}{n}\,\frac{1-\mu}{1+\mu}\left(\frac{1+\mu}{2}\right)^{\frac{2}{n}}\left(1 + \frac{1-\mu}{1+\mu}\cos\lambda\right)^{\frac{2}{n}-1}\sin\lambda \tag{6.9}$$

Substituting equation (6.9) in equation (5.14), and taking $\theta = 0$, then gives

$$c_{t\zeta}^D(0) = -\frac{\Omega r_2^2}{2\pi n}\,\frac{1-\mu}{1+\mu}\left(\frac{1+\mu}{2}\right)^{\frac{2}{n}} \int_{-\pi}^{\pi} \left(1 + \frac{1-\mu}{1+\mu}\cos\lambda\right)^{\frac{2}{n}-1} \sin\lambda\, \cot an\left(\frac{\lambda}{2}\right) d\lambda \tag{6.10}$$

by which equation (6.2) becomes

$$\Gamma_B^D = \frac{\Omega r_2^2}{n}\frac{1-\mu}{1+\mu}\left[\frac{1+\mu}{2}\right]^{\frac{2}{n}}\int_{-\pi}^{\pi}\left[1+\frac{1-\mu}{1+\mu}\cos\lambda\right]^{\frac{2}{n}-1}\left[1+\cos\lambda\right]d\lambda \qquad (6.11)$$

where we have used the identity

$$\operatorname{cotan}\left[\frac{\lambda}{2}\right] = \frac{\sin\lambda}{1-\cos\lambda} \qquad (6.12)$$

to eliminate the singularity of the integral at $\lambda = 0$.

For simplicity we next write equation (6.11) alternatively as

$$n\Gamma_B^D = KI_0 \qquad (6.13)$$

where

$$K = \Omega r_2^2\frac{1-\mu}{1+\mu}\left[\frac{1+\mu}{2}\right]^{\frac{2}{n}} \qquad (6.14)$$

and

$$I_0 = \int_{-\pi}^{\pi}\left[1+\frac{1-\mu}{1+\mu}\cos\lambda\right]^{\frac{2}{n}-1}\left[1+\cos\lambda\right]d\lambda \qquad (6.15)$$

Next putting

$$\alpha = \tfrac{1}{2}\lambda \qquad (6.16)$$

we can write integral (6.15) as

$$I_0 = 8\int_0^{\frac{\pi}{2}}\left[\frac{2\mu}{1+\mu}+2\frac{1-\mu}{1+\mu}\cos^2\alpha\right]^{\frac{2}{n}-1}\cos^2\alpha\,d\alpha \qquad (6.17)$$

Formulated by equation (6.17) the integral I_0 appears to have an equivalent, stated by special functions. Presented in a slightly different way we have according to Gradshteyn and Ryzhik (eq. 3.682, p. 389)

$$\int_0^{\frac{\pi}{2}} \frac{sin^x\alpha\, cos^y\alpha}{(p + q\, cos^2\alpha)^\eta}\, d\alpha = \frac{1}{2p^\eta} B\left[\frac{x+1}{2}, \frac{y+1}{2}\right] F\left[\frac{y+1}{2}, \eta; \frac{x+y}{2}+1; -\frac{q}{p}\right] \tag{6.18}$$

$$(x > -1,\ y > -1,\ p > 0,\ q > 0)$$

where $B(..,..)$ stands for the well-known beta function, and $F(..,..;..;..)$ represents the hypergeometric function or hypergeometric series.

Then putting

$$x = 0 \tag{6.19}$$

$$y = 2 \tag{6.20}$$

$$p = \frac{2\mu}{1+\mu} \tag{6.21}$$

$$q = 2\,\frac{1-\mu}{1+\mu} \tag{6.22}$$

$$\eta = 1 - \frac{2}{n} \tag{6.23}$$

we obtain from equations (6.17) and (6.18)

$$I_0 = 4 \left(\frac{2\mu}{1+\mu}\right)^{\frac{2}{n}-1} B(\tfrac{1}{2},\tfrac{3}{2})\, F\left[\tfrac{3}{2}, 1-\tfrac{2}{n}; 2; -\tfrac{1-\mu}{\mu}\right] \tag{6.24}$$

Furthermore, since

$$B(\tfrac{1}{2},\tfrac{3}{2}) = \frac{\Gamma(\frac{1}{2})\,\Gamma(\frac{3}{2})}{\Gamma(2)} = \frac{\pi}{2} \tag{6.25}$$

and

$$F\left[\tfrac{3}{2},1-\tfrac{2}{n};2;-\tfrac{1-\mu}{\mu}\right] = \mu^{1-\frac{2}{n}} F\left[\tfrac{1}{2},1-\tfrac{2}{n};2;1-\mu\right] \tag{6.26}$$

the latter being an elementary transformation of a hypergeometric function[6] and $\Gamma(..)$ being the well-known gamma function, we may write equation (6.24) also as

$$I_0 = 2\pi \left[\frac{1+\mu}{2}\right]^{1-\frac{2}{n}} F\left[\tfrac{1}{2},1-\tfrac{2}{n};2;1-\mu\right] \tag{6.27}$$

Substitution of equations (6.24) and (6.27) in equation (6.13) then gives for the blade circulation due to the displacement flow

$$n\Gamma_B^D = 2\pi\Omega r_2^2 \frac{1-\mu}{2} F\left[\tfrac{1}{2},1-\tfrac{2}{n};2;1-\mu\right] \tag{6.28}$$

which may also be written as

$$n\Gamma_B^D = \sigma_{p,D}\, 2\pi\Omega r_2^2 \tag{6.29}$$

where

$$\sigma_{p,D} = \frac{1-\mu}{2} F\left[\tfrac{1}{2},1-\tfrac{2}{n};2;1-\mu\right] \tag{6.30}$$

The factor $\sigma_{p,D}$ is generally known as the slip factor although it is merely due to the displacement flow. Similar slip factors may be defined with respect to the source and vortex flow, as will be shown below. To distinguish the various slip factors that are to be discussed throughout this work, we employ a subscript notation where the first subscript refers to the *pump* or *turbine* and the second subscript indicates the nature of the slip factor, i.e. displacement (D), source (Q) or vortex (Γ) flow. The meaning of slip factors, always being less than 1 and expressing the fact that the flow receives imperfect guidance due to the limited number of blades, will be further discussed in chapter 9.

Finally substituting equations (6.7), (6.8), and (6.29) in equation (6.1) we

[6] As can be found in, for instance, Abramowitz and Stegun, Bateman (1953), or Gradshteyn and Ryzhik we have that

$$F(a,b;c;z) = F(b,a;c;z) = (1-z)^{-b} F(c-a,b;c;\tfrac{z}{z-1})$$

obtain for the blade circulation of a pump impeller fitted with (n) straight radial blades

$$n\Gamma_B = \sigma_{p,D}\, 2\pi\Omega r_2^2 - \sigma_{p,\Gamma}\, \Gamma_1 \tag{6.31}$$

where

$$\sigma_{p,\Gamma} = 1 - \sqrt{\mu} = 1 - \left[\frac{r_1}{r_2}\right]^{\frac{n}{2}} \tag{6.32}$$

and $\sigma_{p,D}$ according to equation (6.30).

Perhaps needless to say that the slip factors are all dimensionless and in the interval [0,1], with the limiting value ($n \longrightarrow \infty$) being 1.

6.1.2 Condition of shockless entry

From equation (5.55) we have as the condition of shockless entry for the pump impeller fitted with straight radial blades, putting $\theta_1 = \pi$

$$c^D_{t\zeta}(\pi) - c^D_{t\zeta}(0) + c^Q_{t\zeta}(\pi) - c^Q_{t\zeta}(0) + c^\Gamma_{t\zeta}(\pi) - c^\Gamma_{t\zeta}(0) = 0 \tag{6.33}$$

Individual terms in equation (6.33) to be discussed separately, as far as they have not been obtained previously.

First substituting equation (6.9) we obtain from equation (5.14)

$$c^D_{t\zeta}(\pi) = \frac{\Omega r_2^2}{2\pi n}\,\frac{1-\mu}{1+\mu}\left[\frac{1+\mu}{2}\right]^{\frac{2}{n}} \int_{-\pi}^{\pi} \left[1 + \frac{1-\mu}{1+\mu}\cos\lambda\right]^{\frac{2}{n}-1} \sin\lambda\, \operatorname{cotan}\left[\frac{\pi-\lambda}{2}\right] d\lambda \tag{6.34}$$

Then using the identity

$$\operatorname{cotan}\left[\frac{\pi-\lambda}{2}\right] = \frac{\sin\lambda}{1+\cos\lambda} \tag{6.35}$$

to eliminate the singularity at $\lambda = \pi$, equation (6.34) becomes

$$c_{t\zeta}^{D}(\pi) = \frac{\Omega r_2^2}{2\pi n}\frac{1-\mu}{1+\mu}\left(\frac{1+\mu}{2}\right)^{\frac{2}{n}}\int_{-\pi}^{\pi}\left[1 + \frac{1-\mu}{1+\mu}\cos\lambda\right]^{\frac{2}{n}-1}\left[1 - \cos\lambda\right]d\lambda \qquad (6.36)$$

which we write alternatively as

$$2\pi n c_{t\zeta}^{D}(\pi) = KI_1 \qquad (6.37)$$

where

$$I_1 = \int_{-\pi}^{\pi}\left[1 + \frac{1-\mu}{1+\mu}\cos\lambda\right]^{\frac{2}{n}-1}\left[1 - \cos\lambda\right]d\lambda \qquad (6.38)$$

and K according to equation (6.14).

Next we derive from equation (5.34) and (5.43), putting $\delta = \pi$ and using equation (4.15)

$$c_{t\zeta}^{Q}(\pi) = 0 \qquad (6.39)$$

$$c_{t\zeta}^{\Gamma}(\pi) = -\frac{1-\sqrt{\mu}}{\sqrt{\mu}}\frac{\Gamma_1}{2\pi n} \qquad (6.40)$$

Then substituting equations (6.5), (6.6), (6.13), (6.37), (6.39), and (6.40) in equation (6.33) we obtain for the shockless prerotation

$$K(I_0 + I_1) - \frac{1-\mu}{\sqrt{\mu}}\Gamma_{1,SL} = 0 \qquad (6.41)$$

or

$$\Gamma_{1,SL} = \frac{\sqrt{\mu}}{1-\mu}K(I_0 + I_1) \qquad (6.42)$$

Thus, to obtain the shockless prerotation as given by equation (6.42) we have to compute the integral $I_0 + I_1$. From equations (6.15) and (6.38) we readily obtain that this integral reads

$$I_0 + I_1 = 4 \int_0^{\pi} \left[1 + \frac{1-\mu}{1+\mu} \cos\lambda\right]^{\frac{2}{n}-1} d\lambda \tag{6.43}$$

To evaluate this equation we recall that the integral in equation (6.43) resembles Laplace's integral for Legendre functions, i.e.

$$P_\nu(\xi) = \frac{1}{\pi} \int_0^{\pi} \left[\xi + \sqrt{\xi^2-1}\cos\lambda\right]^{\nu} d\lambda \tag{6.44}$$

where $P_\nu(\xi)$ represents the Legendre function of the first kind.

Then putting

$$\xi = \frac{1+\mu}{2\sqrt{\mu}} \tag{6.45}$$

$$\nu = \frac{2}{n} - 1 \tag{6.46}$$

we obtain from equations (6.43) and (6.44)

$$I_0 + I_1 = 4\pi\xi^{-\nu}P_\nu(\xi) \tag{6.47}$$

which may be written alternatively as

$$I_0 + I_1 = 4\pi\xi^{-\nu}P_\alpha(\xi) \tag{6.48}$$

where

$$\alpha = -\nu - 1 \tag{6.49}$$

or, by equation (6.46),

$$\alpha = -\frac{2}{n} \tag{6.50}$$

Since the Legendre function ($P_\nu(\xi)$) can be expressed by a hypergeometric function, we evaluate equation (6.48) somewhat further. Substituting the elementary transformation

$$P_\alpha(\xi) = \left[\frac{1+\xi}{2}\right]^\alpha F\left[-\alpha, -\alpha; 1; \frac{\xi-1}{\xi+1}\right] \tag{6.51}$$

which is valid for $Re\{\xi\} > 0$, we obtain from equation (6.48)

$$I_0 + I_1 = 4\pi\xi^{-\nu}\left[\frac{1+\xi}{2}\right]^\alpha F\left[-\alpha, -\alpha; 1; \frac{\xi-1}{\xi+1}\right] \tag{6.52}$$

Then substituting equations (6.45), (6.46), and (6.50) in equation (6.52) we get

$$I_0 + I_1 = 2^{1+\frac{6}{n}}\,\pi\,(1+\mu)^{1-\frac{2}{n}}\,(1+\sqrt{\mu})^{-\frac{4}{n}}\,(\sqrt{\mu})^{\frac{4}{n}-1} F\left[\frac{2}{n}, \frac{2}{n}; 1; \left(\frac{1-\sqrt{\mu}}{1+\sqrt{\mu}}\right)^2\right] \tag{6.53}$$

Finally substituting equations (6.14) and (6.53) in equation (6.42), and using equation (4.14), we obtain for the shockless prerotation of a pump impeller fitted with straight radial blades

$$\Gamma_{1,SL} = \tau_{p,D}\, 2\pi\Omega r_1^2 \tag{6.54}$$

where

$$\tau_{p,D} = \left[\frac{2}{1+\sqrt{\mu}}\right]^{\frac{4}{n}} F\left[\frac{2}{n}, \frac{2}{n}; 1; \left(\frac{1-\sqrt{\mu}}{1+\sqrt{\mu}}\right)^2\right] \tag{6.55}$$

Just as we have done for the slip factor we here have introduced a so–called prerotation factor ($\tau_{p,D}$), which is also dimensionless but greater than 1. This prerotation factor will be further discussed in chapter 9.

6.1.3 Velocity distributions in the ζ–plane

Having dealt with the singular behaviour at the blade tips (Kutta condition and shockless operation), we are now to complete our discussion and derive the velocity distributions (in the ζ–plane) along the blades, that is, along the unit circle. Successively we will treat the velocity distributions due to the source flow, the vortex flow, and the displacement flow.

Source Flow

Putting $\delta = \pi$ and substituting equation (4.15), we obtain from equation (5.34)

$$c^{Q}_{t\zeta}(\theta) = -\frac{Q}{2\pi n}\,\frac{\sin\,\theta}{\cos\,\theta + \frac{1+\mu}{1-\mu}} \tag{6.56}$$

Vortex Flow

From equation (5.43) we obtain, again putting $\delta = \pi$ and substituting equation (4.15)

$$c^{\Gamma}_{t\zeta}(\theta) = \frac{\Gamma_1}{2\pi n}\,\frac{\cos\,\theta + \frac{1-V\mu}{1+V\mu}}{\cos\,\theta + \frac{1+\mu}{1-\mu}} \tag{6.57}$$

Displacement Flow

Substitution of equation (6.9) in equation (5.14) gives for the velocity distribution along a blade, in the ζ–plane

$$c^{D}_{t\zeta}(\theta) = \frac{K}{2\pi n}\int_{-\pi}^{\pi}\left[1 + \frac{1-\mu}{1+\mu}\cos\lambda\right]^{\frac{2}{n}-1}\sin\lambda\,\cot an\left[\frac{\theta-\lambda}{2}\right]\,d\lambda \tag{6.58}$$

with K according to equation (6.14).

Next substituting the identity

$$\cot an\left[\frac{\theta-\lambda}{2}\right] = \frac{\sin\lambda + \sin\theta}{\cos\lambda - \cos\theta} \tag{6.59}$$

and taking into account that the trigonometric function

$$G(\lambda) = \left[1 + \frac{1-\mu}{1+\mu}\cos\lambda\right]^{\frac{2}{n}-1}\frac{\sin\lambda\,\sin\theta}{\cos\lambda - \cos\theta} \tag{6.60}$$

is an odd function, we may write equation (6.58) as

$$c^{D}_{t\zeta}(\theta) = \frac{K}{2\pi n} \int_{-\pi}^{\pi} \left[1 + \frac{1-\mu}{1+\mu} \cos\lambda\right]^{\frac{2}{n}-1} \frac{\sin^2\lambda}{\cos\lambda - \cos\theta} d\lambda \tag{6.61}$$

or, employing some elementary trigonometric manipulations,

$$c^{D}_{t\zeta}(\theta) = \frac{K}{2\pi n} \sin^2\theta \int_{-\pi}^{\pi} \left[1 + \frac{1-\mu}{1+\mu} \cos\lambda\right]^{\frac{2}{n}-1} \frac{d\lambda}{\cos\lambda - \cos\theta}$$

$$+ \frac{K}{2\pi n} \left[1 - \cos\theta\right] \int_{-\pi}^{\pi} \left[1 + \frac{1-\mu}{1+\mu} \cos\lambda\right]^{\frac{2}{n}-1} d\lambda$$

$$- \frac{K}{2\pi n} \int_{-\pi}^{\pi} \left[1 + \frac{1-\mu}{1+\mu} \cos\lambda\right]^{\frac{2}{n}-1} \left[1 + \cos\lambda\right] d\lambda \tag{6.62}$$

Using equations (6.15) and (6.43) we may rephrase equation (6.62) as

$$c^{D}_{t\zeta}(\theta) = \frac{K}{2\pi n} \left[\sin^2\theta\, I(\theta) + \left[1 - \cos\theta\right] \frac{I_0 + I_1}{2} - I_0\right] \tag{6.63}$$

where

$$I(\theta) = \int_{-\pi}^{\pi} \left[1 + \frac{1-\mu}{1+\mu} \cos\lambda\right]^{\frac{2}{n}-1} \frac{d\lambda}{\cos\lambda - \cos\theta} \tag{6.64}$$

In equation (6.63) only the integral $I(\theta)$ remains to be discussed, for the integrals I_0 and $I_0 + I_1$ have already been treated in the previous sections. To evaluate the integral $I(\theta)$, as given by equation(6.64), we employ the

following from aerodynamics well–known principle value integral (Milne–Thompson, 1958, p. 80)

$$\int_{-\pi}^{\pi} \frac{\cos k\lambda}{\cos \lambda - \cos \theta} d\lambda = 2\pi \frac{\sin k\theta}{\sin \theta} \tag{6.65}$$

Developing the leading part of integral (6.64) in a Fourier cosine series we may next rephrase integral (6.64) using equation (6.65).

The Fourier expansion that we employ reads

$$\left[1 + \frac{1-\mu}{1+\mu} \cos \lambda\right]^{\frac{2}{n}-1} = \tfrac{1}{2}A_0 + \sum_{k=1}^{\infty} A_k \cos k\lambda \tag{6.66}$$

where the Fourier coefficients of the cosine series are defined by

$$A_k = \frac{2}{\pi} \int_0^{\pi} \left[1 + \frac{1-\mu}{1+\mu} \cos \lambda\right]^{\frac{2}{n}-1} \cos k\lambda \, d\lambda \tag{6.67}$$

Then substituting equation (6.66) in equation (6.64) we obtain, employing equation (6.65)

$$I(\theta) = \frac{2\pi}{\sin \theta} \sum_{k=1}^{\infty} A_k \sin k\theta \tag{6.68}$$

The Fourier coefficients (A_k) can next be expressed by a special function, since equation (6.67) resembles an integral representation of the associated Legendre functions, i.e.

$$P_\nu^k(\xi) = \left[\prod_{m=1}^{k} (\nu+m)\right] \frac{1}{\pi} \int_0^{\pi} \left[\xi + \sqrt{\xi^2-1} \cos \lambda\right]^{\nu} \cos k\lambda \, d\lambda \tag{6.69}$$

where $P_\nu^k(\xi)$ stands for the associated Legendre function of the first kind.

Putting

$$\xi = \frac{1+\mu}{2\sqrt{\mu}} \tag{6.45}$$

$$\nu = \frac{2}{n} - 1 \tag{6.46}$$

we obtain from equations (6.67) and (6.69) that the Fourier coefficients are

$$A_k = 2 \left[\prod_{m=1}^{k} (\nu+m) \right]^{-1} \xi^{-\nu} P_\nu^k(\xi) \tag{6.70}$$

Next expressing the associated Legendre function by a hypergeometric function, i.e.

$$P_\nu^k(\xi) = \frac{1}{k!} \frac{\Gamma(\nu+k+1)}{\Gamma(\nu-k+1)} \left[\frac{\xi-1}{\xi+1} \right]^{\frac{k}{2}} \left[\frac{2}{1+\xi} \right]^{\nu+1} F\left[1+\nu, k+\nu+1; k+1; \frac{\xi-1}{\xi+1}\right] \tag{6.71}$$

which is valid for $Re\{\xi\} > 0$, we may write the Fourier coefficients (6.70) also as

$$A_k = \left[\prod_{m=1}^{k} (\nu+m) \right]^{-1} \frac{2\xi^{-\nu}}{k!} \frac{\Gamma(\nu+k+1)}{\Gamma(\nu-k+1)} \left[\frac{\xi-1}{\xi+1} \right]^{\frac{k}{2}} \left[\frac{2}{1+\xi} \right]^{\nu+1} F\left[1+\nu, k+\nu+1; k+1; \frac{\xi-1}{\xi+1}\right] \tag{6.72}$$

Then substituting equations (6.45) and (6.46) in equation (6.72), and using the identity

$$\Gamma(x+k) = \Gamma(x) \prod_{m=1}^{k} (m+x-1) \tag{6.73}$$

we get

$$A_k = \frac{2^{\frac{6}{n}}}{k!} (1+\mu)^{1-\frac{2}{n}} (1+\sqrt{\mu})^{-\frac{4}{n}} (\sqrt{\mu})^{\frac{4}{n}-1} \left[\frac{1-\sqrt{\mu}}{1+\sqrt{\mu}} \right]^k \frac{\Gamma(\frac{2}{n})}{\Gamma(\frac{2}{n}-k)} F\left[\frac{2}{n}, k+\frac{2}{n}; k+1; \left[\frac{1-\sqrt{\mu}}{1+\sqrt{\mu}}\right]^2\right] \tag{6.74}$$

or, using the identity

$$\Gamma(y) = \Gamma(y-k) \prod_{m=1}^{k} (y-m) \tag{6.75}$$

we may write equation (6.74) as

$$A_k = 2^{\frac{6}{n}} (1+\mu)^{1-\frac{2}{n}} (1+\sqrt{\mu})^{-\frac{4}{n}} (\sqrt{\mu})^{\frac{4}{n}-1} a_k \tag{6.76}$$

where

$$a_k = \frac{1}{k!} \left[\frac{1-\sqrt{\mu}}{1+\sqrt{\mu}}\right]^k F\left[\frac{2}{n}, k+\frac{2}{n}; k+1; \left[\frac{1-\sqrt{\mu}}{1+\sqrt{\mu}}\right]^2\right] \prod_{m=1}^{k} (\tfrac{2}{n}-m) \tag{6.77}$$

Finally substituting equations (6.14), (6.27), (6.53), and (6.68) in equation (6.63) we obtain for the velocity distribution along a blade (in the ζ–plane) due to the displacement flow

$$c^D_{t\zeta}(\theta) = \Omega r_1^2 \frac{1-\mu}{n\sqrt{\mu}} \left[\frac{2}{1+\sqrt{\mu}}\right]^{\frac{4}{n}} \left\{ \sin\theta \sum_{k=1}^{\infty} a_k \sin k\theta + \sin^2\left[\frac{\theta}{2}\right] F\left[\frac{2}{n}, \frac{2}{n}; 1; \left[\frac{1-\sqrt{\mu}}{1+\sqrt{\mu}}\right]^2\right]\right\}$$

$$- \Omega r_2^2 \frac{1-\mu}{2n} F\left[\tfrac{1}{2}, 1-\tfrac{2}{n}; 2; 1-\mu\right] \tag{6.78}$$

where we have also used equations (4.14)[7] and (6.76); the convergence of the Fourier series and thereby the validity of the solution (6.78) still to be proven, as will next be done.

From Fourier analysis we know that the trigonometrical series

$$R(\lambda) = \sum_{k=0}^{\infty} \left[A_k \cos k\lambda + B_k \sin k\lambda\right] \tag{6.79}$$

will converge uniformly if the series of coefficients, i.e.

$$\sum_{k=0}^{\infty} \left[|A_k| + |B_k|\right] \tag{6.80}$$

converges.

7 From equation (4.14) it follows that $(r_1/r_2)^2 = \mu^{2/n}$

Employing d'Alembert's criterion we next easily prove the convergence of the Fourier series. From equations (6.76) and (6.77) it follows that

$$\lim_{k\to\infty} \left| \frac{A_{k+1}}{A_k} \right| = \lim_{k\to\infty} \left| \frac{a_{k+1}}{a_k} \right| = \frac{1-\sqrt{\mu}}{1+\sqrt{\mu}} \tag{6.81}$$

which is always less than 1 ($\mu > 0$), so the Fourier series will converge uniformly.

Q.E.D.

From equation (6.81) we also notice that the rate of convergence of the series will decrease if μ becomes small, that is, when $\mu \ll 1$.

6.1.4 Velocity distribution in the z-plane

The velocity distribution along a blade results from the superposition of all the sub velocities, as mentioned previously. With respect to the velocity in the ζ-plane we thus have

$$c_{t\zeta}(\theta) = c^{D}_{t\zeta}(\theta) + c^{Q}_{t\zeta}(\theta) + c^{\Gamma}_{t\zeta}(\theta) + c^{K}_{t\zeta} \tag{6.82}$$

Then substituting equations (5.46), (6.56), (6.57), and (6.78) in equation (6.82), and employing equations (6.30), (6.31), and (6.32) for the blade circulation ($n\Gamma_B$) we obtain

$$c_{t\zeta}(\theta) = \Omega r_1^2 \frac{1-\mu}{n\sqrt{\mu}} \left[\frac{2}{1+\sqrt{\mu}} \right]^{\frac{4}{n}} \left\{ \sin\theta \sum_{k=1}^{\infty} a_k \sin k\theta + \sin^2\left[\frac{\theta}{2}\right] F\left[\frac{2}{n}, \frac{2}{n}; 1; \left[\frac{1-\sqrt{\mu}}{1+\sqrt{\mu}}\right]^2 \right] \right\}$$

$$- \frac{\sin\theta}{\frac{1+\mu}{1-\mu} + \cos\theta} \frac{Q}{2\pi n} - \sqrt{\mu} \frac{1 - \cos\theta}{\frac{1+\mu}{1-\mu} + \cos\theta} \frac{\Gamma_1}{2\pi n} \tag{6.83}$$

The velocity in the z-plane next following from the transformation (5.19); for that we first obtain from equation (5.35), putting $\beta = 0$, $\delta = \pi$, and substituting equation (4.15)

$$\left| \frac{d\zeta}{dz} \right|_B = \frac{n}{r} \left[\frac{1+\mu}{1-\mu} + \cos\theta \right] \frac{1}{|\sin\theta|} \tag{6.84}$$

Then substituting equations (6.83) and (6.84) in equation (5.19) we finally

get

$$c_r = \frac{Q}{2\pi r} + \sqrt{\mu}\,\frac{1-\cos\theta}{\sin\theta}\,\frac{\Gamma_1}{2\pi r} - \Omega r_1^2\,\frac{1-\mu}{r\sqrt{\mu}}\left[\frac{2}{1+\sqrt{\mu}}\right]^{\frac{4}{n}}\left[\frac{1+\mu}{1-\mu}+\cos\theta\right]\times$$

$$\left\{\sum_{k=1}^{\infty} a_k \sin k\theta + \frac{1-\cos\theta}{2\sin\theta}\,F\left[\frac{2}{n},\frac{2}{n};1;\left[\frac{1-\sqrt{\mu}}{1+\sqrt{\mu}}\right]^2\right]\right\} \tag{6.85}$$

in which we have also used the auxiliary relations

$$c_{tz}^{+} = -c_r \tag{6.86}$$

$$c_{tz}^{-} = +c_r \tag{6.87}$$

where the superscripts + and - again denote the pressure and suction side, and c_r being the radial fluid velocity; in the case of straight radial blades this absolute velocity (c_r) also being the relative fluid velocity (w), direct tangentially to the blades.

To compute the velocity distribution according to equation (6.85) we need to have an indication of the (truncation) error of the partial sum of the Fourier series, so that the requisite number of Fourier coefficients can be determined to obtain a satisfactory significance; this is done by comparing the truncation error with a geometric series, as follows.

First we isolate the Fourier series and write

$$S(\theta) = \sum_{k=1}^{\infty} a_k \sin k\theta = S_p(\theta) + T_p(\theta) \tag{6.88}$$

where $S_p(\theta)$ is the partial sum and $T_p(\theta)$ the truncation error, both after summing the first p terms of the series, i.e.

$$S_p(\theta) = \sum_{k=1}^{p} a_k \sin k\theta \tag{6.89}$$

$$T_p(\theta) = \sum_{k=p+1}^{\infty} a_k \sin k\theta \tag{6.90}$$

Then to estimate the truncation error we notice from the latter that

$$-\sum_{k=p+1}^{\infty}|a_k| \le T_p(\theta) \le \sum_{k=p+1}^{\infty}|a_k| \tag{6.91}$$

Next referring to equations (6.76), (6.77), and (6.81) it follows that

$$L = \lim_{k\to\infty}\left|\frac{a_{k+1}}{a_k}\right| = \frac{1-\sqrt{\mu}}{1+\sqrt{\mu}} > \left|\frac{a_{k+1}}{a_k}\right| \quad \forall\ k < \infty \tag{6.92}$$

and

$$|a_{k+1}| < |a_k| \tag{6.93}$$

so

$$\sum_{k=p+1}^{\infty}|a_k| < |a_{p+1}|\sum_{k=p+1}^{\infty}\left|\frac{a_{k+1}}{a_k}\right| < |a_p|\sum_{m=0}^{\infty}L^m = \frac{|a_p|}{1-L} \tag{6.94}$$

Thus we obtain for the sum of the Fourier series

$$S(\theta) = S_p(\theta) \pm \frac{a_p}{1-L} \tag{6.95}$$

with L as given in equation (6.92).

Employing the above–given expression we have computed the Fourier series in equation (6.85); the error term being judged by the overall result (c_r). The solution according to equation (6.85) is illustrated in figure 6.1, where we have plotted solutions for zero through flow and minimum through flow, with both zero prerotation and shockless entry. The minimum through flow, so that no back flow occurs along the blades, thereby being based on a shockless entry.

From the plots in figure 6.1 we notice that both the displacement flow and the vortex flow seem to be symmetrical. Indeed these flows are symmetrical as can easily proven by equations (6.57) and (6.78). From these equations it follows that

$$c^D_{t\zeta}(\theta) = c^D_{t\zeta}(-\theta) \tag{6.96}$$

$$c^\Gamma_{t\zeta}(\theta) = c^\Gamma_{t\zeta}(-\theta) \tag{6.97}$$

Furthermore we have by equation (4.20)

$$r_B(\theta) = r_B(-\theta) \tag{6.98}$$

so the displacement flow and vortex flow are symmetrical.

Q.E.D.

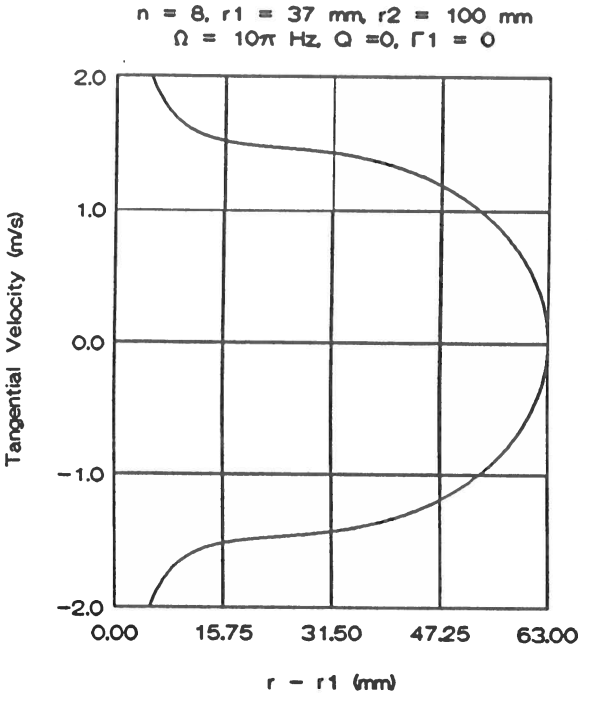

(*i*)

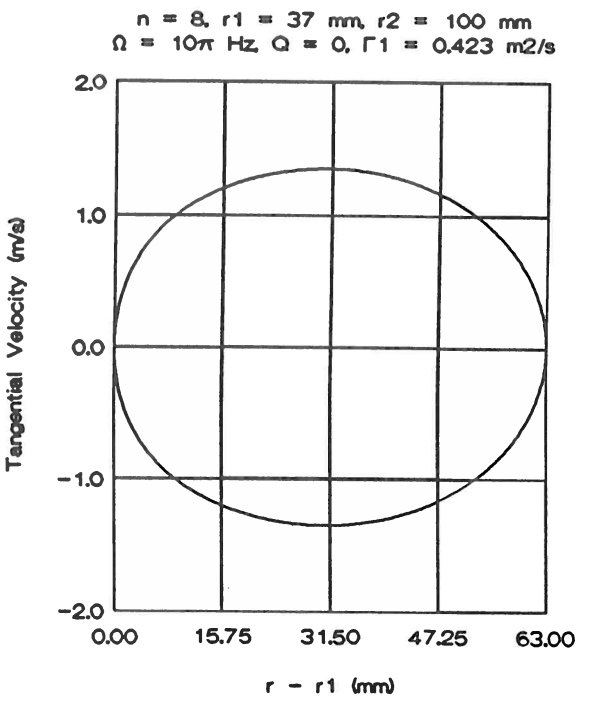

(*ii*)

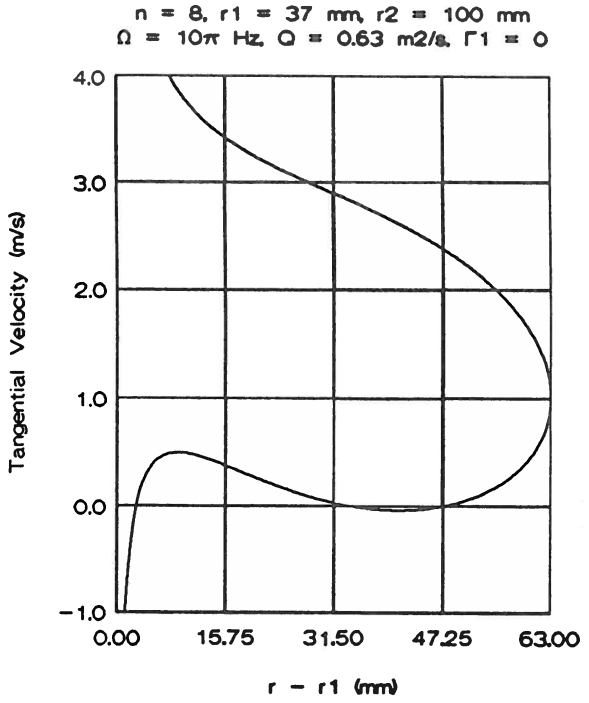

(*iii*)

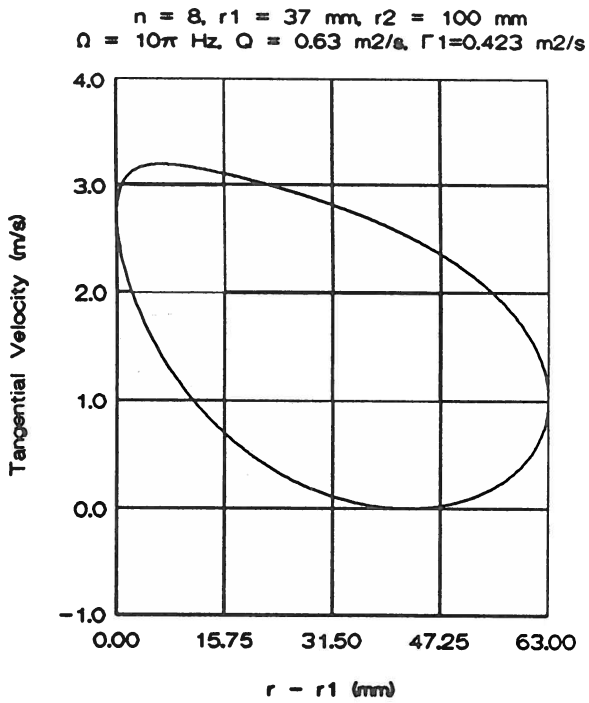

(*iv*)

figure 6.1 *velocity distributions along straight radial blades*

(*i*) *zero through flow and zero prerotation*

(*ii*) *zero through flow and shockless entry*

(*iii*) *minimum through flow and zero prerotation*

(*iv*) *minimum through flow and shockless entry*

6.1.5 Pressure distribution along a blade

Based on the velocity distribution (6.85) we may now also compute the pressure distribution along a blade, by using Bernoulli's theorem for steady two–dimensional fluid motions with respect to rotating axes, i.e.

$$\frac{p}{\rho} + \tfrac{1}{2}w^2 - \tfrac{1}{2}\Omega^2 r^2 = H \tag{6.99}$$

where

p = thermodynamic pressure
ρ = fluid density
w = relative fluid velocity

and H a (more or less) arbitrary constant, often referred to as Bernoulli's constant; the relative fluid velocity w being given by

$$w = |\boldsymbol{w}| = |\boldsymbol{c} - \boldsymbol{\Omega}\times\boldsymbol{r}| \tag{6.100}$$

where

$$r = |\boldsymbol{r}| \tag{6.101}$$

with $\boldsymbol{r}$ the radius vector and $\boldsymbol{w}$ the relative fluid velocity vector.

For points on straight radial blades ($r = r_B$) we further readily have that

$$w = c_r \tag{6.102}$$

Then choosing the constant H equal to zero, we obtain from equation (6.99)

$$p = \tfrac{1}{2}\rho\Omega^2 r_B^2 - \tfrac{1}{2}\rho c_r^2 \tag{6.103}$$

The pressure distribution according to equation (6.103) is graphically illustrated in figure 6.2; these plots are derived from figure 6.1 (iii) and figure 6.1 (iv), where we have taken $\rho = 1000\ kg/m^3$ for convenience.

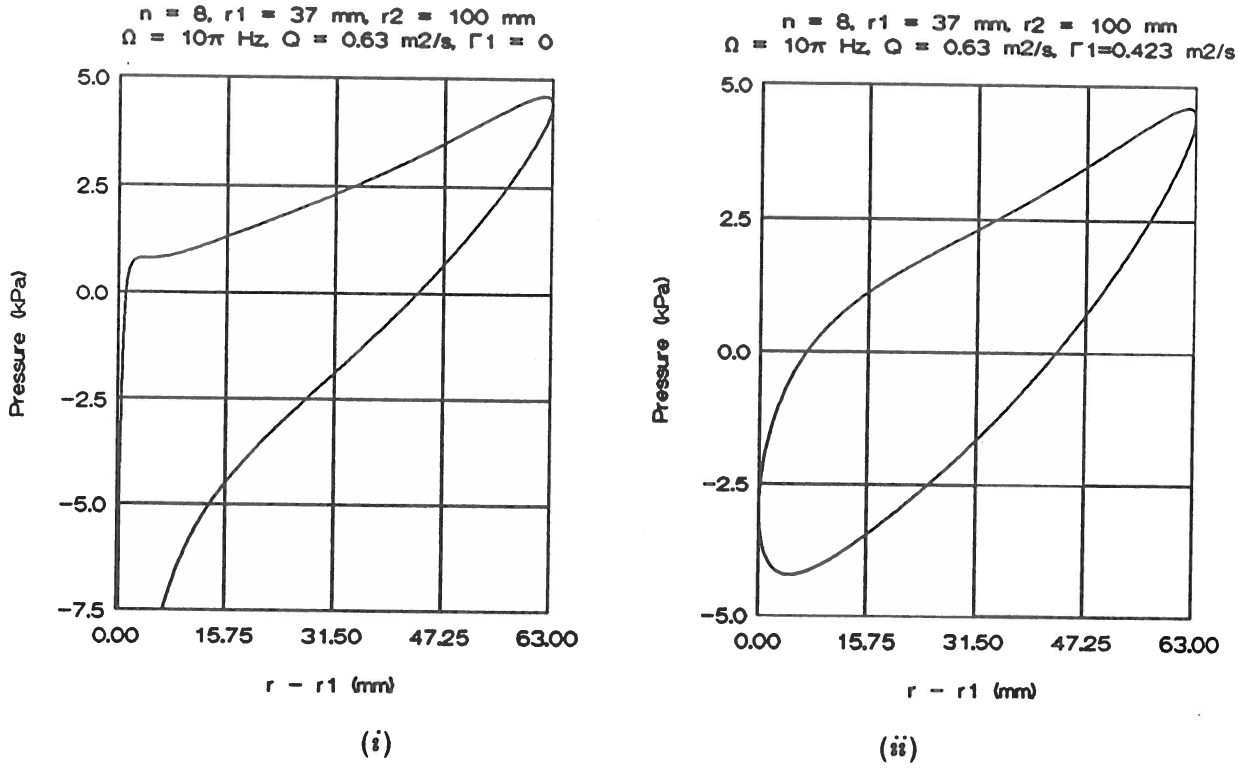

figure 6.2 *pressure distributions along straight radial blades with (i) zero prerotation and (ii) shockless entry*

From the pressure distribution along the blades we may finally obtain the torque ($\boldsymbol{\tau}_0$), about the origin, exerted on the impeller. Since we confine ourselves to strict two–dimensional motions, so the torque has a fixed direction, viz. perpendicular to flow field, we merely have to compute the strength ($\tau_0 = |\boldsymbol{\tau}_0|$) of the torque. This strength is simply obtained by the pressure difference over the blades, i.e.

$$\tau_0 = n \int_{r_1}^{r_2} \left[p^+ - p^- \right] r \, dr \tag{6.104}$$

which will evidently give the same result as to be obtained from the moment of momentum since we consider an isolated impeller.

6.2 Turbine Impeller

As already mentioned in the beginning of this chapter we will, with regard to the turbine, merely discuss the blade circulation and the condition of

shockless entry. The velocity distribution along the blades of the turbine impeller will not be treated. This, however, may be derived analogously to what has been described in the previous paragraph. Incidentally, in case of a shockless operation both pump and turbine will show an identical behaviour, so the results that have been obtained for the pump impeller may then directly be applied to the turbine impeller.

6.2.1 Blade circulation

By the subdivision of equation (6.1) we obtain from equation (5.51), putting $\theta_1 = \pi$

$$\Gamma_B^D = -2\pi c_{t\zeta}^D(\pi) \tag{6.105}$$

$$\Gamma_B^Q = -2\pi c_{t\zeta}^Q(\pi) \tag{6.106}$$

$$\Gamma_B^\Gamma = -2\pi c_{t\zeta}^\Gamma(\pi) \tag{6.107}$$

with

$$c_{t\zeta}^D(\pi) = \frac{KI_1}{2\pi n} \tag{6.37}$$

$$c_{t\zeta}^Q(\pi) = 0 \tag{6.39}$$

$$c_{t\zeta}^\Gamma(\pi) = -\frac{1-\sqrt{\mu}}{\sqrt{\mu}} \frac{\Gamma_1}{2\pi n} \tag{6.40}$$

Substituting the above, equation (5.51) gives

$$n\Gamma_B = -\frac{1-\sqrt{\mu}}{\sqrt{\mu}} \Gamma_1 - KI_1 \tag{6.108}$$

Since in case of a turbine Γ_2 is prescribed rather than Γ_1 (as by a pump), we substitute equation (5.53) in equation (6.108) and obtain

$$n\Gamma_B = (1 - \sqrt{\mu})\,\Gamma_2 - \sqrt{\mu}\,K\,I_1 \tag{6.109}$$

Then writing equation (6.109) alternatively as

$$n\Gamma_B = (1 - \sqrt{\mu})\,\Gamma_2 - \sqrt{\mu}\,K\,(I_1 - I_0) + \sqrt{\mu}\,K\,I_0 \qquad (6.110)$$

and substituting equations (6.14), (6.27), and (6.53) we obtain for the blade circulation of a turbine impeller fitted with straight radial blades

$$n\Gamma_B = \sigma_{t,\Gamma}\,\Gamma_2 - \sigma_{t,D}\,2\pi\Omega r_1^2 \qquad (6.111)$$

where the introduced slip factors are

$$\sigma_{t,\Gamma} = 1 - \sqrt{\mu} \qquad (6.112)$$

and

$$\sigma_{t,D} = (1-\mu)\left(\frac{2}{1+\sqrt{\mu}}\right)^{\frac{4}{n}} F\left(\frac{2}{n},\frac{2}{n};1;\left[\frac{1-\sqrt{\mu}}{1+\sqrt{\mu}}\right]^2\right) + \frac{1}{2}\,\mu^{\frac{1}{2}-\frac{2}{n}}\,(1-\mu)\,F\left[\frac{1}{2},1-\frac{2}{n};2;1-\mu\right] \qquad (6.113)$$

The above-given slip factor (6.113), related to the displacement flow through the turbine impeller, will be further discussed in chapter 9. The slip factor (6.112) related to the prerotation of the turbine impeller is identical to the corresponding slip factor (6.32) for the pump impeller.

6.2.2 Condition of shockless entry

Putting $\theta_1 = \pi$, we obtain from equation (5.59) as the condition of shockless entry for a turbine impeller fitted with straight radial blades

$$c^D_{t\zeta}(0) - c^D_{t\zeta}(\pi) + c^Q_{t\zeta}(0) - c^Q_{t\zeta}(\pi) + c^\Gamma_{t\zeta}(0) - c^\Gamma_{t\zeta}(\pi) = 0 \qquad (6.114)$$

with

$$c^D_{t\zeta}(0) = -\frac{KI_0}{2\pi n} \qquad (6.13)$$

$$c^D_{t\zeta}(\pi) = \frac{KI_1}{2\pi n} \qquad (6.37)$$

$$c^Q_{t\zeta}(0) = 0 \qquad (6.5)$$

$$c^Q_{t\zeta}(\pi) = 0 \qquad (6.39)$$

$$c_{t\zeta}^{\Gamma}(0) = (1 - \sqrt{\mu}) \frac{\Gamma_1}{2\pi n} \tag{6.6}$$

$$c_{t\zeta}^{\Gamma}(\pi) = -\frac{1-\sqrt{\mu}}{\sqrt{\mu}} \frac{\Gamma_1}{2\pi n} \tag{6.40}$$

we thus obtain

$$-K(I_0 + I_1) + \frac{1-\mu}{\sqrt{\mu}} \Gamma_{1,SL} = 0 \tag{6.115}$$

Next substituting equation (5.53) in equation (6.115), and taking the blade circulation according to equation (6.109), gives

$$\Gamma_{2,SL} = \frac{K}{1-\mu} (I_0 + \mu I_1) \tag{6.116}$$

Then writing equation (6.116) alternatively as

$$\Gamma_{2,SL} = KI_0 + \frac{\mu}{1-\mu} K(I_0 + I_1) \tag{6.117}$$

and substituting equations (6.14), (6.27), and (6.53) we obtain for the shockless prerotation of a turbine impeller fitted with straight radial blades

$$\Gamma_{2,SL} = \tau_{t,D}\, 2\pi\Omega r_2^2 \tag{6.118}$$

where the prerotation factor is given by

$$\tau_{t,D} = \mu^{\frac{2}{n}+\frac{1}{2}} \left(\frac{2}{1+\sqrt{\mu}}\right)^{\frac{4}{n}} F\left[\frac{2}{n}, \frac{2}{n}; 1; \left(\frac{1-\sqrt{\mu}}{1+\sqrt{\mu}}\right)^2\right] + \frac{1}{2}(1-\mu) F\left[\frac{1}{2}, 1-\frac{2}{n}; 2; 1-\mu\right] \tag{6.119}$$

Further expatiation on this prerotation factor for the turbine impeller fitted with straight radial blades will be given in chapter 9.

7

SOLUTIONS FOR LOGARITHMIC SPIRAL BLADES

Having completely determined the flow field for the impeller fitted with straight radial blades (previous chapter), we now focus our attention on the analytical solution of the flow field for the impeller fitted with logarithmic spiral blades. Similar to the previous chapter we will discuss the case of a pump rather extensively (paragraph 7.1), while the turbine will merely be considered with respect to the blade circulation and the shockless entry (paragraph 7.2). Furthermore – with respect to the displacement flow – we will restrict ourselves to a brief discussion since arithmetical expressions have not been obtained yet; only an asymptotic solution for the blade circulation due to the displacement flow in case of the pump impeller could be derived and will thus be outlined.

7.1 Pump Impeller

Discussing the pump impeller fitted with logarithmic spiral blades we will generally follow the same procedure as given in paragraph 6.1 for the radially bladed impeller. In the first sections we will successively discuss the blade circulation, the shockless entry, the velocity distributions in the ζ–plane and the z–plane, and the pressure distribution along a blade. In the remaining section of this paragraph we will additionally discuss the asymptotic solution for the blade circulation that we have obtained.

7.1.1 Blade circulation

To obtain the blade circulation for the pump impeller fitted with logarithmic spiral blades we employ the subdivision as given by equation (6.1). The individual contributions to the blade circulation again being given by equations (6.2), (6.3), and (6.4).

From equations (5.34) and (5.43) we readily obtain for the velocity

contributions due to the source flow and the vortex flow (putting $\theta = 0$)

$$c^{Q}_{t\zeta}(0) = -\frac{Q}{\pi n}\,\frac{a\,sin\,\delta}{1 + a^2 - 2a\cos\,\delta} \tag{7.1}$$

$$c^{\Gamma}_{t\zeta}(0) = \frac{\Gamma_1}{\pi n}\,\frac{1 - a\cos\,\delta}{1 + a^2 - 2a\cos\,\delta} \tag{7.2}$$

where a and δ are as given by equations (4.23) and (4.42).

Then substituting equation (7.1) and (7.2) in equations (6.3) and (6.4) we obtain for the individual contributions to the blade circulation due to the source and the vortex

$$n\Gamma^{Q}_{B} = Q\,\frac{2a\,sin\,\delta}{1 + a^2 - 2a\cos\,\delta} \tag{7.3}$$

$$n\Gamma^{\Gamma}_{B} = -\Gamma_1\,\frac{2(1 - a\cos\,\delta)}{1 + a^2 - 2a\cos\,\delta} \tag{7.4}$$

The remaining contribution due to the displacement flow follows next from equation (5.14). Putting $\theta = 0$ and substituting equations (6.12) and (5.26) we get

$$2\pi n c^{D}_{t\zeta}(0) = J_0 \tag{7.5}$$

where we have put for simplicity

$$J_0 = n\Omega \int_{-\pi}^{\pi} r_B(\lambda)\,\frac{dr_B}{d\lambda}\,\frac{sin\,\lambda}{1 - cos\,\lambda}\,d\lambda \tag{7.6}$$

Then by equations (6.2), (7.5), and (7.6) it follows that

$$n\Gamma^{D}_{B} = -J_0 = n\Omega \int_{-\pi}^{\pi} r_B(\lambda)\,\frac{dr_B}{d\lambda}\,\frac{sin\,\lambda}{cos\,\lambda - 1}\,d\lambda \tag{7.7}$$

with the function $r_B(\lambda)$ being further determined by the mapping $Z : z \longleftrightarrow \zeta$.

Since we have not yet obtained arithmetical expressions with respect to the displacement flow, as has been done for the impeller fitted with straight radial blades, we will settle on the solution as given by equation (7.7); this equation will serve as a bases for the asymptotic solution to be discussed in the last section of this paragraph.

Finally substituting equations (7.3), (7.4), and (7.7) in equation (6.1) we obtain for the blade circulation of a pump impeller fitted with logarithmic spiral blades

$$n\Gamma_B = \sigma_{p,D}\, 2\pi\Omega r_2^2 + \sigma_{p,Q}\, Q\tan\beta - \sigma_{p,\Gamma}\, \Gamma_1 \tag{7.8}$$

where the slip factors are

$$\sigma_{p,D} = \frac{n}{2\pi r_2^2} \int_{-\pi}^{\pi} r_B(\lambda) \frac{dr_B}{d\lambda} \frac{\sin\lambda}{\cos\lambda - 1} d\lambda \tag{7.9}$$

$$\sigma_{p,Q} = \frac{2a \sin\delta \cot an\, \beta}{1 - 2a\cos\delta + a^2} \tag{7.10}$$

$$\sigma_{p,\Gamma} = \frac{2(1 - a\cos\delta)}{1 - 2a\cos\delta + a^2} \tag{7.11}$$

For most (practical) situations one will find that the slip factors (7.10) and (7.11) are practically equal to 1. In case of an infinite number of blades these slip factors become (logically) equal to 1, for we then have that $a \rightarrow 1$ and $\delta \rightarrow \pi - 2\beta$. The above-given slip factors and some related aspects will be further discussed in chapter 9.

7.1.2 Condition of shockless entry

By equation (5.55) we have as the condition of shockless entry

$$c^D_{t\zeta}(\theta_1) - c^D_{t\zeta}(0) + c^Q_{t\zeta}(\theta_1) - c^Q_{t\zeta}(0) + c^\Gamma_{t\zeta}(\theta_1) - c^\Gamma_{t\zeta}(0) = 0 \tag{5.55}$$

with the contributions $c^D_{t\zeta}(\theta_1)$, $c^Q_{t\zeta}(\theta_1)$, and $c^\Gamma_{t\zeta}(\theta_1)$ next to be obtained.

Substituting equation (4.55) we obtain from equations (5.34) and (5.43)

$$c_{t\zeta}^{Q}(\theta_1) = \frac{Q}{\pi n} \frac{a \sin \varepsilon}{1 + a^2 - 2a\cos \varepsilon} \tag{7.12}$$

$$c_{t\zeta}^{\Gamma}(\theta_1) = \frac{\Gamma_1}{\pi n} \frac{1 - a\cos \varepsilon}{1 + a^2 - 2a\cos \varepsilon} \tag{7.13}$$

From equation (5.14) we obtain, after substitution of equations (5.26) and (6.59)

$$c_{t\zeta}^{D}(\theta_1) = -\frac{\Omega}{2\pi} \int_{-\pi}^{\pi} r_B(\lambda) \frac{dr_B}{d\lambda} \frac{\sin \lambda + \sin \theta_1}{\cos \lambda - \cos \theta_1} d\lambda \tag{7.14}$$

which we write alternatively as

$$2\pi n c_{t\zeta}^{D}(\theta_1) = J_1 \tag{7.15}$$

where

$$J_1 = n\Omega \int_{-\pi}^{\pi} r_B(\lambda) \frac{dr_B}{d\lambda} \frac{\sin \theta_1 + \sin \lambda}{\cos \theta_1 - \cos \lambda} d\lambda \tag{7.16}$$

Then substituting equations (6.2), (7.1), (7.2), (7.12), (7.13), and (7.15) in equation (5.55) we obtain (condition of shockless entry)

$$\frac{1}{2}(J_1 - J_0) + Q \left[\frac{a \sin \varepsilon}{1 + a^2 - 2a\cos \varepsilon} + \frac{a \sin \delta}{1 + a^2 - 2a\cos \delta} \right]$$

$$+ \Gamma_{1,SL} \left[\frac{1 - a\cos \varepsilon}{1 + a^2 - 2a\cos \varepsilon} - \frac{1 - a\cos \delta}{1 + a^2 - 2a\cos \delta} \right] = 0 \tag{7.17}$$

or employing some elementary trigonometrical manipulations, and using equations (4.23) and (4.45), we can write equation (7.17) as

$$\tfrac{1}{2}(J_1 - J_0) + \frac{\left[\frac{1}{a} - a\right]\left[\cos\varepsilon - \cos\delta\right]}{\left[\frac{1}{a} + a - 2\cos\varepsilon\right]\left[\frac{1}{a} + a - 2\cos\delta\right]}(\Gamma_{1,SL} - Q\tan\beta) = 0 \tag{7.18}$$

Next we put

$$\Gamma_1 = \Gamma_1^D + \Gamma_1^Q \tag{7.19}$$

Then from equations (7.18) and (7.19) we obtain

$$\Gamma_{1,SL}^D = \frac{\left[\frac{1}{a} + a - 2\cos\varepsilon\right]\left[\frac{1}{a} + a - 2\cos\delta\right]}{2\left[\frac{1}{a} - a\right]\left[\cos\delta - \cos\varepsilon\right]}(J_1 - J_0) \tag{7.20}$$

$$\Gamma_{1,SL}^Q = Q\tan\beta \tag{7.21}$$

Equation (7.21) exactly gives (as was to be expected) the circulation that accompanies a vortex source flow, by which the blades of the pump impeller will be (directed along) streamlines.

Since for most practical situations the mapping constants (a and δ) may be derived from their first order approximations (section 4.3.2), we may simplify equation (7.20) accordingly. Substituting equations (4.45) and (4.48) in equation (7.20) we obtain by equation (4.46) as a first order approximation (in ε) for the shockless prerotation due to the displacement flow

$$\Gamma_{1,SL}^D \approx \frac{\varepsilon\,(J_1 - J_0)}{\sin 2\beta} \tag{7.22}$$

Without further stipulation we give that

$$|J_0| \ll |J_1| \tag{7.23}$$

by which equation (7.22) may be reduced to

$$\Gamma_{1,SL}^D \approx \frac{\varepsilon\, J_1}{\sin 2\beta} \tag{7.24}$$

In conclusion of this section we summarize the above, and write the shockless prerotation for an impeller fitted with logarithmic spiral blades as

$$\Gamma_{1,SL} = \tau_{p,D}\, 2\pi\Omega r_1^2 + Q tan\, \beta \tag{7.25}$$

where the prerotation factor is

$$\tau_{p,D} = \frac{\left[\frac{1}{a} + a - 2cos\,\varepsilon\right]\left[\frac{1}{a} + a - 2cos\,\delta\right]}{2\left[\frac{1}{a} - a\right]\left[cos\,\delta - cos\,\varepsilon\right]} \frac{(J_1 - J_0)}{2\pi\Omega r_1^2} \tag{7.26}$$

exactly, or using equations (7.16), (7.22) and (7.23)

$$\tau_{p,D} \approx \frac{\varepsilon\, n}{2\pi r_1^2 sin\, 2\beta} \int_{-\pi}^{\pi} r_B(\lambda) \frac{dr_B}{d\lambda} \frac{sin\,\theta_1 + sin\,\lambda}{cos\,\theta_1 - cos\,\lambda} d\lambda \tag{7.27}$$

approximately.

7.1.3 Velocity distributions in the ζ-plane

In this section we briefly recollect the velocity distributions in the ζ-plane as they have been discussed previously.

Displacement flow

Substitution of equations (5.26) and (6.59) in equation (5.14) gives for the velocity due to the displacement flow

$$c^D_{t\zeta}(\theta) = \frac{\Omega}{2\pi} \int_{-\pi}^{\pi} r_B(\lambda) \frac{dr_B}{d\lambda} \frac{sin\,\theta + sin\,\lambda}{cos\,\theta - cos\,\lambda} d\lambda \tag{7.28}$$

The source flow, vortex flow, and Kutta condition are next readily obtained from the preceding.

Source flow

$$c_{t\zeta}^{Q}(\theta) = \frac{Q}{\pi n} \frac{a\,sin(\theta-\delta)}{1 + a^2 - 2a\,cos(\theta-\delta)} \tag{5.32}$$

Vortex flow

$$c_{t\zeta}^{\Gamma}(\theta) = \frac{\Gamma_1}{\pi n} \frac{1 - a\,cos(\theta-\delta)}{1 + a^2 - 2a\,cos(\theta-\delta)} \tag{5.43}$$

Kutta condition

$$c_{t\zeta}^{K} = \frac{\Gamma_B}{2\pi} \tag{5.47}$$

with Γ_B according to equation (7.8).

7.1.4 Velocity distribution in the z-plane

Referring to figure 7.1 we have that the absolute velocity (c_s, c_n) along the blades in the z-plane is given by

$$c_s = \begin{cases} -c_{tz}^{+} \\ +c_{tz}^{-} \end{cases} \tag{7.29}$$

$$c_n = \Omega r_B cos\,\beta \tag{7.30}$$

with the latter being a boundary condition (paragraph 5.1), and where the subscripts s and n denote that the velocity components are tangential or normal to the blades; the superscripts + and - again denote the pressure side and the suction side of the blades.

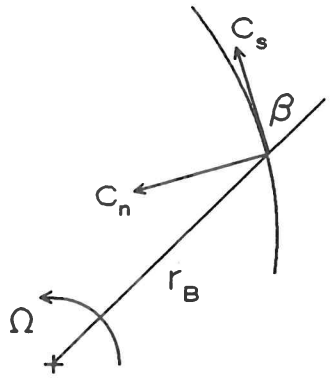

figure 7.1 *absolute velocities along a logarithmic spiral blade*

From the foregoing we have that the absolute velocity along a blade is given by

$$c_{tz} = c_{t\zeta} \left| \frac{d\zeta}{dz} \right|_B \tag{5.17}$$

$$\left| \frac{d\zeta}{dz} \right|_B = \frac{n}{2r_B} \left| \frac{1 + a^2 - 2a\cos(\delta-\theta)}{a\sin(\delta+\beta-\theta) - \sin\beta} \right| \tag{5.35}$$

$$c_{t\zeta}(\theta) = c^D_{t\zeta}(\theta) + c^Q_{t\zeta}(\theta) + c^\Gamma_{t\zeta}(\theta) + c^K_{t\zeta} \tag{6.82}$$

with the (sub) velocities in equation (6.82) as given in the previous section.

From the absolute velocity we next obtain the relative velocity by

$$\boldsymbol{w} = \boldsymbol{c} - \boldsymbol{\Omega}\times\boldsymbol{r} \tag{6.92}$$

which gives for the velocity components along a logarithmic spiral blade

$$w_s = c_s - \Omega r\sin\beta \tag{7.31}$$

$$w_n = 0 \tag{7.32}$$

with the latter being a trivial result.

Since no simple arithmetical function ($r_B(\lambda)$) for the mapping of logarithmic spiral blades, as generally given by equations (4.43) and (4.44), could be derived like it has been done for the impeller fitted with straight radial blades, we have computed the velocity distribution, the Kutta condition, and the condition of shockless entry – all with respect to the displacement flow – by a direct numerical evaluation of the integrals (trapezium rule), taking an illustrative impeller as a test case (see paragraph 8.2 for a detailed specification).

The computed velocity distribution (w_s) relative to the blades is illustrated graphically in figure 7.2. In this figure we have plotted the relative velocities for zero through flow and minimum through flow with both zero prerotation and shockless entry, as was also done for the impeller fitted with straight radial blades (figure 6.1). The velocities in figure 7.2 are plotted as a function of the blade coordinate (s), which is defined by

$$s = \frac{r_B - r_1}{cos\ \beta} \tag{7.33}$$

This coordinate simply represents the traversed length along a blade starting from the inner tip.

Comparing the velocity distributions for logarithmic spiral blades (figure 7.2) with the velocity distributions for straight radial blades (figure 6.1) – both impellers having the same inner/outer–tip ratio – we notice that due to the curvature of the blades the minimum source strength (so that no back flow occurs) has decreased significantly. Defining a source ratio (q_β) by

$$q_\beta = \frac{Q^\beta_{min,LSB}}{Q_{min,SRB}} \tag{7.34}$$

where

$Q^\beta_{min,LSB}$ = minimum source strength for logarithmic spiral blades

$Q_{min,SRB}$ = minimum source strength for straight radial blades

we obtain from our computed examples (figure 6.1 and figure 7.2)

$$q_{60} = \frac{0.215}{0.630} = 0.34$$

This result is in fairly good accordance with the asymptotic approach[8] of the flow through the impeller(s). By this asymptotic approach (see appendix B) it follows that the minimum source flow, so that no back flow will occur along the blades, is inversely proportional to the square of the cosine of the blade angle; thus we have as the limiting value for the source ratio

$$q_{60,\mathrm{lim}} = \cos^{-2}60 = 0.25$$

8 The asymptotic approach referred to is based on a large number of extremely long logarithmic spiral blades (see appendix B).

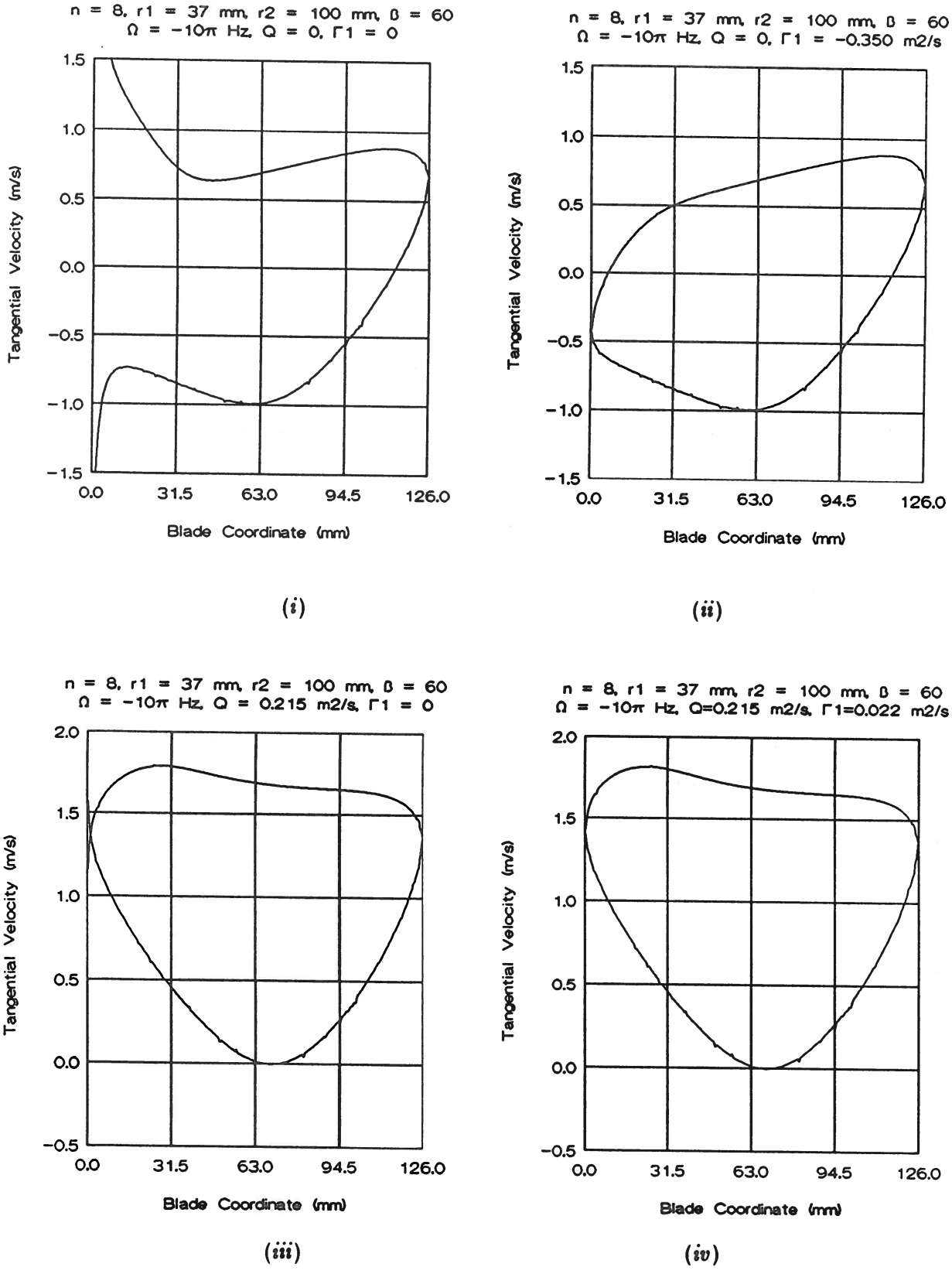

figure 7.2 velocity distributions along logarithmic spiral blades

- *(i) zero through flow and zero prerotation*
- *(ii) zero through flow and shockless entry*
- *(iii) minimum through flow and zero prerotation*
- *(iv) minimum through flow and shockless entry*

7.1.5 Pressure distribution along a blade

Referring to section 6.1.5 it follows that the pressure distribution along a logarithmic spiral blade can be obtained from the velocities given in the previous section by

$$p = \tfrac{1}{2}\rho\Omega^2 r_B^2 - \tfrac{1}{2}\rho w_s^2 \qquad (7.35)$$

Based on equation (7.35) we have plotted in figure 7.3 the pressure distribution along a logarithmic spiral blade as a function of the blade coordinate (s). These figures are obtained from figure 7.2, where we again have taken $\rho = 1000\ kg/m^3$ for convenience.

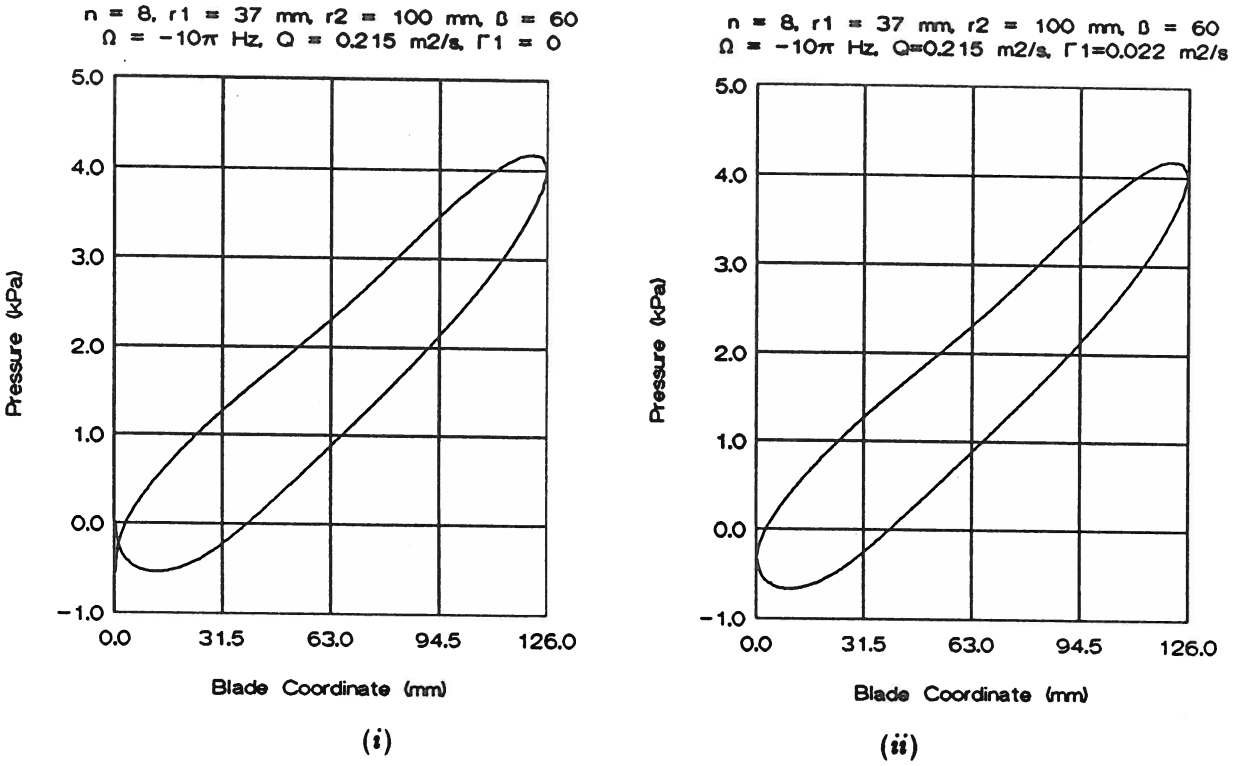

figure 7.3 pressure distributions along logarithmic spiral blades with (i) zero prerotation and (ii) shockless entry

Comparing the above-given pressure plots for the logarithmic spiral blades with the corresponding pressure plots for the straight radial blades (figure 6.2) we notice that, due to the curvature, the pressure distribution has flattened out. This means that an impeller fitted with curved blades will

have a favourable blade loading, which will improve when the curvature increases.

7.1.6 Asymptotic solution for the blade circulation

In the last section of this paragraph we will discuss the asymptotic solution of the blade circulation due to the displacement flow, for the impeller fitted with logarithmic spiral blades. To that end we will consider the special case of $\mu = (r_1/r_2)^n \rightarrow 0$, which will obvious be the case if $r_1 \rightarrow 0$ and/or $n \rightarrow \infty$. This presumption ($\mu \rightarrow 0$) implies that the origin and the inner tip will (approximately) be mapped in the same point on the unit circle, i.e.

$$\zeta_0 \rightarrow \zeta_1 \tag{7.36}$$

So

$$a \rightarrow 1 \tag{7.37}$$

$$\delta \rightarrow \pi - 2\beta \tag{7.38}$$

which readily follows from equations (4.23) and (4.42) when $\mu \rightarrow 0$.

Considering the above, our asymptotic solution will be based on the assumptions

$$a = 1 \tag{7.39}$$

$$\delta = \pi - 2\beta \tag{7.40}$$

These assumptions result in the map that is given in figure 7.4. From this figure we obtain by some elementary trigonometric manipulations

$$|1 - \zeta_0| = |\zeta_2 - \zeta_0| = 2\cos\beta \tag{7.41}$$

$$|\zeta_B - \zeta_0| = |\zeta_B - \zeta_1| = 2\cos(\beta + \tfrac{1}{2}\lambda) \tag{7.42}$$

$$arg(1 - \zeta_0) = -\beta \tag{7.43}$$

$$arg(\zeta_B - \zeta_0) = -\beta + \tfrac{1}{2}\lambda \tag{7.44}$$

so

$$1-\zeta_0 = \zeta_2-\zeta_0 = 2\cos\beta\ e^{-i\beta} \tag{7.45}$$

$$\zeta_B-\zeta_0 = \zeta_B-\zeta_1 = 2\cos(\beta+\tfrac{1}{2}\lambda)\ e^{-(\beta-\frac{1}{2}\lambda)i} \tag{7.46}$$

where the argument (λ) must be

$$(\delta-2\pi < \lambda < \delta) \tag{7.47}$$

or

$$(-\pi-2\beta < \lambda < \pi-2\beta) \tag{7.48}$$

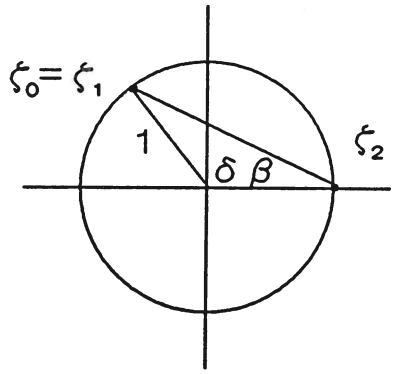

figure 7.4 mapping of an impeller with the inner tip near the origin

Next substituting equations (7.45) and (7.46) in equation (4.44) we obtain from equation (4.43)

$$\left[\frac{r_B}{r_2}\right]^{\frac{n}{\cos\beta}} = \left|\left[\left[\frac{\cos(\beta+\frac{1}{2}\lambda)}{\cos\beta}\right] e^{\frac{1}{2}\lambda i}\right]^{\cos\beta - i\sin\beta}\right|^2 \tag{7.49}$$

or

$$\left[\frac{r_B}{r_2}\right]^{\frac{n}{\cos\beta}} = \left[\frac{\cos(\beta+\frac{1}{2}\lambda)}{\cos\beta}\right]^{2\cos\beta} e^{\lambda\sin\beta} \tag{7.50}$$

So the mapping function for points on a logarithmic spiral blade, with $\mu = 0$, reads

$$r_B(\lambda) = r_2 \left[\frac{\cos(\beta + \frac{1}{2}\lambda)}{\cos \beta} \right]^{\frac{2\cos^2\beta}{n}} e^{\frac{\lambda \sin 2\beta}{2n}} \qquad (7.51)$$

which is valid under the restriction of equation (7.47) or (7.48). To illustrate the usefulness of equation (7.51) we have plotted in figure 7.5 the function $r_B(\lambda)$ according to equation (7.51) vs. the exact value as generally given by equations (4.43) and (4.44). Putting $\lambda = \delta = \pi - 2\beta$ it is easily verified by equation (7.51) that $\mu = (r_1/r_2)^n = 0$, as we have assumed.

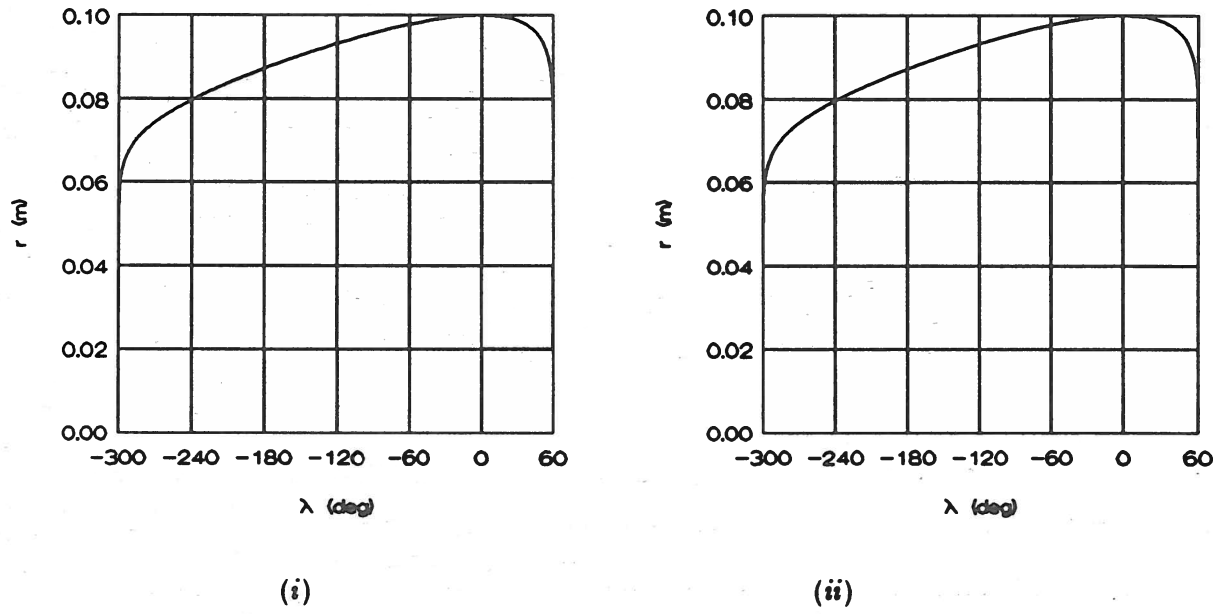

figure 7.5 mapping function $r_B(\lambda)$ for an impeller fitted with logarithmic spiral blades with: $r_1 = 0.37$, $r_2 = 0.1$, $n = 8$, $\beta = \frac{\pi}{3}$; (i) exact, (ii) approximation ($\mu = 0$)

Having a relatively simple relation $r_B(\lambda)$ between corresponding blade points in the z–plane and the ζ–plane we may now determine the blade circulation (approximately). First we derive from equation (7.51)

$$\frac{dr_B}{d\lambda} = -\frac{r_B}{n}\,\frac{\sin\left(\frac{\lambda}{2}\right)\,\cos\beta}{\cos\left(\beta+\frac{1}{2}\lambda\right)} \tag{7.52}$$

Then substituting equations (7.51) and (7.52) in equation (7.7), and altering the interval of integration as given by equation (7.48), we obtain for the blade circulation due to the displacement flow

$$n\Gamma_B^D = \Omega r_2^2 \int_{-\pi-2\beta}^{\pi-2\beta} \left[\frac{\cos(\beta+\frac{1}{2}\lambda)}{\cos\beta}\right]^{\frac{4\cos^2\beta}{n}-1} e^{\frac{\lambda\sin 2\beta}{n}} \cos\left(\frac{\lambda}{2}\right)\,d\lambda \tag{7.53}$$

where we have also used the identity

$$\frac{\sin\lambda}{\cos\lambda - 1}\sin\left(\frac{\lambda}{2}\right) = -\cos\left(\frac{\lambda}{2}\right) \tag{7.54}$$

Next using a transformation

$$\alpha = \beta + \tfrac{1}{2}\lambda \tag{7.55}$$

equation (7.53) becomes

$$n\Gamma_B^D = MJ_0^* \tag{7.56}$$

where we have introduced for simplicity

$$M = 2\Omega r_2^2\,(\cos\beta)^{1-\frac{4\cos^2\beta}{n}}\, e^{-\frac{2\beta\sin 2\beta}{n}} \tag{7.57}$$

$$J_0^* = \int_{-\frac{\pi}{2}}^{\frac{\pi}{2}} (\cos\alpha)^{\frac{4\cos^2\beta}{n}-1}\, e^{\frac{2\alpha\sin 2\beta}{n}} \cos(\alpha-\beta)\,d\alpha \tag{7.58}$$

To evaluate the integral J_0^* we will alter it by some simple trigonometry. From equation (7.58) it follows that

$$J_0^* = \cos\beta \int_{-\frac{\pi}{2}}^{\frac{\pi}{2}} (\cos\alpha)^{\frac{4\cos^2\beta}{n}} e^{\frac{2\alpha\sin 2\beta}{n}} d\alpha$$

$$+ \sin\beta \int_{-\frac{\pi}{2}}^{\frac{\pi}{2}} \sin\alpha\, (\cos\alpha)^{\frac{4\cos^2\beta}{n}-1} e^{\frac{2\alpha\sin 2\beta}{n}} d\alpha \qquad (7.59)$$

Then using the identity

$$\int_{-\frac{\pi}{2}}^{\frac{\pi}{2}} \sin\alpha\, (\cos\alpha)^{\frac{4\cos^2\beta}{n}-1} e^{\frac{2\alpha\sin 2\beta}{n}} d\alpha = \frac{\sin\beta}{\cos\beta} \int_{-\frac{\pi}{2}}^{\frac{\pi}{2}} (\cos\alpha)^{\frac{4\cos^2\beta}{n}} e^{\frac{2\alpha\sin 2\beta}{n}} d\alpha \qquad (7.60)$$

which can easily be verified by partial integration, we may write equation (7.59) as

$$J_0^* = \frac{1}{\cos\beta} \int_{-\frac{\pi}{2}}^{\frac{\pi}{2}} (\cos\alpha)^{\frac{4\cos^2\beta}{n}} e^{\frac{2\alpha\sin 2\beta}{n}} d\alpha \qquad (7.61)$$

Formulated by equation (7.61) the integral J_0^* appears to have an equivalent, stated by the beta function. According to Gradshteyn and Ryzhik (eq. 3.892.2, p. 476) we have

$$\int_{-\frac{\pi}{2}}^{\frac{\pi}{2}} e^{i\eta\alpha} \cos^{\nu-1}\alpha\, d\alpha = \frac{\pi}{2^{\nu-1}\nu} B^{-1}\left[\frac{\nu+\eta+1}{2}, \frac{\nu-\eta+1}{2}\right] \qquad (7.62)$$

where $B^{-1}(..,..)$ denotes the reciprocal of $B(..,..)$, NOT the inversion.

Then putting

$$\nu = 1 + \frac{4cos^2\beta}{n} \tag{7.63}$$

$$\eta = -\frac{2sin\ 2\beta}{n}i \tag{7.64}$$

we obtain from equations (7.61) and (7.62)

$$J_0^* = \frac{\pi}{cos\ \beta}\left[2^{\frac{4cos^2\beta}{n}}\left[1 + \frac{4cos^2\beta}{n}\right]B(\chi,\bar{\chi})\right]^{-1} \tag{7.65}$$

where

$$\chi = 1 + \frac{2cos^2\beta}{n} + \frac{sin\ 2\beta}{n}i \tag{7.66}$$

Substitution of equations (7.57) and (7.65) in equation (7.56) finally gives for the asymptotic solution of the blade circulation due to the displacement flow ($\mu = 0$)

$$n\Gamma_B^D = \sigma_{p,D}\ 2\pi\Omega r_2^2 \tag{7.67}$$

where the slip factor is

$$\sigma_{p,D} = \left[(2cos\ \beta)^{\frac{4cos^2\beta}{n}}\left[1 + \frac{4cos^2\beta}{n}\right]e^{\frac{2\beta sin\ 2\beta}{n}}B(\chi,\bar{\chi})\right]^{-1} \tag{7.68}$$

and the complex number χ according to equation (7.66).

The slip factor $\sigma_{p,D}$ according to equation (7.68) will further be discussed in chapter 9; there we will illustrate (among other things) the influence of both the blade angle and the number of blades.

7.2 Turbine Impeller

With regard to the turbine impeller fitted with logarithmic spiral blades we will briefly consider the blade circulation and the condition of shockless entry. Again, since no arithmetical expressions have been derived yet, we will merely discuss the solutions.

7.2.1 Blade circulation

From equations (5.51) and (6.1) it follows that

$$\Gamma_B^D = -2\pi c_{t\zeta}^D(\theta_1) \tag{7.69}$$

$$\Gamma_B^Q = -2\pi c_{t\zeta}^Q(\theta_1) \tag{7.70}$$

$$\Gamma_B^\Gamma = -2\pi c_{t\zeta}^\Gamma(\theta_1) \tag{7.71}$$

with

$$c_{t\zeta}^Q(\theta_1) = \frac{Q}{\pi n} \frac{a \sin \varepsilon}{1 + a^2 - 2a\cos \varepsilon} \tag{7.12}$$

$$c_{t\zeta}^\Gamma(\theta_1) = \frac{\Gamma_1}{\pi n} \frac{1 - a\cos \varepsilon}{1 + a^2 - 2a\cos \varepsilon} \tag{7.13}$$

$$c_{t\zeta}^D(\theta_1) = \frac{J_1}{2\pi n} \tag{7.15}$$

where equation (7.13) may be stated alternatively as, using equation (4.47)[9]

$$c_{t\zeta}^\Gamma(\theta_1) = -\frac{\Gamma_1}{\pi n} \frac{a \sin \varepsilon \cot \beta}{1 + a^2 - 2a\cos \varepsilon} \tag{7.72}$$

Then substituting the above-given equations in equation (6.1) we obtain

$$-n\Gamma_B = J_1 + \frac{2a \sin \varepsilon \cot \beta}{1 + a^2 - 2a\cos \varepsilon} \left[Q \tan \beta - \Gamma_1\right] \tag{7.73}$$

9 From equation (4.47) it readily follows that 1-acos ε = -asin ε cotan β.

Again, since Γ_2 is predetermined rather than Γ_1, we employ equation (5.53) to eliminate Γ_1 in equation (7.73), and obtain for the blade circulation of the turbine impeller

$$n\Gamma_B = \sigma_{t,\Gamma}\,\Gamma_2 - \sigma_{t,Q}\,Q\tan\beta - \sigma_{t,D}\,2\pi\Omega r_1^2 \tag{7.74}$$

where the slip factors are

$$\sigma_{t,\Gamma} = \frac{2(1 - a\cos\varepsilon)}{1 - a^2} = \frac{2a\sin\varepsilon\ \cot\beta}{a^2 - 1} \tag{7.75}$$

$$\sigma_{t,Q} = \frac{2a\sin\varepsilon\ \cot\beta}{a^2 - 1} \tag{7.76}$$

$$\sigma_{t,D} = \frac{1 - a^2 + 2a\cos\varepsilon}{1 - a^2}\,\frac{J_1}{2\pi\Omega r_1^2} \tag{7.77}$$

Substituting equation (7.16) the latter becomes

$$\sigma_{t,D} = \frac{1 - a^2 + 2a\cos\varepsilon}{1 - a^2}\,\frac{n}{2\pi r_1{}^2}\int_{-\pi}^{\pi} r(\lambda)\,\frac{dr_B}{d\lambda}\,\frac{\sin\theta_1 + \sin\lambda}{\cos\theta_1 - \cos\lambda}\,d\lambda \tag{7.78}$$

The (turbine) slip factors (7.75) and (7.76), related to the source flow and the vortex flow, appear to be identical. Using equation (4.47) it is easily verified that the limiting value ($n \to \infty$) of these slip factors equals the Eulerian value (1), since then $\varepsilon \to 0$. Finally we may remind the reader, to avoid misinterpretation of equation (7.74), that $Q < 0$ in case of a turbine.

7.2.2 Condition of shockless entry

From equation (5.58) we have as the condition of shockless entry

$$c^D_{t\zeta}(0) - c^D_{t\zeta}(\theta_1) + c^Q_{t\zeta}(0) - c^Q_{t\zeta}(\theta_1) + c^\Gamma_{t\zeta}(0) - c^\Gamma_{t\zeta}(\theta_1) = 0 \tag{5.58}$$

where the velocities are

$$c^Q_{t\zeta}(0) = -\frac{Q}{\pi n}\,\frac{a\sin\delta}{1 + a^2 - 2a\cos\delta} \tag{7.1}$$

$$c_{t\zeta}^{\Gamma}(0) = \frac{\Gamma_1}{\pi n} \frac{1 - a\cos\delta}{1 + a^2 - 2a\cos\delta} \tag{7.2}$$

$$c_{t\zeta}^{D}(0) = \frac{J_0}{2\pi n} \tag{7.5}$$

$$c_{t\zeta}^{Q}(\theta_1) = \frac{Q}{\pi n} \frac{a\sin\varepsilon}{1 + a^2 - 2a\cos\varepsilon} \tag{7.12}$$

$$c_{t\zeta}^{\Gamma}(\theta_1) = \frac{\Gamma_1}{\pi n} \frac{1 - a\cos\varepsilon}{1 + a^2 - 2a\cos\varepsilon} \tag{7.13}$$

$$c_{t\zeta}^{D}(\theta_1) = \frac{J_1}{2\pi n} \tag{7.15}$$

Substituting these velocities, equation (5.58) gives

$$\tfrac{1}{2}(J_0 - J_1) + Q\left[\frac{a\sin\delta}{1 + a^2 - 2a\cos\delta} + \frac{a\sin\varepsilon}{1 + a^2 - 2a\cos\varepsilon}\right]$$

$$+ \Gamma_{1,SL}\left[\frac{1 - a\cos\delta}{1 + a^2 - 2a\cos\delta} - \frac{1 - a\cos\varepsilon}{1 + a^2 - 2a\cos\varepsilon}\right] = 0 \tag{7.79}$$

Since equation (7.79) is identical to equation (7.17) we may simply use the results obtained previously for the pump impeller, viz. equations (7.19), (7.20), and (7.21).

First we substitute equation (7.73) in equation (5.53) and obtain, using equation (4.47)

$$\Gamma_2 = \frac{a^2 - 1}{1 - 2a\cos\varepsilon + a^2}\Gamma_1 - \frac{2a\sin\varepsilon}{1 - 2a\cos\varepsilon + a^2}Q - J_1 \tag{7.80}$$

Next putting

$$\Gamma_2 = \Gamma_2^D + \Gamma_2^Q \tag{7.81}$$

by which equation (7.80) gives

$$\Gamma_2^D = \frac{a^2 - 1}{1 - 2a\cos\varepsilon + a^2}\Gamma_1^D - J_1 \tag{7.82}$$

and

$$\Gamma_2^Q = \frac{a^2 - 1}{1 - 2a\cos\varepsilon + a^2}\,\Gamma_1^Q - \frac{2a\sin\varepsilon}{1 - 2a\cos\varepsilon + a^2}\,Q \tag{7.83}$$

we obtain for the shockless prerotation of the turbine impeller fitted with logarithmic spiral blades, after substituting equations (7.20) and (7.21) in equations (7.82) and (7.83), using equation (4.47)[10] and summing the results

$$\Gamma_{2,SL} = \tau_{t,D}\,2\pi\Omega r_2^2 + Q\tan\beta \tag{7.84}$$

where

$$\tau_{t,D} = \frac{\frac{1}{a} + a - 2\cos\delta}{\cos\delta - \cos\varepsilon}\,\frac{(J_1 - J_0)}{4\pi\Omega r_2^2} - \frac{J_1}{2\pi\Omega r_2^2} \tag{7.85}$$

The prerotation factor (7.85) is not treated in further detail since no arithmetical expressions for the integrals J_0 and J_1 have been obtained yet.

[10] See footnote 9.

8

ANALYTICAL SOLUTION VS FINITE ELEMENT SOLUTION

Besides the analytical solution, discussed in the previous chapters, we have also computed finite element solutions of (sub) flows, taking a pump impeller – fitted with logarithmic spiral blades – as a test case. The obtained finite element solutions primarily serve to illustrate the flow through the impeller; they are not to verify the analytical solution, though it has to be said that numerous deficiencies in the analytical solution have been traced by the finite element solution. After having first generally outlined the finite element procedure (paragraph 8.1) we will briefly discuss the flows that we have computed (paragraph 8.2), where we will compare the finite element solution with the analytical result(s).

8.1 Finite Element Procedure

The finite element solutions of the (sub) flows through the pump impeller have all been obtained using the finite element package SEPRAN. This package may be regarded as a toolbox of subroutines that are to be implemented in a suitable solver – a FORTRAN computer program – so that a particular problem, i.e. a differential equation with boundary condition(s), may be solved numerically. This toolbox idea gives great flexibility in solving problems, and moreover allows the user to implement his own subroutines. Furthermore the definition of (boundary) contours and mesh generation is rather sophisticated within SEPRAN, which makes a numerical treatment relatively easy. The general treatment, not specifically confined to SEPRAN, to obtain finite element solutions of the flow through the impeller is briefly outlined below.

First of all to determine the flow through the impeller numerically we may either solve the velocity potential (φ) or the stream function (ψ), both satisfying the Laplace equation as was mentioned in paragraph 3.1. From an illustrative point of view (streamlines) we choose to solve the stream function, i.e.

$$\nabla^2\psi = 0 \tag{3.6}$$

The ellipticity of the Laplace equation (3.6) next requires the choice of a representative region with appropriate boundary conditions so that the finite element solution may be compared with the analytical solution. Basically this means that an inner and outer boundary enclosing the impeller have to be chosen, such that the behaviour at the origin and the behaviour at infinity may be imposed on those boundaries. This region may simply be chosen as given in figure 8.1 (i). Then, by the periodicity of the flow through the impeller, we may further restrict ourselves to a periodical sub region as given in figure 8.1 (ii).

Having specified the region to treat the flow numerically we next need to impose the boundary conditions. First both the shockless entry ($\Gamma_{1,SL}$) and the blade circulation (Γ_B), the latter being given by the Kutta condition, are directly obtained from the analytical results. These circulations are subsequently imposed on the circular shaped inner and outer boundaries, say with radii R_1 and R_2, according to (so–called natural boundary conditions or Neumann conditions)

$$\text{inner boundary } (R_1): \left.\frac{\partial\psi}{\partial n}\right|_{R_1} = -\frac{\Gamma_1}{2\pi R_1} \tag{8.1}$$

$$\text{outer boundary } (R_2): \left.\frac{\partial\psi}{\partial n}\right|_{R_2} = \frac{\Gamma_2}{2\pi R_2} \tag{8.2}$$

with the circulations Γ_1 and Γ_2 being related by equation (5.53).

Next the periodic boundaries of the sub region, say B_1 and B_2, are (mesh) connected by

$$\psi\,|_{B_1} = \psi\,|_{B_2} + \frac{Q}{n} \tag{8.3}$$

By this condition we thus impose the fluid flux through the sub region.

The boundary condition on the blade finally is given by the fact that the relative stream function[11] (κ) is constant along a blade, say $\kappa = 0$, so the

[11] Like the absolute flow, the relative flow is also solenoidal so we may likewise define a relative stream function (κ); for two-dimensional flows the two type of stream functions are related by $\psi = \kappa - \frac{1}{2}\Omega r^2$ (see appendix B).

absolute stream function equals

$$\psi = -\tfrac{1}{2}\Omega r^2 \tag{8.4}$$

on the blade.

In conclusion of this paragraph we give the two meshes (figure 8.2) that we have used for the finite element solution(s). Both meshes are generated with simple triangular shaped elements, where especially the mesh of the sub region is refined rather severely near the blade tips to minimize the singular behaviour of the solution (intersecting streamlines). The mesh of the whole region (figure 8.2 (i)) has only been used to obtain an illustrative picture of the flow, whereas the mesh of the sub region (figure 8.2 (ii)) served for the finite element solution(s). To indicate the mesh size we finally give that the mesh of the whole region consisted of nearly 5800 elements with about 3300 nodal points, and that the mesh of the sub region consisted of nearly 3150 elements with about 1750 corresponding nodal points.

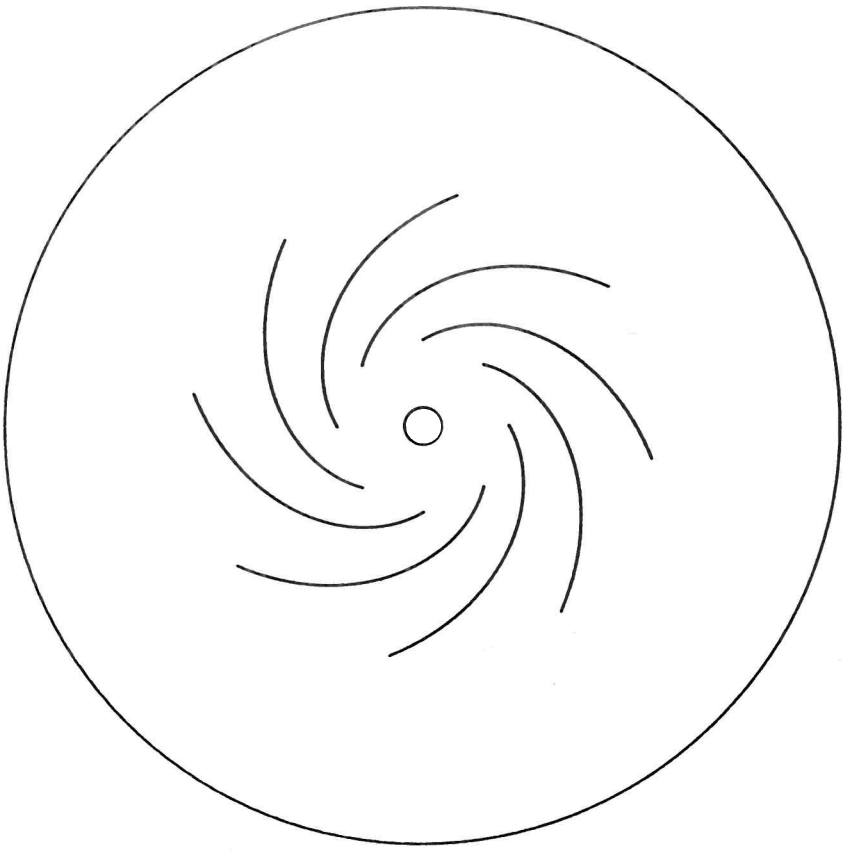

(*i*)

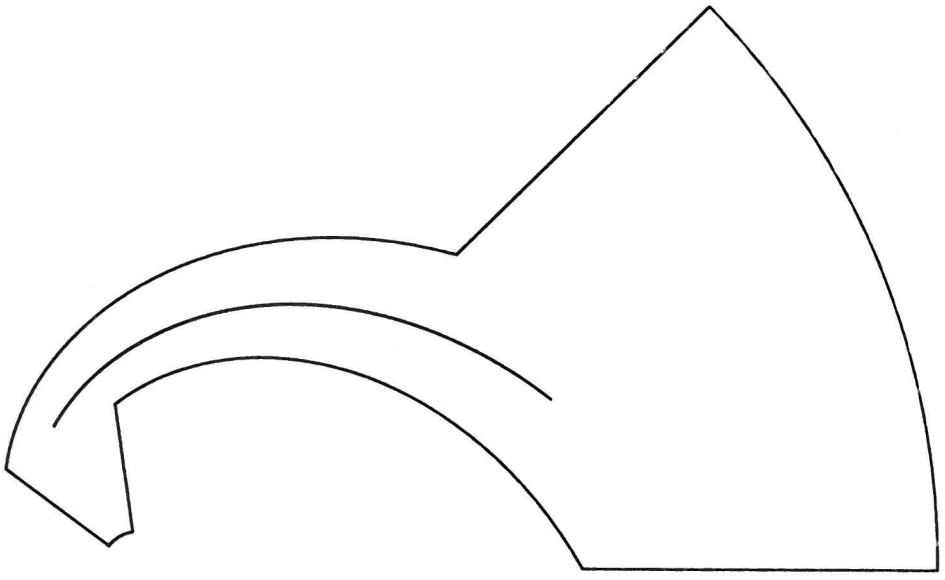

(*ii*)

figure 8.1 (*i*) *finite element region and* (*ii*) *periodical sub region*

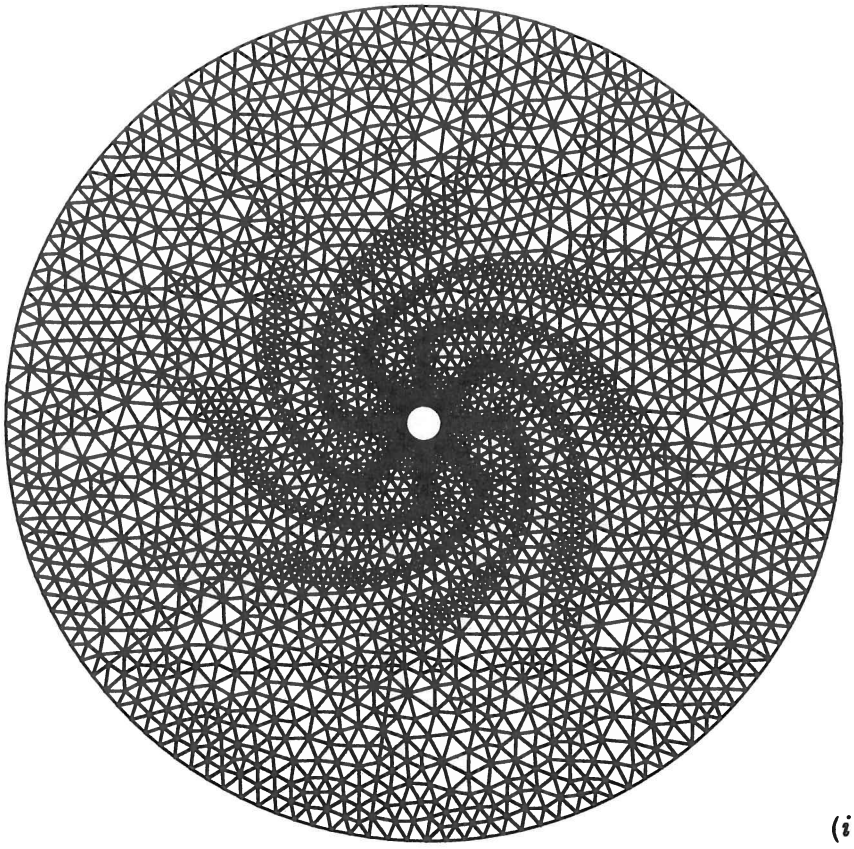

(*i*)

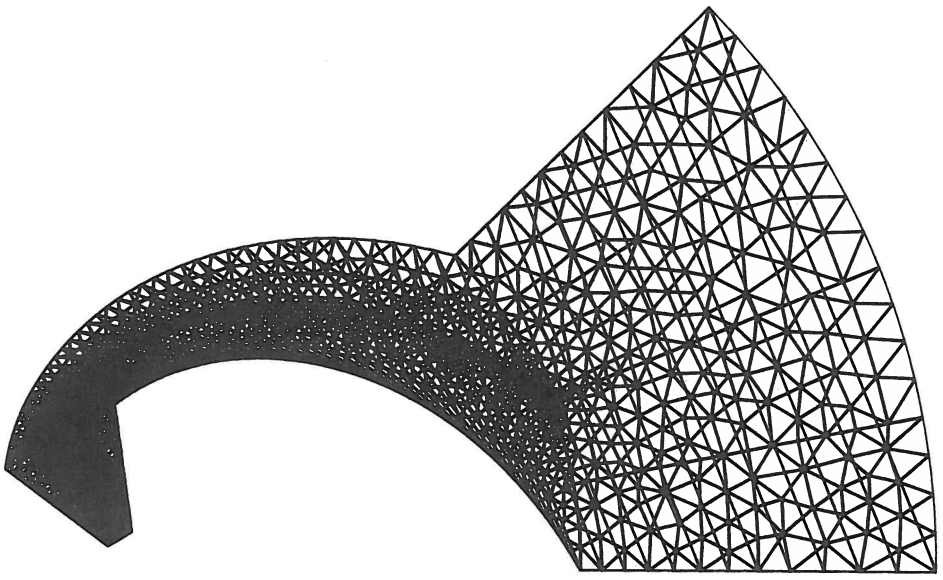

(*ii*)

figure 8.2 *finite element mesh of* (*i*) *whole region and* (*ii*) *periodical sub region*

8.2 Computed Flows

By manipulating the boundary conditions, as given in the previous paragraph, we have derived finite element solutions of velocity distributions along a blade of the pump impeller (earlier mentioned in section 7.1.4). All sub flows have been computed, both numerically and analytically.

The impeller that we have used was characterized by

number of blades	$n = 8$
inner tip	$r_1 = 37\ mm$
outer tip	$r_2 = 100\ mm$
blade angle	$\beta = 60^o = \frac{\pi}{3}$

and where we further had

inner boundary	$R_1 = 8\ mm$
outer boundary	$R_2 = 180\ mm$
angular speed	$\Omega = -10\pi\ s^{-1}$
minimum source strength	$Q_{min} = 0.215\ m^2/s$
blade circulations	$\Gamma_B^D = -0.200\ m^2/s$
	$\Gamma_B^Q = 0.046\ m^2/s$
	$\Gamma_B^\Gamma \approx -\frac{\Gamma_1}{n} = -0.125\,\Gamma_1$
shockless prerotations	$\Gamma_{1,SL}^D = -0.350\ m^2/s$
	$\Gamma_{1,SL}^Q = 0.372\ m^2/s$

As a preliminary and illustrative example we have first solved the (shockless) displacement flow numerically in both the entire finite element region and the periodical sub region. The result of this exercise is presented in figure 8.3 by relative streamlines. Figure 8.3 (i) clearly shows the recirculation areas or relative eddies that are due to the irrotationality of the absolute flow (see also appendix B). These relative eddies cause a back flow ($w_s < 0$) along the pressure side of the blades, if the source or through flow is not strong enough to compensate the eddy velocity. The prevention of back flow is clearly illustrated by the next given velocity distributions of the examined (sub) flows.

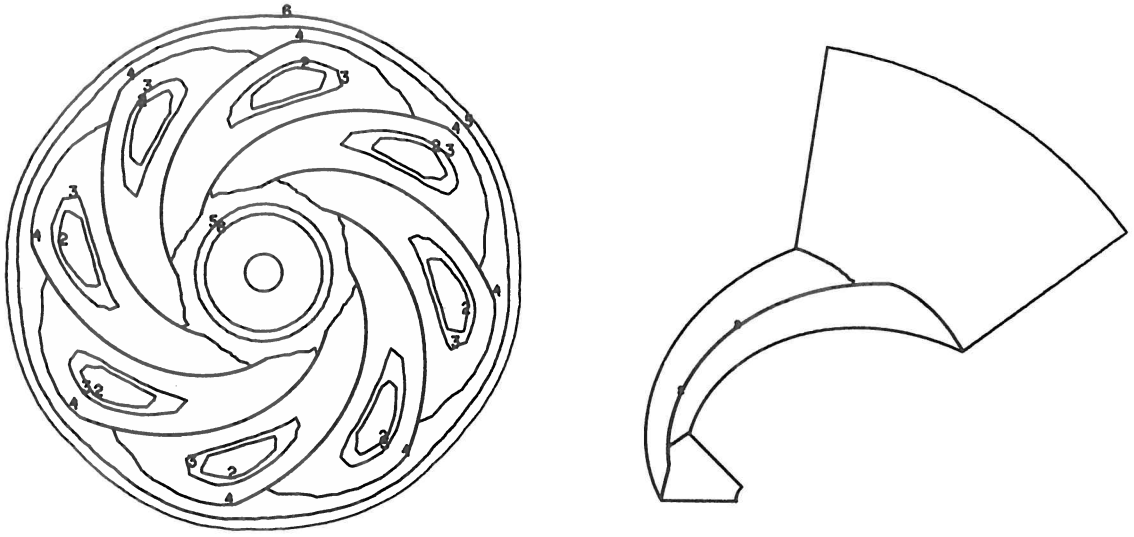

(*i*) (*ii*)

figure 8.3 (*i*) *relative eddies and* (*ii*) *relative streamline* ($\kappa = 0$) *due to the displacement flow* (*shockless*)

The velocity distributions along the blades, given on the next pages, are all relative to the blades and plotted as a function of the blade coordinate (s), previously defined by equation (7.33).

The (10) flows that we have computed are:

- displacement flow
- displacement flow with Kutta condition
- displacement flow with Kutta condition and shockless entry
- source flow
- source flow with Kutta condition
- source flow with Kutta condition and shockless entry
- vortex flow
- vortex flow with kutta condition
- displacement flow with source and Kutta condition
- displacement flow with source, shockless entry and Kutta condition

Besides velocity distributions we have also computed the pressure distribution for the latter two (displacement flow with source), using equation (7.35).

All finite element solutions show excellent agreement with the analytical results, as was to be expected. With regard to the Kutta condition and the shockless entry we further notice that the fluid flows smoothly at the blade tips, i.e. the singular behaviour at the blade tips is properly eliminated.

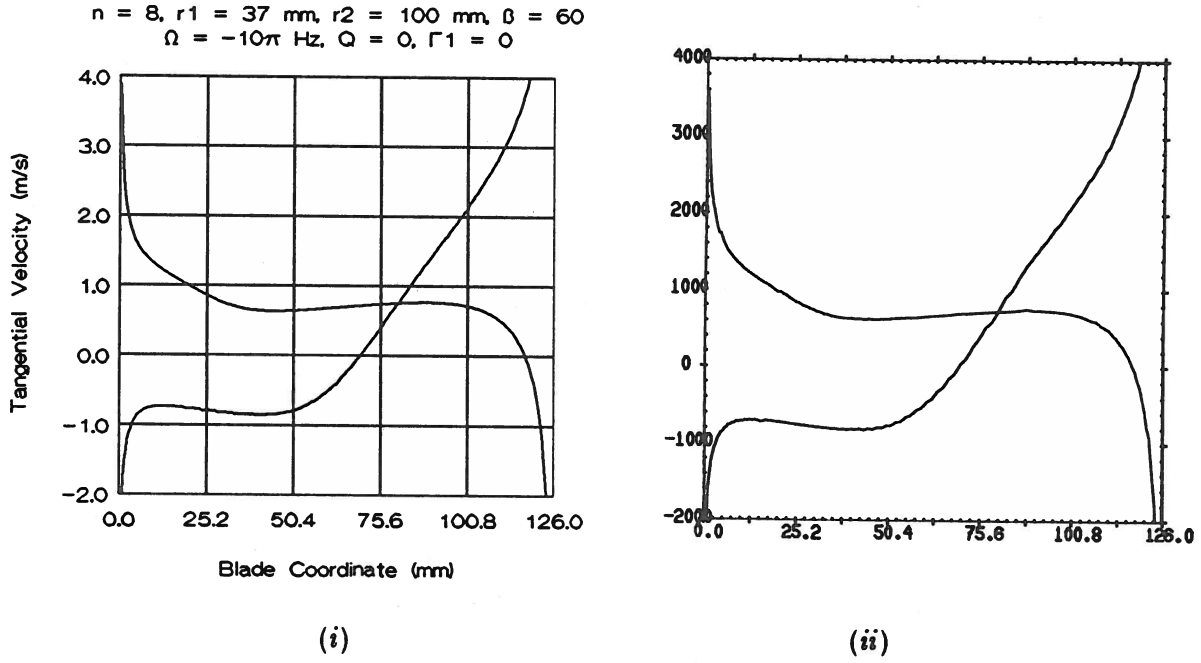

(*i*) (*ii*)

figure 8.4 *velocity distribution along a logarithmic spiral blade; displacement flow; (i) analytical solution, (ii) numerical solution*

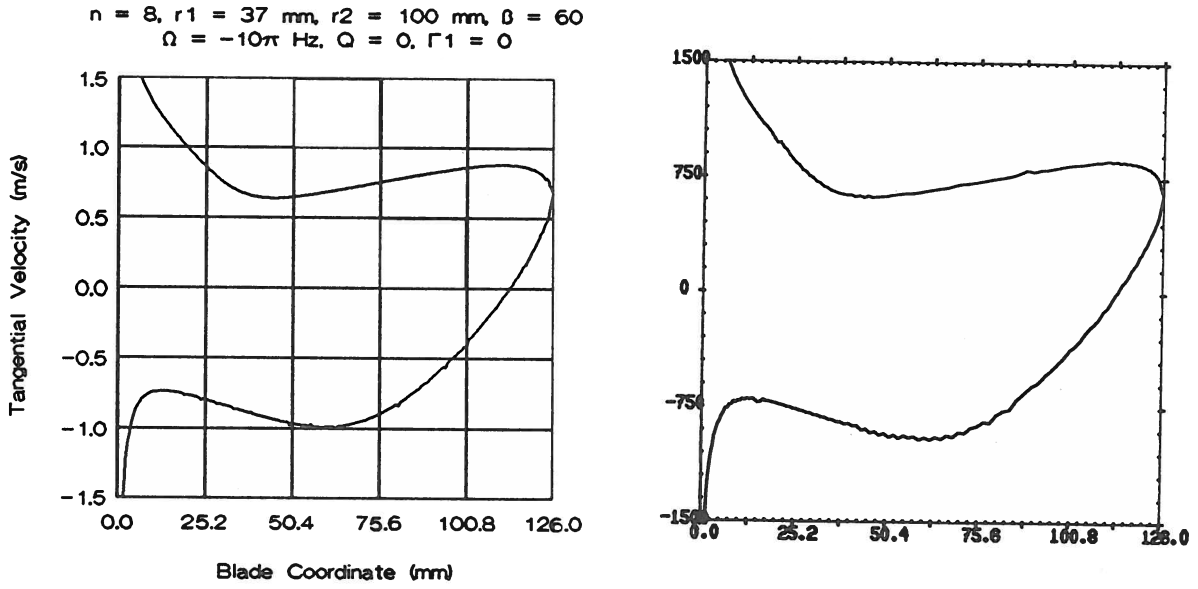

(*i*) (*ii*)

figure 8.5 *velocity distribution along a logarithmic spiral blade; displacement flow with Kutta condition; (i) analytical solution, (ii) numerical solution*

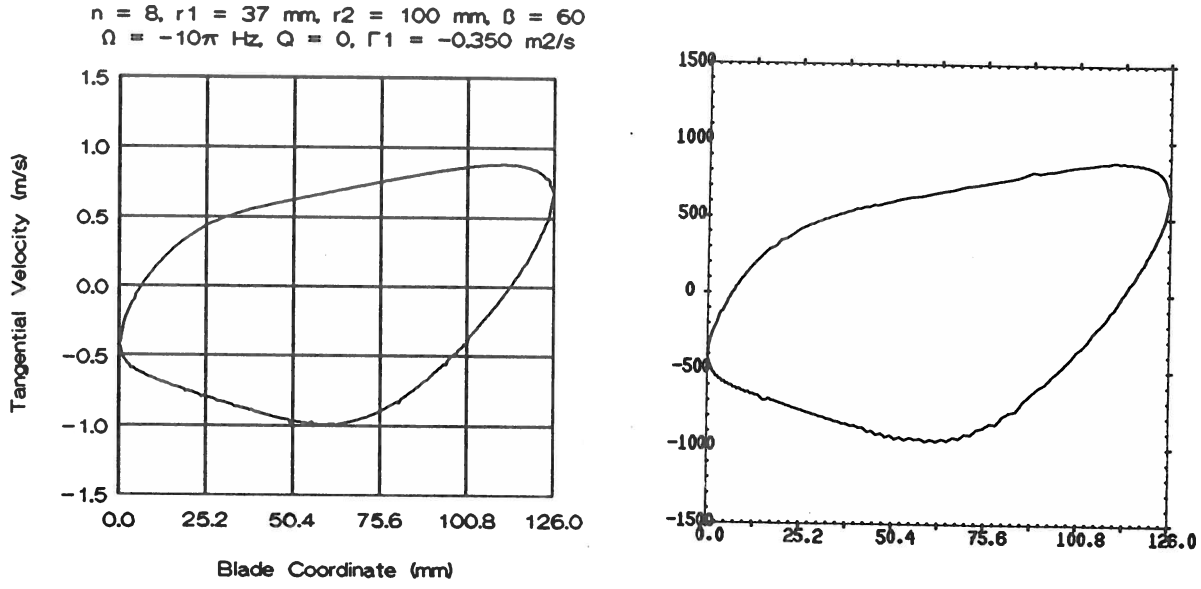

(*i*) (*ii*)

figure 8.6 *velocity distribution along a logarithmic spiral blade; displacement flow with Kutta condition and shockless entry; (i) analytical solution, (ii) numerical solution*

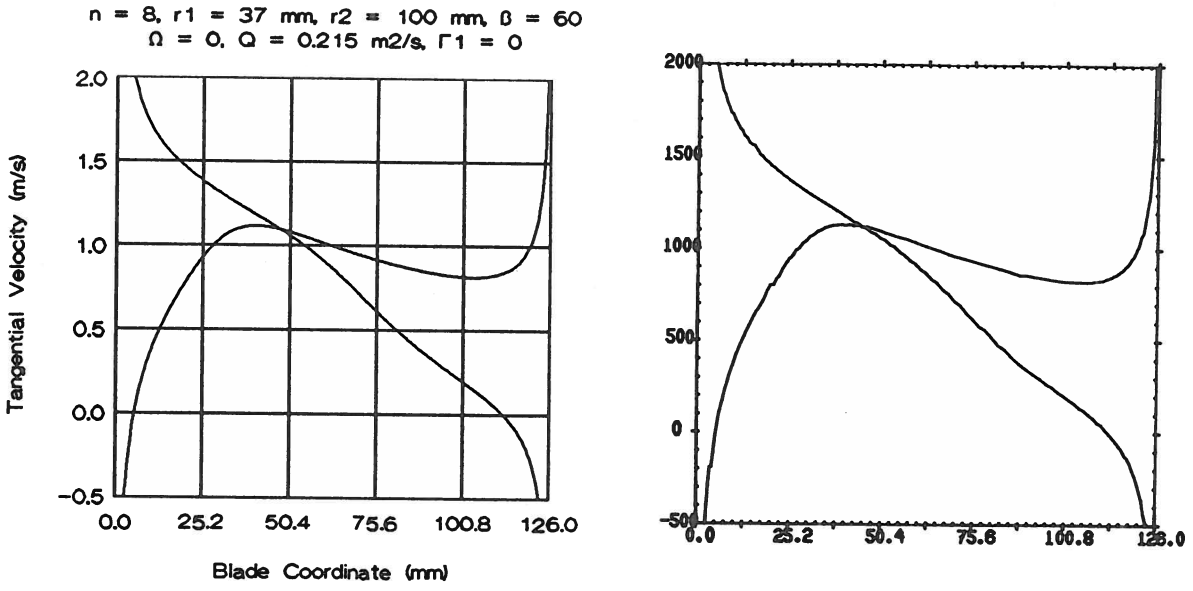

(*i*) (*ii*)

figure 8.7 *velocity distribution along a logarithmic spiral blade; source flow; (i) analytical solution, (ii) numerical solution*

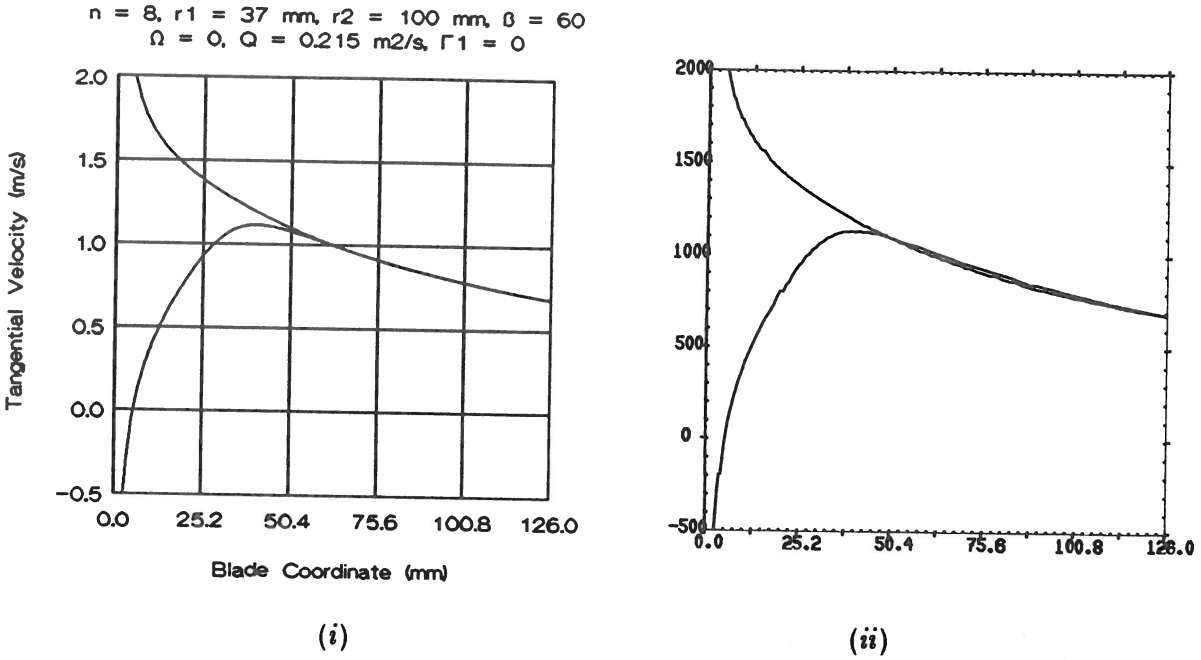

figure 8.8 *velocity distribution along a logarithmic spiral blade; source flow with Kutta condition;* (*i*) *analytical solution,* (*ii*) *numerical solution*

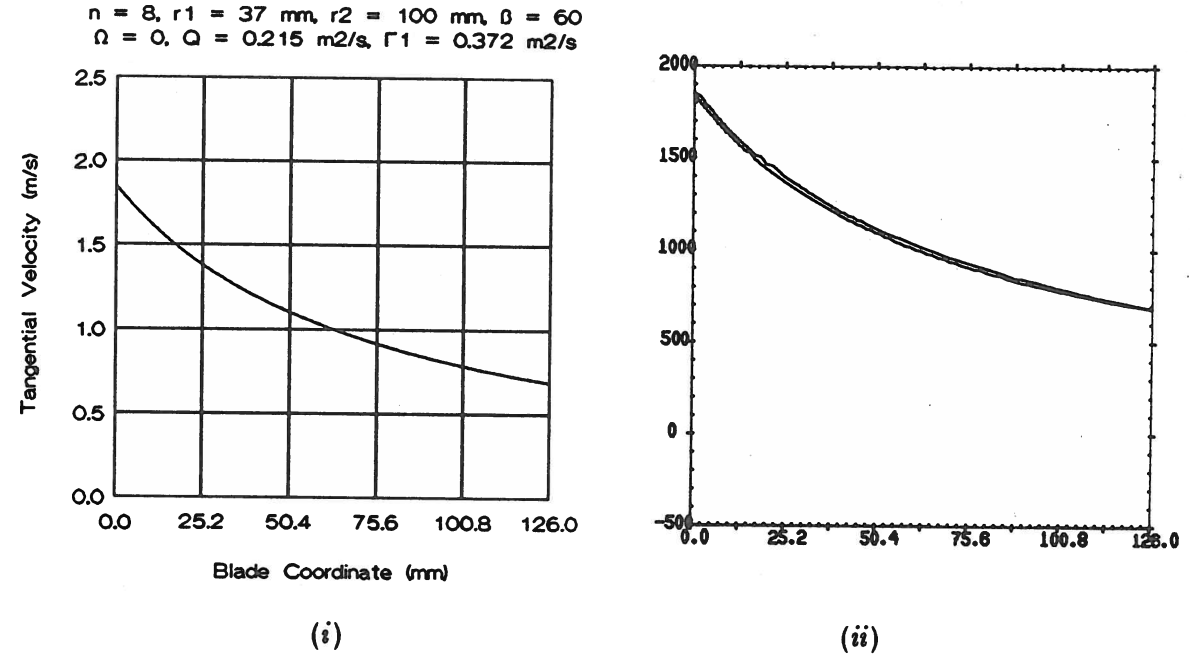

figure 8.9 *velocity distribution along a logarithmic spiral blade; source flow with Kutta condition and shockless entry;* (*i*) *analytical solution,* (*ii*) *numerical solution*

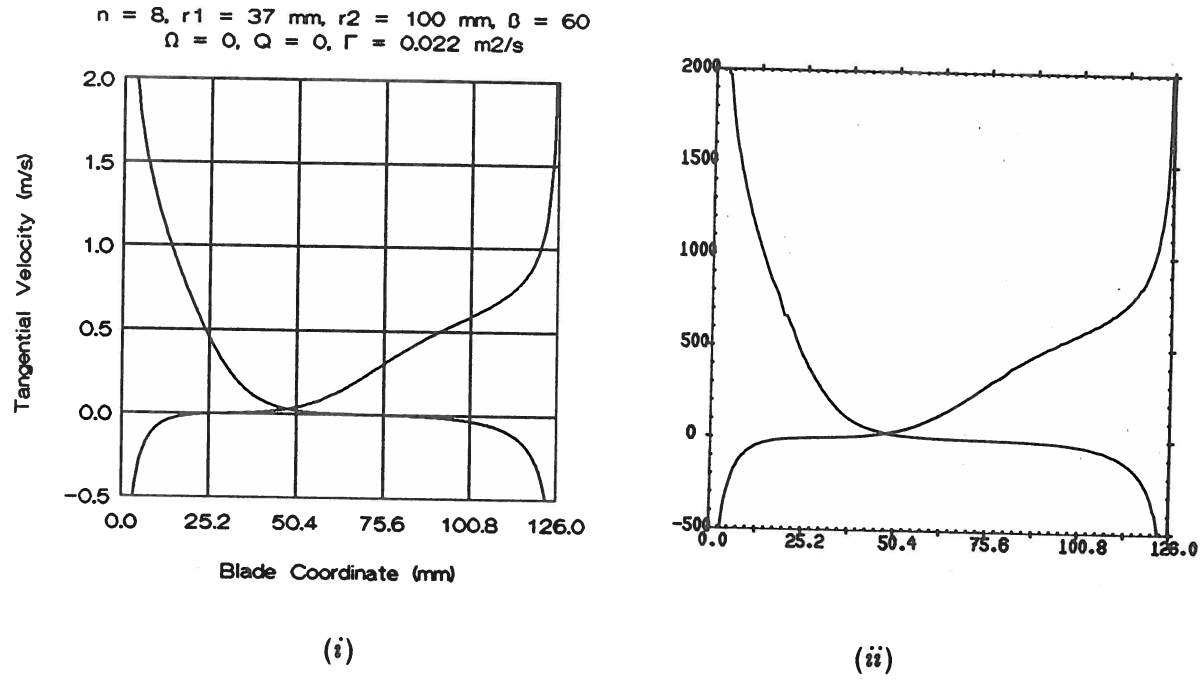

(*i*) (*ii*)

figure 8.10 *velocity distribution along a logarithmic spiral blade; vortex flow; (i) analytical solution, (ii) numerical solution*

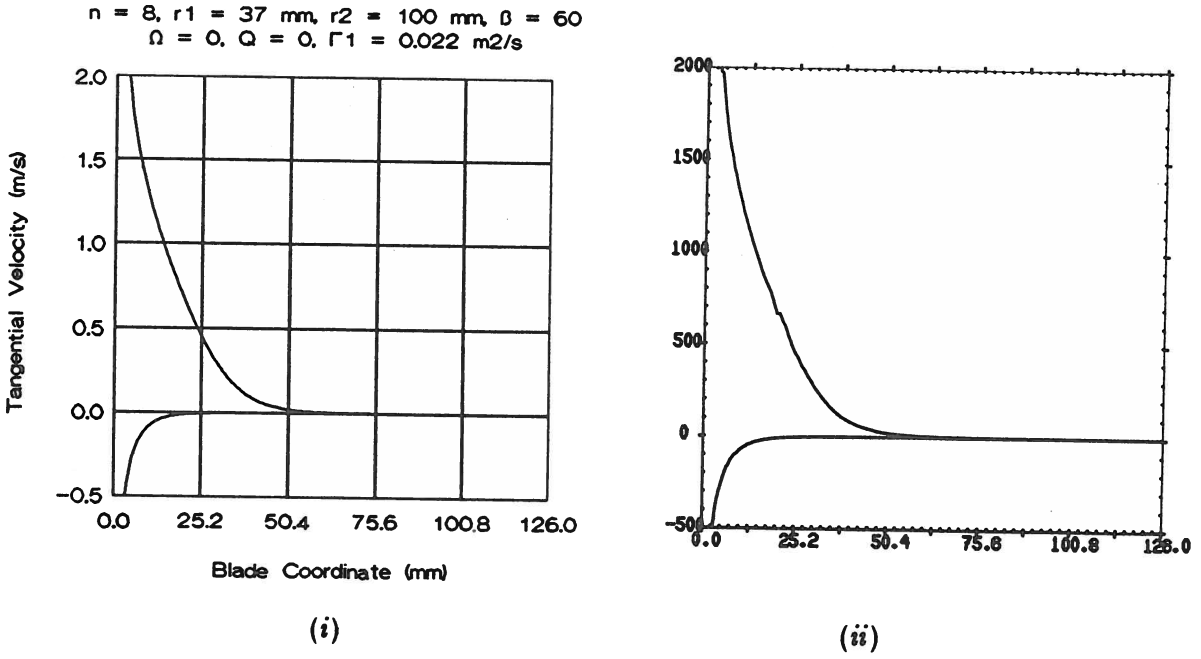

(*i*) (*ii*)

figure 8.11 *velocity distribution along a logarithmic spiral blade; vortex flow with Kutta condition; (i) analytical solution, (ii) numerical solution*

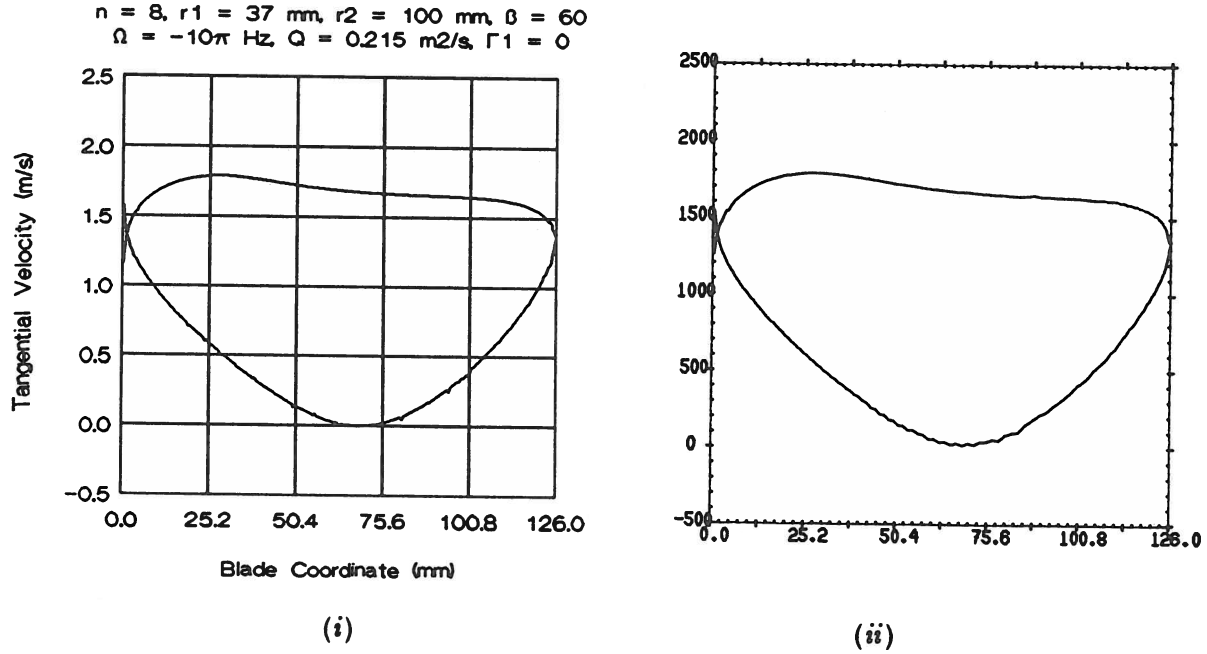

(*i*) (*ii*)

figure 8.12 *velocity distribution along a logarithmic spiral blade; displacement flow with source and Kutta condition; (i) analytical solution, (ii) numerical solution*

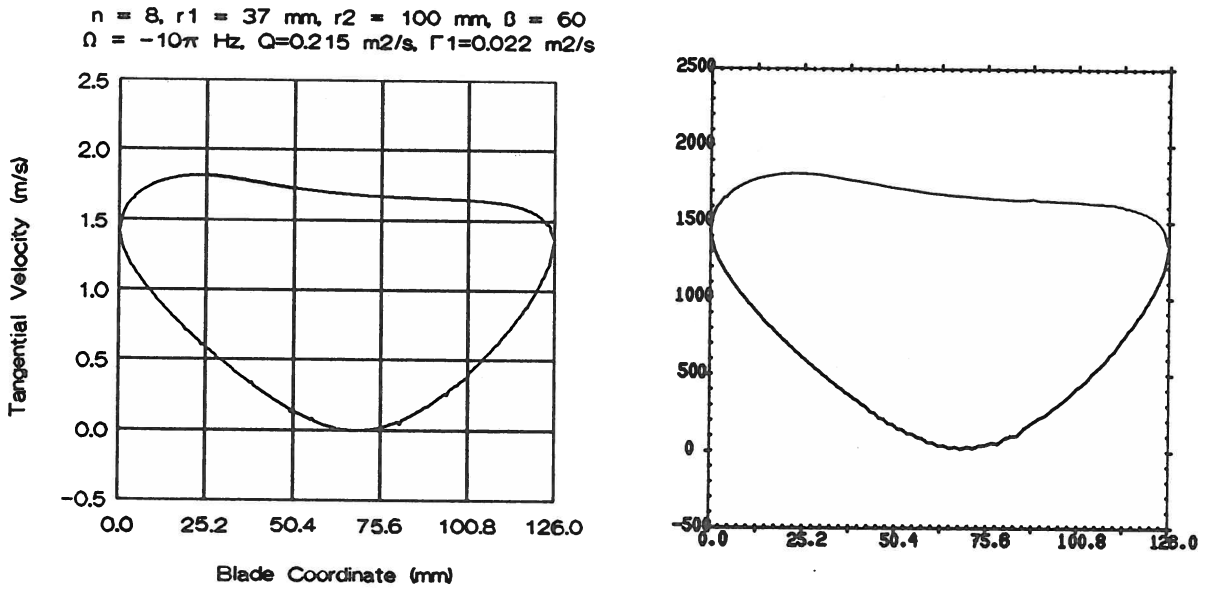

(*i*) (*ii*)

figure 8.13 *velocity distribution along a logarithmic spiral blade; displacement flow with source, Kutta condition and shockless entry; (i) analytical solution, (ii) numerical solution*

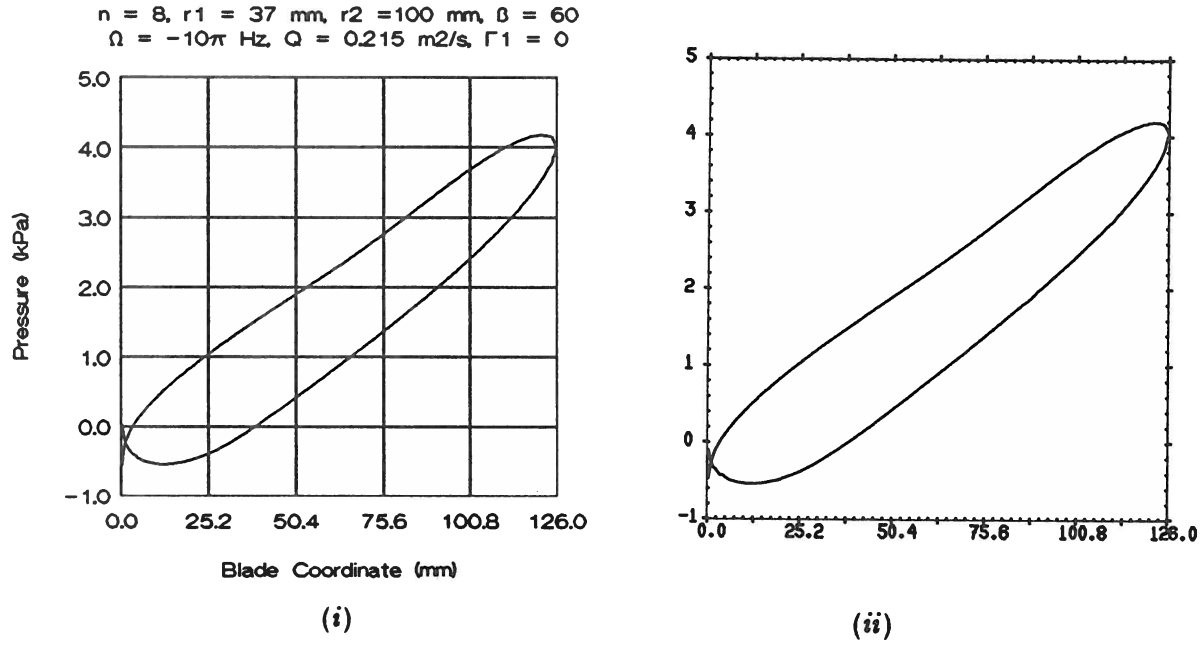

figure 8.14 *pressure distribution along a logarithmic spiral blade; displacement flow with source and Kutta condition; (i) analytical solution, (ii) numerical solution*

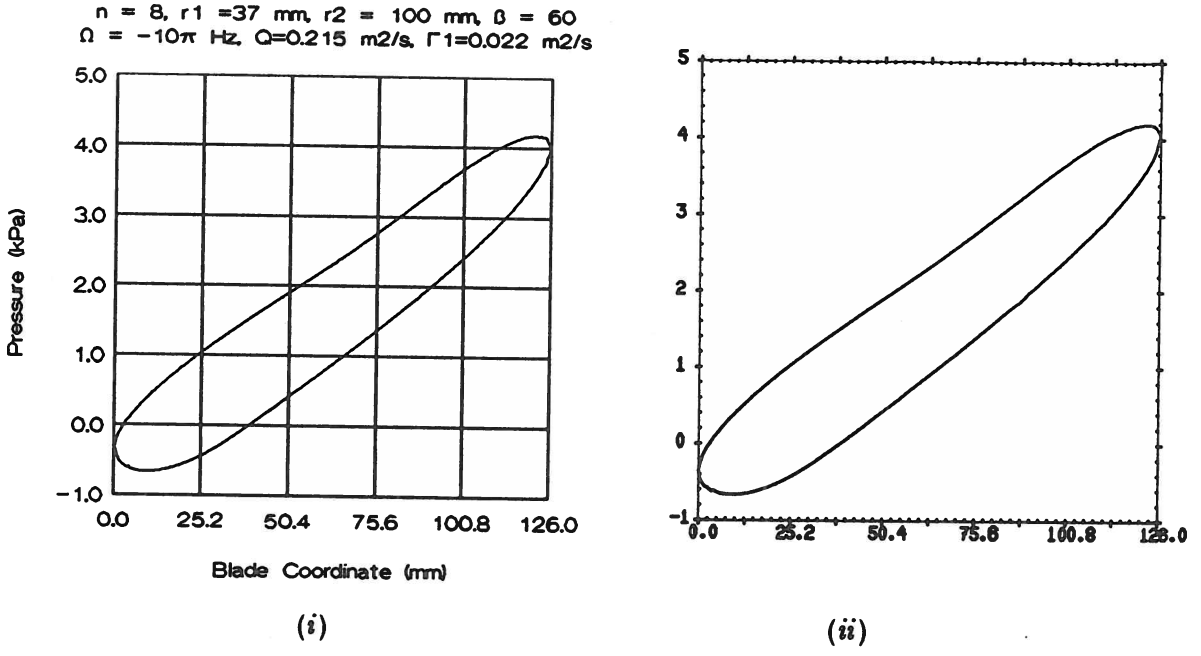

figure 8.15 *pressure distribution along a logarithmic spiral blade; displacement flow with source, Kutta condition and shockless entry; (i) analytical solution, (ii) numerical solution*

9

APPLICATION OF RESULTS IN COMPARISON WITH ONE-DIMENSIONAL FLOW THEORY

The previously derived results, based on our two–dimensional analysis of the flow through the impeller, will be further discussed in this chapter. The applications that we are about to give are basically related to the classical one–dimensional flow theory, and may be regarded as a relative simple and practical extension.

As a preliminary we first give a short review of some elementary formulas, that will serve as a basis discussing the applications; though these formulas have appeared previously we will rephrase them for the completeness of this chapter. Next the applications will be discussed, where we will make a distinction between the pump impeller and the turbine impeller. First applications for the pump will be discussed and secondly some features of the turbine will be outlined.

9.1 Review of Basic Formulas

The first important relation that we have relates the circulations around the origin (Γ_1), the impeller (Γ_2), and the blades (Γ_B); this relation generally reads

$$\Gamma_2 = \Gamma_1 + \sum_{j=1}^{n} \Gamma_B \tag{9.1}$$

Then by the periodicity of the flow through the impeller, for we base our analysis on a so–called isolated impeller, equation (9.1) may be simplified as

$$\Gamma_2 = \Gamma_1 + n\Gamma_B \tag{9.2}$$

Equation (9.2) simply states that the circulation (Γ_2) around the impeller equals the circulation (Γ_1) around the origin plus n times the circulation

(Γ_B) around an impeller blade, with n being the number of blades.

The second important relation that we recollect is the general equation for the blade circulation. Based on our two dimensional analysis of the flow through an impeller fitted with logarithmic spiral blades we have for the pump impeller

$$n\Gamma_B = \sigma_{p,D}\, 2\pi\Omega r_2^2 + \sigma_{p,Q}\, Q\tan\beta - \sigma_{p,\Gamma}\, \Gamma_1 \qquad (9.3)$$

and for the turbine impeller

$$n\Gamma_B = \sigma_{t,\Gamma}\, \Gamma_2 - \sigma_{t,Q}\, Q\tan\beta - \sigma_{t,D}\, 2\pi\Omega r_1^2 \qquad (9.4)$$

where Ω is the angular speed of the impeller, Q is the fluid flux, and β the blade angle; the latter being equal to zero in case of straight radial blades. To avoid confusion all positive directions are defined counter clock wise (Γ_1, Γ_2, Γ_B, β, Ω) and radially outward (Q). The subscripts of the slip factors ($\sigma_{.,.}$) simply denote their origin, that is, displacement flow (D), source flow (Q) or vortex flow (Γ), and indicate whether it concerns the *pump* or the *turbine*.

In case of an infinite number of blades ($n \longrightarrow \infty$) all the slip factors become 1, and the equations (9.3) and (9.4) then reduce to the well known Eulerian expressions.

9.2 Applications for the Pump Impeller

The applications that we will discuss in this paragraph successively are: the influence of the prerotation with respect to the circulation, the shockless entry, the develop head and slip factor(s), and the choice of a volute fitting the pump impeller.

9.2.1 Influence of the prerotation

The influence of the prerotation, with respect to the circulation around the impeller, is best demonstrated by substituting equation (9.3) in equation (9.2). We thus obtain

$$\Gamma_2 = \sigma_{p,D}\, 2\pi\Omega r_2^2 + \sigma_{p,Q}\, Q\tan\beta + (1 - \sigma_{p,\Gamma})\, \Gamma_1 \tag{9.5}$$

Next to examine the influence of the prerotation we recollect the expressions for the slip factor ($\sigma_{p,\Gamma}$) obtained previously.

For straight radial blades we had

$$\sigma_{p,\Gamma} = 1 - V\mu = 1 - \left[\frac{r_1}{r_2}\right]^{\frac{n}{2}} \tag{6.32}$$

and for logarithmic spiral blades

$$\sigma_{p,\Gamma} = \frac{2(1 - a\cos\delta)}{1 - 2a\cos\delta + a^2} \tag{7.11}$$

where

$$\delta = \pi - 2\beta + \varepsilon \tag{4.45}$$

$$a \approx \frac{1}{1 - \varepsilon\, \mathrm{cotan}\, \beta} \tag{4.48}$$

with

$$\varepsilon \approx \left[\frac{r_1}{r_2}\right]^{\frac{n}{2\cos^2\beta}} e^{2\beta \tan\beta}\, \sin 2\beta \tag{4.53}$$

The latter two being valid for $|\varepsilon| \ll 1$ and $|\varepsilon| \ll |\beta|$.

From the above-given relations it will be evident that

$$1 - \sigma_{p,\Gamma} \ll 1 \tag{9.6}$$

for impellers with a respectable number of blades, i.e. $n \gg 1$, and/or a sufficiently large inner/outer tip ratio. We may thus conclude from equation (9.5) that the prerotation gives an insignificant contribution to the circulation around the impeller. One might therefore think that the prerotation plays an unimportant role on the whole. This, however, is a misconception since the object of our concern should be the blade circulation

($n\Gamma_B$) when discussing the efficiency of the impeller. Furthermore, the importance of the prerotation is primarily the possibility to impose a shockless entry, so that impact losses are omitted, rather than the contribution to the circulation.

9.2.2 Shockless entry

From our two–dimensional analysis it follows that the shockless prerotation for a pump impeller fitted with logarithmic spiral blades reads

$$\Gamma_{1,SL} = \tau_{p,D}\, 2\pi\Omega r_1^2 + Q\tan\beta \tag{7.25}$$

Since we have not obtained an arithmetical expression for the prerotation factor ($\tau_{p,D}$) in case of logarithmic spiral blades, we will further (have to) confine ourselves to the solution that has been obtained for the impeller fitted with straight radial blades ($\beta = 0$), i.e.

$$\tau_{p,D} = \left[\frac{2}{1+\sqrt{\mu}}\right]^{\frac{4}{n}} F\left[\frac{2}{n},\frac{2}{n};1;\left[\frac{1-\sqrt{\mu}}{1+\sqrt{\mu}}\right]^2\right] \tag{6.55}$$

To judge this prerotation factor we will briefly discuss the given relation.

From equation (6.55) we first of all notice the remarkable fact that

$$\tau_{p,D} > 1 \tag{9.7}$$

since the hypergeometric function – $F(a,b;c;z)$ – always exceeds the value 1 for positive arguments (a,b,c). So the shockless prerotation actually required for the pump impeller will be higher than the one–dimensional (Eulerian) value.

Secondly we notice from equation (6.55) that a numerical evaluation of the prerotation factor becomes rather awkward, due to the decreasing rate of convergence of the hypergeometric series, if the parameter μ becomes small. It would therefore be convenient to have an easily computable approximation of the prerotation factor (6.55). To obtain this we may reasonably impose

$$\sqrt{\mu} = \left[\frac{r_1}{r_2}\right]^{\frac{n}{2}} \ll 1 \tag{9.8}$$

by which we may approximate equation (6.55) by

$$\tau_{p,D} \approx 2^{\frac{4}{n}} F\left[\tfrac{2}{n},\tfrac{2}{n};1;1\right] \tag{9.9}$$

which can be stated alternatively as a quotient of gamma functions[12], i.e.

$$\tau_{p,D} \approx 2^{\frac{4}{n}} \frac{\Gamma(1-\frac{4}{n})}{\Gamma^2(1-\frac{2}{n})} \tag{9.10}$$

where it is provided that $n > 4$.

Equation (9.10) gives us a relative simple approximation of the prerotation factor for impellers fitted with (n) straight radial blades. The decrease of this prerotation factor, when increasing the number of blades, is graphically illustrated in figure 9.1. This figure clearly shows that the prerotation factor tends to the Eulerian value (1) for a large number of blades, as can readily be proven by equation (9.10), i.e.

$$\lim_{n\to\infty} \tau_{p,D} = 1 \tag{9.11}$$

Thus we also obtain the well-known Eulerian expression of the prerotation for a pump impeller

$$\Gamma_{1,Eu} = \lim_{n\to\infty} \Gamma_{1,SL} = 2\pi\Omega r_1^2 + Q\tan\beta \tag{9.12}$$

12 As can be found in, for instance, Abramowitz and Stegun, Bateman (1953), or Gradshteyn and Ryzhik we have that $F(a,b;c;1) = \frac{\Gamma(c-b-a)\Gamma(c)}{\Gamma(c-b)\Gamma(c-a)}$ where Re{c-b-a} > 0 and c not zero or a negative integer.

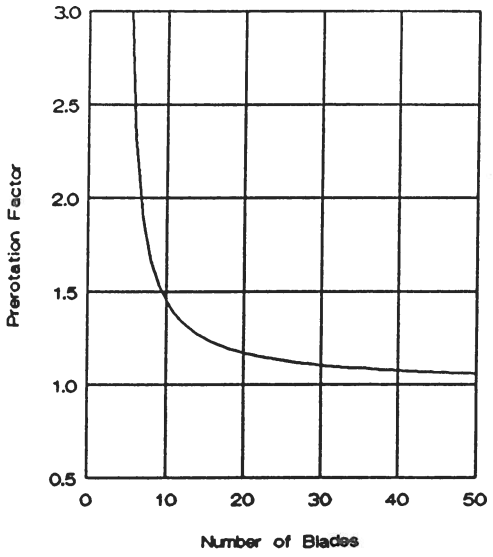

figure 9.1 *prerotation factor for straight radial blades (approximately)*

9.2.3 Developed head and slip factor(s)

From the classical (two–dimensional) approach by the moment of momentum it follows that the theoretically developed head (H_{th}) of an isolated centrifugal impeller may be written as

$$H_{th} = \frac{(\Gamma_2 - \Gamma_1)\Omega}{2\pi g} = \frac{n\Gamma_B\Omega}{2\pi g} \tag{9.13}$$

where g is the acceleration due to gravity.

Substitution of equation (9.3) in equation (9.13) next gives

$$gH_{th} = \sigma_{p,D}\,\Omega^2 r_2^2 + \sigma_{p,Q}\,\frac{\Omega Q \tan\beta}{2\pi} - \sigma_{p,\Gamma}\,\frac{\Omega\Gamma_1}{2\pi} \tag{9.14}$$

or using dimensionless groups

$$\Psi_{th} = \sigma_{p,D} + \sigma_{p,Q}\,\Phi\tan\beta - \sigma_{p,\Gamma}\,\Upsilon_1 \tag{9.15}$$

where we have introduced:

$$\text{head coefficient,} \quad \Psi_{th} = \frac{gH_{th}}{\Omega^2 r_2^2} \tag{9.16}$$

$$\text{flow coefficient,} \qquad \Phi = \frac{Q}{2\pi\Omega r_2^2} \tag{9.17}$$

$$\text{vortex coefficient,} \qquad \Upsilon_1 = \frac{\Gamma_1}{2\pi\Omega r_2^2} \tag{9.18}$$

Next letting the number of blades become infinitely large all the slip factors ($\sigma_{p,D}$, $\sigma_{p,Q}$, $\sigma_{p,\Gamma}$) become 1, and equation (9.15) then reduces to the well–known expression for the Eulerian head (coefficient)

$$\Psi_{Eu} = 1 + \Phi tan\,\beta - \Upsilon_1 \tag{9.19}$$

where the subscript Eu is used to indicate the Eulerian value.

Based on this Eulerian head we may next define a head reduction factor[13] (*HRF*) by

$$HRF = \frac{H_{th}}{H_{Eu}} = \frac{\Psi_{th}}{\Psi_{Eu}} \tag{9.20}$$

Substituting equations (9.15) and (9.19) this becomes

$$HRF = \frac{\sigma_{p,D} + \sigma_{p,Q}\,\Phi tan\beta - \sigma_{p,\Gamma}\,\Upsilon_1}{1 + \Phi tan\beta - \Upsilon_1} \tag{9.21}$$

where it will be evident that the limiting value ($n \rightarrow \infty$) of the head reduction factor equals 1 since then all slip factors become 1.

Equations (9.14), (9.15), and (9.21) clearly illustrate the importance of the slip factors for the pump impeller ($\sigma_{p,D}$, $\sigma_{p,Q}$, $\sigma_{p,\Gamma}$). Separately for both the straight radial blades and the logarithmic spiral blades we will further expand on the relations previously obtained for the respective slip factors.

Straight Radial Blades

For the impeller fitted with straight radial blades ($\beta = 0$) only $\sigma_{p,D}$ and $\sigma_{p,\Gamma}$ are of interest. These slip factors are given by

[13] In some literature the head reduction factor is (incorrectly) addressed as the slip factor; this is a rejectable conception since there is a strong flow dependence of the head reduction factor, whereas the slip factor(s) (should) only depend on the size and shape of the impeller.

$$\sigma_{p,D} = \frac{1-\mu}{2} F\left[\tfrac{1}{2}, 1-\tfrac{2}{n}; 2; 1-\mu\right] \tag{6.30}$$

$$\sigma_{p,\Gamma} = 1 - \sqrt{\mu} = 1 - \left[\frac{r_1}{r_2}\right]^{\frac{n}{2}} \tag{6.32}$$

As we have said in the previous section we again have (and even more strongly) that the evaluation of the hypergeometric series, given in equation (6.30), will be rather laborious if the parameter μ becomes small. Likewise we will therefore derive an approximation – of equation (6.30) – to evaluate the slip factor ($\sigma_{p,D}$) conveniently; the slip factor ($\sigma_{p,\Gamma}$) should give no problems to compute.

In reason we now impose

$$\mu = \left[\frac{r_1}{r_2}\right]^n \ll 1 \tag{9.22}$$

so equation (6.30) may be approximated by

$$\sigma_{p,D} \approx \tfrac{1}{2} F\left[\tfrac{1}{2}, 1-\tfrac{2}{n}; 2; 1\right] \tag{9.23}$$

which can be stated alternatively as[14]

$$\sigma_{p,D} \approx \frac{1}{\sqrt{\pi}} \frac{\Gamma(\frac{1}{2}+\frac{2}{n})}{\Gamma(1+\frac{2}{n})} \tag{9.24}$$

Equation (9.24) may be used as a fairly good approximation for computing the slip factor due to the displacement flow for (two–dimensional) impellers fitted with straight radial blades. If an exact value is required, or when condition (9.22) is not fulfilled equation (6.30) should be used.

Logarithmic Spiral Blades

For the impeller fitted with logarithmic spiral blades we have previously obtained the following expressions for the slip factors

[14] See footnote 12

$$\sigma_{p,Q} = \frac{2a\,sin\,\delta\;cotan\;\beta}{1 - 2acos\;\delta + a^2} \tag{7.10}$$

$$\sigma_{p,\Gamma} = \frac{2(1 - acos\;\delta)}{1 - 2acos\;\delta + a^2} \tag{7.11}$$

$$\sigma_{p,D} = \left[(2cos\,\beta)^{\frac{4cos^2\beta}{n}} \left(1+\frac{4cos^2\beta}{n}\right) e^{\frac{2\beta sin\,2\beta}{n}} B(\chi,\bar{\chi})\right]^{-1} \tag{7.68}$$

where

$$\chi = 1 + \frac{2cos^2\beta}{n} + \frac{sin\,2\beta}{n}i \tag{7.66}$$

and the constants a and δ as given herein before. Equations (7.10) and (7.11) are exact solutions for the respective slip factors while equation (7.68) is valid for $\mu = (r_1/r_2)^n = 0$. The latter, however, is no major restriction since most impellers found in practice are characterized by $\mu \ll 1$. Thus we have a useful relation to obtain, approximately, the slip factor due to the displacement flow for impellers fitted with logarithmic spiral blades. The numerical evaluation of the beta function in equation (7.68) should cause no severe problems despite the appearance of complex arguments; practical algorithms to compute this function are given in many handbooks as for instance Abramowitz and Stegun, and Press *et al.* Furthermore it will not always be necessary to compute the slip factor according to equation (7.68); for we can simplify equation (7.68) if

$$\left[\frac{sin\,2\beta}{n}\right]^2 \ll \left[1 + \frac{2cos^2\beta}{n}\right]^2 \tag{9.25}$$

Thus we obtain by some elementary manipulations[15]

[15] As can be found in, for instance, Abramowitz and Stegun, Bateman (1953), or Gradshteyn and Ryzhik we have that:

$B(x,x) = B(z,\bar{z})_k \prod_{k=0}^{\infty}(1 + y^2/(x+k)^2)$ where $z = x + iy$ and $x \neq 0, -1, -2, \ldots$

$B(z,w) = \frac{\Gamma(z)\Gamma(w)}{\Gamma(z+w)}$

$\Gamma(2z) = (2\pi)^{-\frac{1}{2}}2^{2x-\frac{1}{2}}\Gamma(z)\Gamma(z+\frac{1}{2})$, duplication formula

$\Gamma(z+1) = z\Gamma(z)$, recurrence formula

$$\sigma_{p,D} \approx \left[(\cos\beta)^{\frac{4\cos^2\beta}{n}} \, e^{\frac{2\beta \sin 2\beta}{n}} \, \sqrt{\pi} \, \frac{\Gamma\left(1 + \frac{2\cos^2\beta}{n}\right)}{\Gamma\left(\frac{1}{2} + \frac{2\cos^2\beta}{n}\right)} \right]^{-1} \qquad (9.26)$$

Equations (9.26) provides a more convenient relation to compute the slip factor ($\sigma_{p,D}$) numerically, than equation (7.68). One should however bear in mind the restrictions that lead to this convenient equation. Putting $\beta = 0$ in equation (9.26) we further readily obtain the result for straight radial blades as given by equation (9.24).

To illustrate the effect of curvature we have plotted the slip factor ($\sigma_{p,D}$) in figure 9.2 for several numbers of blades and various blade angles, using equation (7.68). The plot given in figure 9.2 (i) is identical to the figure presented by Busemann (fig. 17, p. 384), for the limiting value $r_1 \to 0$. Busemann however obtained his results by a direct numerical treatment while we have obtained an arithmetical expression. The plot of figure 9.2 (ii) is identical to the figures given by both Csanady and Dixon (fig. 7.10, p. 205), who based their results on the work of Busemann.

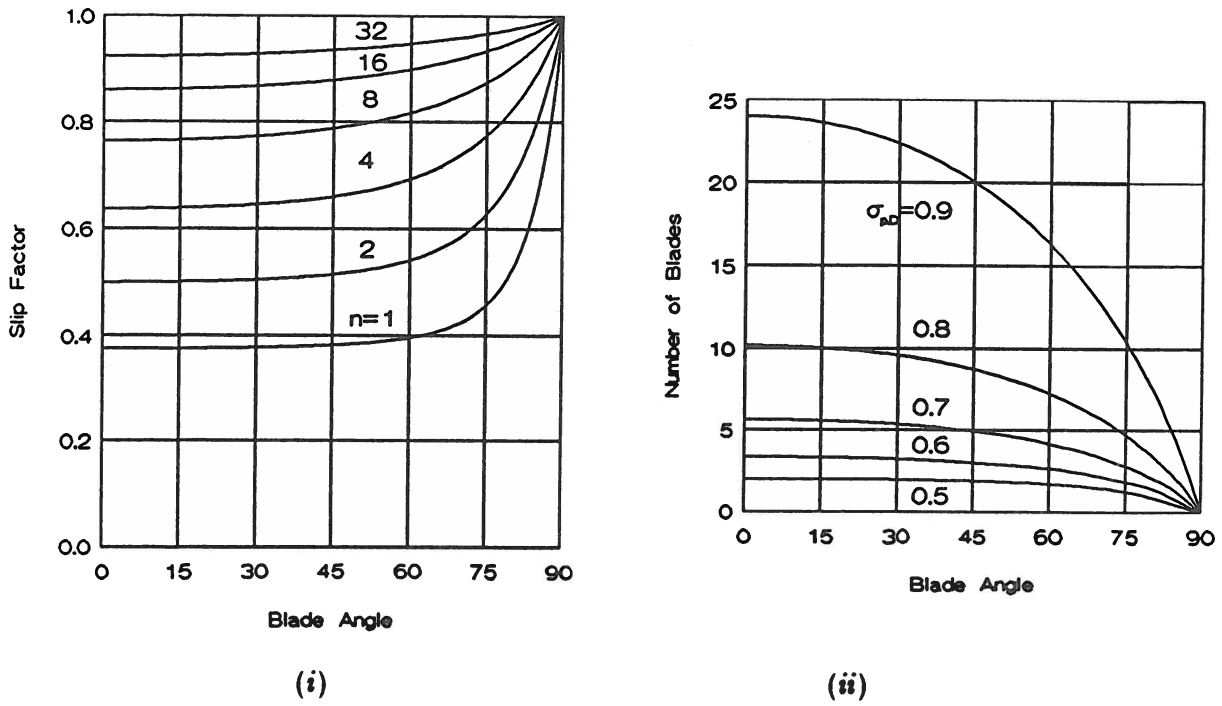

figure 9.2 slip factors for (two-dimensional) centrifugal impellers with the inner tip near the origin or large inner/outer tip ratios

Finally to illustrate the effect of the slip factors with respect to the head (coefficient) we have illustrated in figure 9.3 the theoretical, the Eulerian, and the actual head[16] (all with zero prerotation). To avoid misinterpretation we emphasize that this figure merely illustrates the effect of the slip factor ($\sigma_{p,D}$) due to the displacement flow since the slip factors related to the source flow and vortex flow ($\sigma_{p,Q}$ and $\sigma_{p,\Gamma}$) are practically equal to 1.

From figure 9.3 we clearly see the limiting effect of the number of blades. The remaining difference between theoretical and actual head is due to friction losses, impact losses, and off design operation. These off design losses originate from the fact that the volute does not fit the impeller at off design operation. Choosing a volute to fit the impeller properly at the design operation point will be treated in the remaining section of this paragraph. The impact losses can simply be reduced by giving the flow, entering the impeller, the requisite prerotation so that a shockless operation will be obtained.

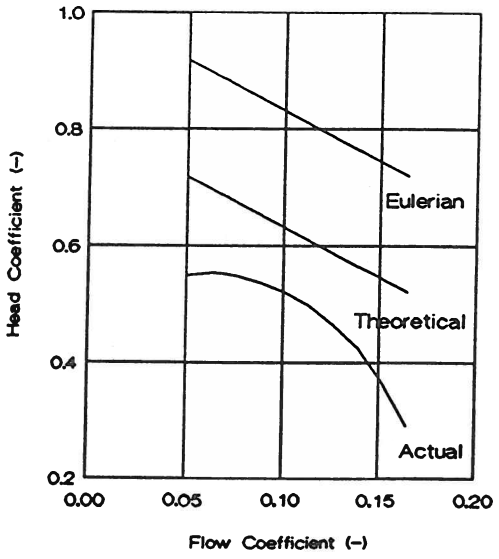

figure 9.3 head coefficient vs flow coefficient for a logarithmically bladed impeller receiving zero prerotation
($n = 8,\ r_1 = 37\ mm,\ r_2 = 100\ mm,\ \beta = \frac{\pi}{3}$)

16 The actual head given is that of a (perspex) test impeller - used for flow visualization - at the von Karman institute for fluid dynamics, which resembles our impeller quite well; for further information on the test impeller one is referred to Elholm (et al).

9.2.4 Choice of a volute

Now that we have a thorough understanding of the two–dimensional flow through the pump impeller we are also able to expatiate on the choice of a volute that fits the impeller. For simplicity we will confine ourselves to a so–called logarithmically curved volute (see figure 9.4). The curvature of such a volute is – like the logarithmic spiral blade – simply described by, using polar coordinates

$$r(\phi) = r_0 \, e^{\frac{\phi - \phi_0}{\tan \alpha_v}} \tag{9.27}$$

or

$$\phi(r) = \phi_0 + \tan \alpha_v \, ln\left[\frac{r}{r_0}\right] \tag{9.28}$$

with the choice of ϕ_0 and r_0 being arbitrary (provided that $r_0 > r_1$), and where the volute angle α_v is to be obtained from the flow leaving the impeller. This may simply be done knowing that the volute is a (logarithmically spiraled) streamline, so we can obtain the volute angle α_v from the circulation/flux ratio of the flow leaving the impeller, i.e.

$$\tan \alpha_v = \frac{\Gamma_2}{Q} \tag{9.29}$$

or, substituting equation (9.2)

$$\tan \alpha_v = \frac{\Gamma_1 + n\Gamma_B}{Q} \tag{9.30}$$

When next imposing a shockless entry ($\Gamma_1 = \Gamma_{1,SL}$) and thus substituting equation (7.25), as well as equation (9.3), in equation (9.30) we obtain, using dimensionless groups

$$\tan \alpha_{v,SL} = (1 + \sigma_{p,Q} - \sigma_{p,\Gamma}) \tan \beta + \frac{\sigma_{p,D} + (1 - \sigma_{p,\Gamma}) \, (r_1/r_2)^2 \, \tau_{p,D}}{\Phi} \tag{9.31}$$

where Φ is the previously defined flow coefficient, and where the slip factors ($\sigma_{p,D}$, $\sigma_{p,Q}$, $\sigma_{p,\Gamma}$) and the prerotation factor ($\tau_{p,D}$) are as given in the previous sections.

With zero prerotation ($\Gamma_1 = 0$) we obtain from equation (9.30) and (9.3), again using dimensionless groups

$$\tan \alpha_{v,0} = \sigma_{p,Q} \tan \beta + \frac{\sigma_{p,D}}{\Phi} \tag{9.32}$$

To demonstrate the above we will compute the angle α_v of a volute fitting the pump impeller defined in paragraph 8.2.

Supposing zero prerotation we obtain from equations (7.10) and (9.26), approximately

$$\sigma_{p,Q} \approx 1$$

$$\sigma_{p,D} \approx 0.816$$

Then taking the design operating point at

$$Q = 0.20 \ m^3/s$$

so

$$\Phi = -0.10$$

A negative sign appearing before the flow coefficient since we are dealing with backward curved blades, i.e.

$$\beta > 0 \iff \Omega < 0.$$

Equation (9.30) next gives

$$\tan \alpha_{v,0} \approx \tan 60 - \frac{0.816}{0.10} = -6.43$$

so

$$\alpha_{v,0} \approx -81^\circ$$

Conclusively we have plotted in figure 9.4 the pump impeller and the computed volute, where we have also added a diffuser at the volute exit (diffuser angle chosen at approximately 10°).

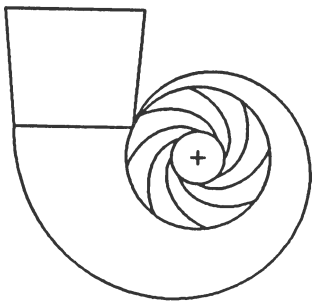

figure 9.4 *impeller with volute*

9.3 Applications for the Turbine Impeller

Regarding the turbine we will confine ourselves to discussing the prerotation and the shockless entry, and the theoretically delivered work and the work reduction factor.

9.3.1 Prerotation and shockless entry

In case of a turbine the circulation (Γ_2) around the impeller represents the prerotation. This prerotation highly determines the work to be delivered by the impeller, as will be discussed in the next section of this paragraph. The circulation (Γ_1) around the origin is merely to be seen as a residual or loss of energy.

The prerotation (Γ_2), required to obtain a shockless operation of the turbine impeller fitted with logarithmic spiral blades, may – based on our two–dimensional analysis – generally be written as

$$\Gamma_{2,SL} = \tau_{t,D}\, 2\pi\Omega r_2^2 + Q\tan\beta \qquad (9.33)$$

Since the prerotation factor ($\tau_{t,D}$) has yet only been worked out for the impeller fitted with straight radial blades we will further (have to) confine ourselves to this type of impeller, as we have likewise done for the pump

impeller. We obtained previously

$$\tau_{t,D} = \mu^{\frac{2}{n}+\frac{1}{2}} \left(\frac{2}{1+\sqrt{\mu}}\right)^{\frac{4}{n}} F\left(\frac{2}{n},\frac{2}{n};1;\left(\frac{1-\sqrt{\mu}}{1+\sqrt{\mu}}\right)^2\right) + \frac{1}{2}(1-\mu)\, F\left(\frac{1}{2},1-\frac{2}{n};2;1-\mu\right) \quad (6.119)$$

Since equation (6.112) embodies the same hypergeometric series that have been discussed in the previous paragraph, we may treat the prerotation factor (6.112) analogously and simply adopt the results.

Thus putting $\sqrt{\mu} \ll 1$ we obtain

$$\tau_{t,D} \approx \frac{1}{2} F\left(\frac{1}{2},1-\frac{2}{n};2;1\right) \quad (9.34)$$

or

$$\tau_{t,D} \approx \frac{1}{\sqrt{\pi}} \frac{\Gamma(\frac{1}{2}+\frac{2}{n})}{\Gamma(1+\frac{2}{n})} \quad (9.35)$$

Equation (9.35) provides a simple relation to approximate the prerotation factor (6.112). From equation (9.35) we further notice that the requisite prerotation for the turbine impeller to obtain a shockless operation is less than the Eulerian value (contrary to the case of a pump). When the number of blades become infinitely large we obtain by equation (9.35) the Eulerian value for the prerotation factor

$$\lim_{n\to\infty} \tau_{t,D} = 1 \quad (9.36)$$

as well as the Eulerian expression of the prerotation

$$\Gamma_{2,Eu} = \lim_{n\to\infty} \Gamma_{2,SL} = 2\pi\Omega r_2^2 + Q\tan\beta \quad (9.37)$$

9.3.2 Delivered work and work reduction factor

By the classical two–dimensional approach, using the moment of momentum, it follows from the energy equation that the theoretically delivered work (P_{th}) is given by

$$P_{th} = \frac{(\Gamma_2 - \Gamma_1)\rho Q\Omega}{2\pi} = \frac{n\Gamma_B \rho Q\Omega}{2\pi} \tag{9.38}$$

To judge this theoretically delivered work we introduce – analogous to the head reduction factor that was defined for the case of a pump – a work reduction factor (*WRF*), defined by

$$WRF = \frac{P_{th}}{P_{Eu}} \tag{9.39}$$

with P_{Eu} being the Eulerian work for an impeller fitted with logarithmic spiral blades, i.e.

$$P_{Eu} = \frac{\rho Q\Omega}{2\pi} (\Gamma_2 - Q\tan\beta - 2\pi\Omega r_1^2) \tag{9.40}$$

Next substituting equations (9.38) and (9.40) in equation (9.39) and using equation (9.4) for the blade circulation we obtain for the work reduction factor, again using dimensionless groups

$$WRF = \frac{(\sigma_{t,\Gamma}\,\Upsilon_2 - \sigma_{t,Q}\,\Phi\tan\beta) - \sigma_{t,D}\,(r_1/r_2)^2}{\Upsilon_2 - \Phi\tan\beta - (r_1/r_2)^2} \tag{9.41}$$

where we have additionally introduced

$$\Upsilon_2 = \frac{\Gamma_2}{2\pi\Omega r_2^2} \tag{9.42}$$

In case of a shockless entry we obtain by substituting equation (9.33) in equation (9.41), using equation (9.42) and employing the fact that by the Eulerian approach the prerotation factor ($\tau_{t,D}$) will be equal to 1,

$$WRF_{SL} = \frac{(\sigma_{t,\Gamma}\,\tau_{t,D} + (1 - \sigma_{t,Q})\,\Phi\tan\beta)\,r_2^2 - \sigma_{t,D}\,r_1^2}{r_2^2 - r_1^2} \tag{9.43}$$

From equation (9.43) we notice that the influence of the source is limited since $\sigma_{t,Q} \approx 1$ as mentioned before. Furthermore it will be evident that the limiting value ($n \rightarrow \infty$) of the work reduction factor equals 1 since then all slip factors as well as the prerotation factor become 1.

Finally, confining ourselves to turbine impellers fitted with straight radial

blades, we shall explore equation (9.43) somewhat further.

Putting $\beta = 0$ equation (9.43) becomes

$$WRF_{SL} = \frac{f_2 r_2^2 - f_1 r_1^2}{r_2^2 - r_1^2} \tag{9.44}$$

where the newly introduced degenerated work reduction factors are

$$f_1 = \sigma_{t,D} \tag{9.45}$$

$$f_2 = \sigma_{t,\Gamma} \tau_{t,D} \tag{9.46}$$

Next imposing for simplicity that $\sqrt{\mu} \ll 1$, the slip factors ($\sigma_{t,D}$ and $\sigma_{t,\Gamma}$) as given by equations (6.112) and (6.113) become (approximately)

$$\sigma_{t,\Gamma} \approx 1 \tag{9.47}$$

$$\sigma_{t,D} \approx 2^{\frac{4}{n}} F\left[\tfrac{2}{n}, \tfrac{2}{n}; 1; 1\right] \tag{9.48}$$

where the latter can be written as[17]

$$\sigma_{t,D} \approx 2^{\frac{4}{n}} \frac{\Gamma(1-\frac{4}{n})}{\Gamma^2(1-\frac{2}{n})} \tag{9.49}$$

which is valid for $n > 4$

Then substituting equations (9.35), (9.47), and (9.49) in equations (9.45) and (9.46) we get

$$f_1 \approx 2^{\frac{4}{n}} \frac{\Gamma(1-\frac{4}{n})}{\Gamma^2(1-\frac{2}{n})} \tag{9.50}$$

$$f_2 \approx \frac{1}{\sqrt{\pi}} \frac{\Gamma(\frac{1}{2}+\frac{2}{n})}{\Gamma(1+\frac{2}{n})} \tag{9.51}$$

The behaviour of the degenerated work reduction factors, as given by equations

[17] See footnote 12

(9.50) and (9.51), is illustrated graphically in figure 9.5; the result being evident.

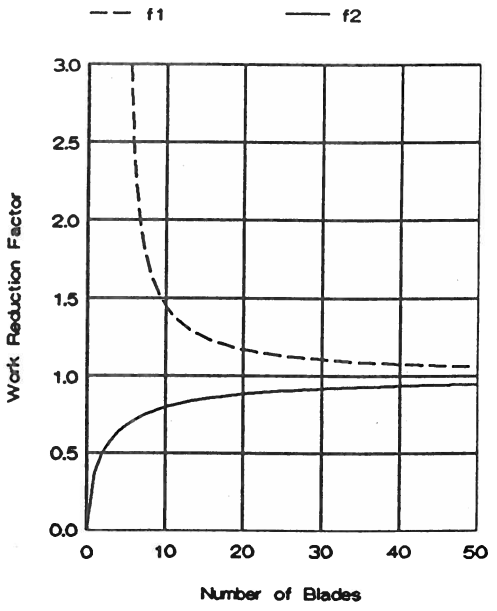

figure 9.5 *degenerated work reduction factors*

10

CONCLUSIONS AND RECOMMENDATIONS

In the foregoing the two–dimensional velocity and pressure distribution along straight radial blades and logarithmic spiral blades of isolated centrifugal pump impellers have been computed successfully. Additionally some interesting features like slip factors and shockless entry have been discussed, with arithmetical solutions being derived.

The solutions for the radially bladed impeller are all fully obtained, that is, arithmetical expressions for the velocity distributions have been derived for both the vortex flow and the displacement flow. The solution for the vortex flow appeared to be a relatively simple expression, whereas the solution for the displacement flow was somewhat more complicated, viz. a Fourier sine series, with the Fourier coefficients given by the hypergeometric series. Circumstantially we also obtained arithmetical expressions for the slip factors and the prerotation factors (shockless entry), for both the pump and the turbine impeller fitted with straight radial blades. As was to be expected the slip factors were all less than their Eulerian value (1), and properly equalled this value for an infinite number of blades. Furthermore the prerotation factor for the pump impeller appeared to exceed (!) the Eulerian value (1), whereas the prerotation factor for the turbine impeller was less (!) than the Eulerian value; both prerotation factors became properly equal to 1 in the Eulerian approach.

The solutions (velocity distribution, prerotation, and slip factors) for the impeller fitted with logarithmic spiral blades are all formulated analytically, with the solutions for the vortex flow and source flow being expressed arithmetically. An arithmetical solution for the displacement flow has not been obtained yet; instead the equations concerned are treated both numerically and asymptotically. By an asymptotic approach arithmetical expressions for the blade circulation and the slip factor, both related to the displacement flow, have been obtained.

All results show, as far as a comparison is permitted, an excellent agreement

with the works of various authors who have studied the same or comparable problems. Moreover, the results in this work add substantially to the previous works, that is, (better) arithmetical solutions have been obtained to compute velocity distributions along straight radial blades, and slip factors for both radially bladed and logarithmically bladed impellers; though improvements are still to be made.

The first recommendation is to express the velocity distribution along a logarithmic spiral blade, due to the displacement flow, like it has been done for the radially bladed impeller, that is, employing a (similar) series development. When doing so it is emphatically advised to treat this velocity distribution in the first instance asymptotically, by taking a low inlet–to–outlet radius ratio ($\mu \longrightarrow 0$).

The second point of interest concerns the shockless prerotation and the blade circulation. Like it has been done for the radially bladed impeller, it may very well be possible to obtain similar arithmetical expressions for the impeller fitted with logarithmic spiral blades. Alternatively one may think of employing a (direct) numerical treatment and presenting the solutions graphically.

Another interesting sequel is to examine if there exists an impeller with blades having a varying blade angle ($\beta_1 \longrightarrow \beta_2$) that can be treated as in this work. The difficulty would there probably be to find a suitable mapping. If such is to succeed and the flow problem can thus be solved, we may improve our understanding of (the flow in) turbomachinery.

Finally one may think of applying the (potential flow) solutions to perform boundary layer analyses, both laminar and turbulent, and study the (occurrence of) boundary layer separation. In this context it may also be interesting to take a closer look at the flow field in and around the back flow areas that occur if the source flow is not strong enough to compensate the flow due to the relative eddy.

APPENDIX A

CONFORMAL MAPPING OF A LOGARITHMIC SPIRAL BLADE ON A CIRCLE (KONIG TRANSFORMATION)

The transformation that maps a piece of a logarithmic spiral conformally on a circle is originally credited to König (1922)[Δ]. This transformation is based on the fact that a (two–dimensional) flow field will not be altered or influenced if we place a barrier of infinitesimal thickness along a streamline. To derive the transformation we start with the (complex) potential $f(z)$ of a so–called vortex–source, i.e.

$$f(z) = \frac{Q}{2\pi} \ln z + \frac{\Gamma}{2\pi i} \ln z \qquad \text{(A.1)}$$

where the source (Q) and the vortex (Γ) are placed in the origin of the z–plane.

Next substituting polar coordinates ($z = re^{i\phi}$) in potential (A.1) we readily obtain, by the constancy of the stream function (the imaginary part of the complex potential), that the streamlines of flow field (A.1) are given by

$$Q\phi - \Gamma \ln r = \textit{constant} \qquad \text{(A.2)}$$

Then defining a known point on a particular streamline by (r_0,ϕ_0), we obtain from equation (A.2) that a streamline of a vortex–source is described by

$$\phi(r) = \phi_0 + \frac{\Gamma}{Q} \ln(r/r_0) \qquad \text{(A.3)}$$

or

$$r(\phi) = r_0 \, e^{\frac{Q}{\Gamma} \ln (\phi - \phi_0)} \qquad \text{(A.4)}$$

Equations (A.3) and (A.4) each exactly describe a logarithmic spiral, as

Δ See also Betz (1964, pp. 245–255).

illustrated in figure A.1, where

$$r \frac{d\phi}{dr} = \tan\beta = \frac{\Gamma}{Q} \tag{A.5}$$

Since a logarithmic spiral blade, with a blade angle β equal to $\arctan(\Gamma/Q)$, placed along a streamline of flow field (A.1) will not alter the potential of the flow field, we may write potential (A.1) also as

$$f^*(z) = \frac{Q}{2\pi}(1 - i\tan\beta)\ln z \tag{A.6}$$

where the asterisk is added for clarity of the remainder.

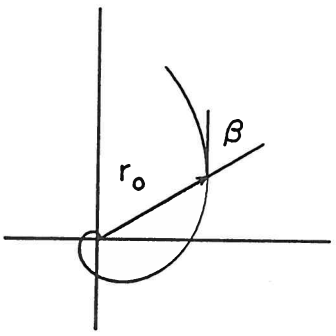

figure A.1 logarithmic spiral

Next we consider the desired image of the mapping, that is, we are interested in a transformation $(z \rightarrow \zeta)$ that maps the blade conformally on a circle. Though it is no restriction we thereby choose the unit circle as image; the reason for this will become apparent at the end of this appendix.

Placing the image of the origin of the z–plane, and the vortex–source, in a point (say ζ_0) outside the unit circle of the ζ–plane, we get the configuration as illustrated in figure A.2. Then without the unit circle as a barrier the potential would be

$$f(\zeta) = \frac{Q}{2\pi}(1 - i\tan\beta)\ln(\zeta - \zeta_0) \tag{A.7}$$

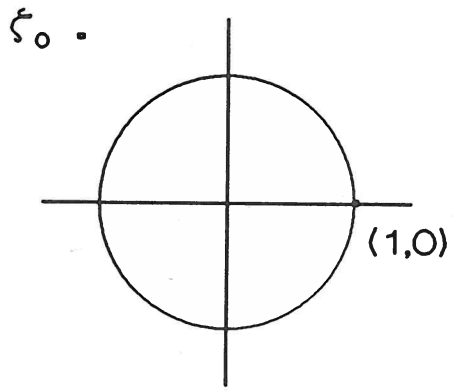

figure A.2 image of the transformation (ζ – plane)

Next applying the circle theorem (Milne–Thomson, 1958, pp. 84–85) we impose the boundary condition in the ζ–plane (unit circle as streamline) and obtain

$$f^*(\zeta) = \frac{Q}{2\pi}\left[(1 - i\tan\beta)\ ln(\zeta - \zeta_0) + (1 + i\tan\beta)\ ln(\tfrac{1}{\zeta} - \bar{\zeta}_0)\right] \qquad (A.8)$$

which can be written alternatively as

$$f^*(\zeta) = \frac{Q}{2\pi}(1 - i\tan\beta)\left[ln(\zeta - \zeta_0) + e^{2i\beta}ln(\tfrac{1}{\zeta} - \bar{\zeta}_0)\right] \qquad (A.9)$$

and where the over bar denotes a complex conjugate.

Since the potentials (A.6) and (A.9) represent (by admission) the same flow, only in different planes, we obtain from equations (A.6) and (A.9) the transformation that maps a logarithmic spiral blade conformally on the unit circle; the transformation reads

$$z = (\zeta - \zeta_0)\ (\tfrac{1}{\zeta} - \bar{\zeta}_0)^{e^{2i\beta}} \qquad (A.10)$$

Next taking the image (say ζ_*) of an arbitrary point (say z_*) as a reference, we may scale the transformation (A.10), and obtain the mapping function that is generally known as König's transformation, i.e.

$$\frac{z}{z_*} = \left[\frac{\zeta - \zeta_0}{\zeta_* - \zeta_0}\right]\left[\frac{\frac{1}{\zeta} - \bar{\zeta}_0}{\frac{1}{\zeta_*} - \bar{\zeta}_0}\right]^{e^{2i\beta}} \tag{A.11}$$

Conclusively, when confining ourselves to points on a blade ($z = z_B$, $\zeta = \zeta_B = e^{i\theta}$) and taking ζ_* on the unit circle (say $\zeta_* = e^{i\lambda}$), the transformation (A.11) can be written as

$$\frac{z_B}{z_*} = \left|\left[\frac{e^{i\theta} - \zeta_0}{e^{i\lambda} - \zeta_0}\right]^{e^{-i\beta}}\right|^{2e^{i\beta}} \tag{A.12}$$

Thus, by choosing the unit circle as the image we have the possibility to simplify the transformation of blade located points (ζ_B), since the complex conjugate ($\bar{\zeta}_B$) equals the reciprocal (ζ_B^{-1}) for points on the unit circle.

Though it should be apparent from the above we finally emphasize that the flow field of the z–plane is mapped *outside* the unit circle of the ζ–plane; this is an essential to apply the circle theorem, that is, the interior of the circle has to be free from singularities (Milne–Thomson, 1958, pp. 84–85).

APPENDIX B

ASYMPTOTIC SOLUTION OF THE TWO-DIMENSIONAL POTENTIAL FLOW THROUGH A CENTRIFUGAL IMPELLER

In this appendix we consider the asymptotic solution of the two–dimensional irrotational solenoidal flow (generally known as potential flow) through a so–called isolated centrifugal impeller. We will start with a short description of the model that we use (section B.1), followed by the governing equations (section B.2), where we will outline the bases of our asymptotic solution. Next we will solve the flow field asymptotically (section B.3), and discuss the solution for a large number of blades (section B.4). Finally we will briefly consider the pressure distribution along a blade (section B.5).

B.1 Model for the Asymptotic Solution

To obtain an asymptotic solution of the two–dimensional flow through a centrifugal impeller, we use a model that consists of n equally spaced logarithmic spirals (see figure B.1). The blades of this impeller are simply described by, using polar coordinates $(r,\phi)^{\Delta}$

$$r^j(\phi) = r_o \, e^{\frac{\phi-\phi_o^j}{\tan\beta}} \tag{B.1}$$

or

$$\phi^j(r) = \phi_o^j + \tan\beta \, ln\left[\frac{r}{r_o}\right] \tag{B.2}$$

where

β = blade angle ($\tan\beta = r\frac{d\phi}{dr}$)
j = blade index, $\{j \in \mathbb{N} | 1 \leq j \leq n\}$

$^{\Delta}$ Implicitly we have that the polar coordinates (r,ϕ) are fixed on the impeller, and thus rotate with the angular speed of the impeller (relative frame of reference).

ϕ_o = offset angle, $\{\phi_o^{j+1} = \phi_o^j + 2\pi/n\}$
r_o = offset radius

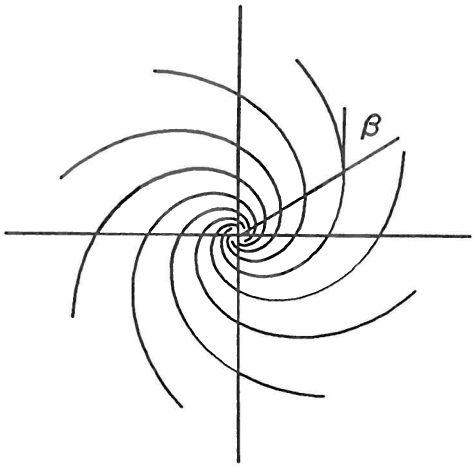

figure B.1 simple two-dimensional model of a centrifugal impeller, fitted with logarithmically curved blades

B.2 Governing Equations

We start this section by recalling that we may confine ourselves to the flow field between two consecutive blades, since the flow through the impeller is periodical. To compute this flow field (asymptotically) we will briefly discuss the general equations that describe the flow field, immediately followed by a simplification so that the flow field can be solved.

First we recall the general equations for the absolute velocity ($\boldsymbol{c}$) of an irrotational solenoidal flow field, i.e.

$$\nabla \times \boldsymbol{c} = 0 \tag{B.3}$$

$$\nabla \bullet \boldsymbol{c} = 0 \tag{B.4}$$

Since our problem is best solved when referring to rotating axes, we substitute the well-known relation between the absolute velocity ($\boldsymbol{c}$) and relative velocity ($\boldsymbol{w}$), i.e.

$$\boldsymbol{c} = \boldsymbol{w} + \boldsymbol{\Omega} \times \boldsymbol{r} \tag{B.5}$$

in equations (B.3) and (B.4), and obtain by elementary vector analysis

$$\nabla \times \boldsymbol{w} = -2\boldsymbol{\Omega} \tag{B.6}$$

$$\nabla \cdot \boldsymbol{w} = 0 \tag{B.7}$$

provided that we have a constant angular speed ($\boldsymbol{\Omega}$).

Equations (B.6) and (B.7) state that the relative flow will possess vorticity (having a constant value $-2\boldsymbol{\Omega}$), and that it will be solenoidal, like the absolute flow. By equation (B.7) we may next define a relative stream function ($\boldsymbol{\kappa}$) according to

$$\boldsymbol{w} = \nabla \times \boldsymbol{\kappa} \tag{B.8}$$

Then substituting equation (B.8) in equation (B.6), and using the identity

$$\nabla^2 \boldsymbol{\kappa} = \nabla(\nabla \cdot \boldsymbol{\kappa}) - \nabla \times \nabla \times \boldsymbol{\kappa} \tag{B.9}$$

and imposing additionally

$$\nabla \cdot \boldsymbol{\kappa} = 0 \tag{B.10}$$

we obtain the Poisson equation

$$\nabla^2 \boldsymbol{\kappa} = 2\boldsymbol{\Omega} \tag{B.11}$$

For two dimensional flow fields, the vector functions ($\boldsymbol{\kappa}$ and $\boldsymbol{\Omega}$) reduce to scalar functions (κ and Ω), so the relative two–dimensional flow through the impeller, that is, between two consecutive blades, is described by

$$\nabla^2 \kappa = 2\Omega \tag{B.12}$$

where we have as – incomplete – boundary conditions that the impeller blades are streamlines of the relative flow, say

$$\kappa \big|_j = \kappa^j \tag{B.13}$$

$$\kappa \big|_{j+1} = \kappa^{j+1} \tag{B.14}$$

Recalling the known Laplace equation for the absolute stream function (two–dimensional), i.e.

$$\nabla^2\psi = 0 \tag{B.15}$$

it follows from equation (B.12) that the two types of stream functions are related by

$$\psi = \kappa - \tfrac{1}{2}\Omega r^2 \tag{B.16}$$

Returning to our elliptic problem (B.12), (B.13), (B.14), we notice that this can not be solved unless additional boundary conditions are imposed on (extra) curves connecting two consecutive blades, since the region where we want to solve our flow problem has to be enclosed by a simple connected contour. Alternatively, however, we will alter the elliptic problem into a parabolic problem so that the two boundary conditions (B.13) and (B.14) will suffice for the solution. For that purpose we will employ a coordinate transformation and judge the elliptic problem, using dimensionless groups.

The transformation that we employ reads

$$\xi = \cos\beta \, \ln(r/r_o) + \phi \sin\beta \tag{B.17}$$

$$\eta = -\sin\beta \, \ln(r/r_o) + \phi \cos\beta \tag{B.18}$$

By this transformation the impeller blades (B.2) are represented in the (ξ,η)–plane by

$$\xi^j(r) = \cos^{-1}\beta \, \ln(r/r_o) + \phi_o^j \sin\beta \tag{B.19}$$

$$\eta^j = \phi_o^j \cos\beta \tag{B.20}$$

where the latter is constant for a particular blade. So the region between two consecutive blades is mapped between two parallels of the ξ–axis, as is illustrated in figure B.2.

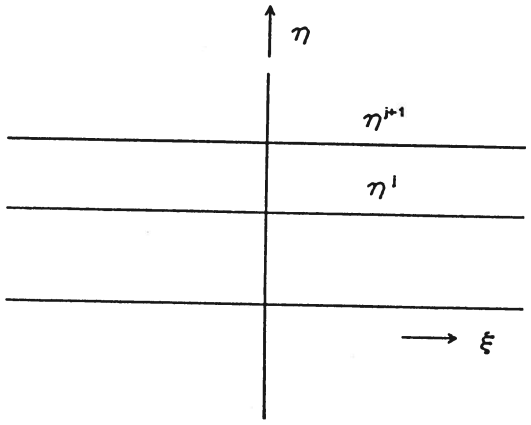

figure B.2 mapped flow region

Next we have to express the Laplace operator (∇^2) by the new (ξ,η) coordinates. From the transformation (B.17), (B.18) it follows that

$$\frac{\partial}{\partial \phi} = \sin\beta \frac{\partial}{\partial \xi} + \cos\beta \frac{\partial}{\partial \eta} \tag{B.21}$$

$$\frac{\partial}{\partial r} = \frac{\cos\beta}{r} \frac{\partial}{\partial \xi} - \frac{\sin\beta}{r} \frac{\partial}{\partial \eta} \tag{B.22}$$

$$r = r_o \, e^{\xi\cos\beta - \eta\sin\beta} \tag{B.23}$$

$$\phi = \xi\sin\beta + \eta\cos\beta \tag{B.24}$$

Then recalling the expression for the Laplace operator in polar coordinates, i.e.

$$\nabla^2 = \nabla^2_{r,\phi} = \frac{1}{r}\frac{\partial}{\partial r} r \frac{\partial}{\partial r} + \frac{1}{r^2}\frac{\partial^2}{\partial \phi^2} \tag{B.25}$$

we obtain by substituting equations (B.21) and (B.22)

$$\nabla^2_{r,\phi} = \frac{1}{r^2}\left[\frac{\partial^2}{\partial \xi^2} + \frac{\partial^2}{\partial \eta^2}\right] \tag{B.26}$$

or, using equation (B.23)

$$\nabla^2_{r,\phi} = \frac{1}{r_o^2} \frac{e^{2\eta \sin \beta}}{e^{2\xi \cos \beta}} \left(\frac{\partial^2}{\partial \xi^2} + \frac{\partial^2}{\partial \eta^2} \right) \tag{B.27}$$

Equation (B.12) then gives

$$\nabla^2_{\xi,\eta} \kappa = \frac{\partial^2 \kappa}{\partial \xi^2} + \frac{\partial^2 \kappa}{\partial \eta^2} = \frac{e^{2\eta \sin \beta}}{e^{2\xi \cos \beta}} 2\Omega r_o^2 \tag{B.28}$$

To judge this newly introduced Laplace operator ($\nabla^2_{\xi,\eta}$), that is, the contribution of the respective derivatives, we will distillate dimensionless groups. For that we switch from the (ξ,η) coordinates to the scale coordinates $(\xi_*,\eta_*) \in [0,1]$, by

$$\xi = \xi_1^j + \xi_*(\xi_2^j - \xi_1^j) \tag{B.29}$$

$$\eta = \eta^j + \eta_*(\eta^{j+1} - \eta^j) \tag{B.30}$$

for a region

$$\xi_1^j < \xi < \xi_2^j \tag{B.31}$$

$$\eta^j < \eta < \eta^{j+1} \tag{B.32}$$

located between two consecutive blades, where ξ_1^j and ξ_2^j are two arbitrary points on the j^{th}–blade, say $\xi_1^j = \xi^j(r_1)$ and $\xi_2^j = \xi^j(r_2)$.

Next substituting equations (B.19) and (B.20), equations (B.29) and (B.30) become

$$\xi = \xi_1^j + \frac{\xi_*}{\cos \beta} \ln(r_2/r_1) \tag{B.33}$$

$$\eta = \eta^j + \eta_* \frac{2\pi \cos \beta}{n} \tag{B.34}$$

where we have used the fact that the offset angles of two consecutive blades differ a factor $2\pi/n$, and where the ratio r_2/r_1 can be seen as a characteristic, e.g. the outlet–to–inlet ratio of the impeller.

By equations (B.33) and (B.34) we next obtain for the Laplace operator (B.28)

$$\nabla^2_{\xi,\eta} = \frac{n^2}{4\pi^2}\left[\left[\frac{2\pi cos\ \beta}{n\ ln(r_2/r_1)}\right]^2 \frac{\partial^2}{\partial \xi_*^2} + \frac{\partial^2}{\partial \eta_*^2}\right] \tag{B.35}$$

Then imposing

$$\left[\frac{2\pi cos\ \beta}{n\ ln(r_2/r_1)}\right]^2 \ll 1 \tag{B.36}$$

which will be valid for a respectable number of blades, we may put

$$\nabla^2_{\xi,\eta} = \frac{n^2}{4\pi^2}\frac{\partial^2}{\partial \eta_*^2} \tag{B.37}$$

Thus equation (B.28) may be approximated by

$$\frac{\partial^2 \kappa}{\partial \eta^2} = \frac{e^{2\eta sin\ \beta}}{e^{2\xi cos\ \beta}} 2\Omega r_o^2 \tag{B.38}$$

This equation has the desired parabolic shape so that our flow problem can be solved; the boundary conditions (B.13) and (B.14) become more specifically

$$\kappa(\xi,\eta^j) = \kappa(\xi,\phi_o^j cos\ \beta) = \kappa^j \tag{B.39}$$

$$\kappa(\xi,\eta^{j+1}) = \kappa(\xi,\phi_o^{j+1} cos\ \beta) = \kappa^{j+1} \tag{B.40}$$

B.3 Solving the Flow Field

The parabolic problem (B.38), (B.39), (B.40) is easily solved; the solution reads

$$\kappa(\xi,\eta) = \kappa^j + \frac{Q}{2\pi}\left[\frac{\eta}{cos\ \beta} - \phi_o^j\right]$$

$$+ \frac{\Omega r_o^2}{2sin^2\beta}\, e^{2\xi cos\ \beta}\left[e^{-2\eta sin\ \beta} - e^{-\phi_o^j sin\ 2\beta}\right]$$

$$+ \frac{n\Omega r_o^2}{4\pi sin^2\beta}\, e^{2\xi cos\ \beta}\left[e^{-\phi_o^j sin\ 2\beta} - e^{-\phi_o^{j+1} sin\ 2\beta}\right]\left[\frac{\eta}{cos\ \beta} - \phi_o^j\right] \tag{B.41}$$

where

$$Q = n(\kappa^{j+1} - \kappa^j) \tag{B.42}$$

which represents the fluid flux.

The stream function (B.41) describes (approximately) the flow field between two logarithmic spiral blades, which rotate with a constant angular speed Ω. Based on solution (B.41) we may next compute the velocity field between/along the blades. To do so we will express the velocities as derivatives of the stream function (B.41) with respect to ξ and η.

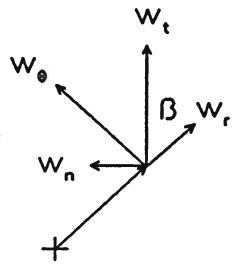

figure B.3 relative fluid velocities

Referring to figure B.3 it follows that the relative fluid velocities (w_t,w_n), tangential and normal to a blade, are related to the the common polar velocities (w_r,w_ϕ) by

$$w_t = w_r \cos\beta + w_\phi \sin\beta \tag{B.43}$$

$$w_n = -w_r \sin\beta + w_\phi \cos\beta \tag{B.44}$$

Then substituting

$$w_r = \frac{1}{r}\frac{\partial\kappa}{\partial\phi} \tag{B.45}$$

$$w_\phi = -\frac{\partial\kappa}{\partial r} \tag{B.46}$$

and using equations (B.21) and (B.22), we obtain from equations (B.43) and (B.44)

$$w_t = \frac{1}{r}\frac{\partial\kappa}{\partial\eta} \tag{B.47}$$

$$w_n = -\frac{1}{r}\frac{\partial\kappa}{\partial\xi} \tag{B.48}$$

From equation (B.41) we next obtain for the derivatives

$$\frac{\partial\kappa}{\partial\eta} = \frac{\Omega r_o^2}{\sin\beta} e^{2\xi\cos\beta}\left[\frac{n}{2\pi\sin 2\beta}\left[e^{-\phi_o^j \sin 2\beta} - e^{-\phi_o^{j+1}\sin 2\beta}\right] - e^{-2\eta\sin\beta}\right]$$

$$+ \frac{Q}{2\pi\cos\beta} \tag{B.49}$$

$$\frac{\partial\kappa}{\partial\zeta} = \frac{\Omega r_o^2}{\sin^2\beta}\cos\beta\, e^{2\xi\cos\beta}$$

$$\left\{\left[e^{-2\eta\sin\beta} - e^{-\phi_o^j\sin 2\beta}\right] + \frac{n}{2\pi}\left[e^{-\phi_o^j\sin 2\beta} - e^{-\phi_o^{j+1}\sin 2\beta}\right]\left[\frac{\eta}{\cos\beta} - \phi_o^j\right]\right\} \tag{B.50}$$

By equations (B.19) and (B.20) we may further represent a point on an arbitrary, say the m^{th}, logarithmic spiral between the blades (with offset angle ϕ_o^m) by

$$\xi = \xi^m = \xi = \cos^{-1}\beta \ln(r/r_o) + \phi_o^m \sin\beta \tag{B.51}$$

$$\eta = \eta^m = \eta(\phi_o^m) = \phi_o^m \cos\beta \tag{B.52}$$

where

$$\phi_o^j \le \phi_o^m \le \phi_o^{j+1} \tag{B.53}$$

Then substituting the derivatives (B.49) and (B.50) in equations (B.44) and (B.45), and using equations (B.52) and (B.53), we obtain for the fluid velocities

$$w_t(r,\phi_o^m) = \frac{\Omega r}{\sin\beta}\left[\frac{ne}{2\pi\sin 2\beta}\phi_o^m \sin 2\beta \left(e^{-\phi_o^j \sin 2\beta} - e^{-\phi_o^{j+1}\sin 2\beta}\right) - 1\right] + \frac{Q}{2\pi r\cos\beta} \tag{B.54}$$

$$w_n(r,\phi_o^m) = -\frac{\Omega r}{\sin^2\beta}\cos\beta \left\{\left[1 - e^{(\phi_o^m-\phi_o^j)\sin 2\beta}\right] + \frac{n}{2\pi}(\phi_o^m-\phi_o^j)\, e^{\phi_o^m \sin 2\beta}\left[e^{-\phi_o^j \sin 2\beta} - e^{-\phi_o^{j+1}\sin 2\beta}\right]\right\} \tag{B.55}$$

B.4 Solutions for a Large Number of Blades

Since we have, by admission, an impeller with a large number of blades, so $\phi_o^{j+1} - \phi_o^j = 2\pi/n \ll 1$ and $\phi_o^m - \phi_o^j \ll 1$, we may simplify solutions (B.54) and (B.55) by using some simple Taylor expansions. These expansions read

$$e^{-\phi_o^j \sin 2\beta} - e^{-\phi_o^{j+1}\sin 2\beta} = \frac{2\pi}{n}\sin 2\beta\, e^{-\phi_o^j \sin 2\beta}\left[1 - \frac{\pi \sin 2\beta}{n}\right] \tag{B.56}$$

$$e^{\phi_o^m \sin 2\beta} = e^{\phi_o^j \sin 2\beta}\left[1 + (\phi_o^m-\phi_o^j)\sin 2\beta\right] \tag{B.57}$$

$$e^{\phi_o^m \sin 2\beta} = e^{\phi_o^j \sin 2\beta} \left[1 + (\phi_o^m - \phi_o^j) \sin 2\beta \left[1 + (\phi_o^m - \phi_o^j) \frac{\sin 2\beta}{2} \right] \right] \quad \text{(B.58)}$$

Equations (B.57) and (B.58) are expansions of the same function, with the expansion (B.58) being of a higher order. The reason to employ these two expansions will become apparent in the following.

Substituting expansions (B.56) and (B.57) in equation (B.54) we obtain for the tangential velocity

$$w_t(r,\phi_o^m) = \frac{Q}{2\pi r \cos\beta} + 2\Omega r \cos\beta \, (\phi_o^m - \phi_o^j - \frac{\pi}{n}) \quad \text{(B.59)}$$

and substituting the expansions (B.56) and (B.58) in equation (B.55) we obtain for the normal velocity

$$w_n(r,\phi_o^m) = -2\Omega r \cos^3\beta \, (\phi_o^m - \phi_o^j)(\phi_o^m - \phi_o^{j+1}) \quad \text{(B.60)}$$

If we had used expansion (B.57) instead of expansion (B.58) to simplify the normal velocity (B.56) we would have obtained the erroneous result

$$w_n(r,\phi_o^m) = -\frac{2\Omega r \cos^2\beta}{\sin\beta} (\phi_o^m - \phi_o^j)\left[1 + (\phi_o^m - \phi_o^j)\sin 2\beta\right]\left[1 - \frac{\pi \sin 2\beta}{n}\right] \quad \text{(B.61)}$$

or, approximately

$$w_n(r,\phi_o^m) = -\frac{2\Omega r \cos^2\beta}{\sin\beta} (\phi_o^m - \phi_o^j) \quad \text{(B.62)}$$

By this result the boundary conditions (zero velocity normal to the blades) are not entirely fulfilled, whereas solution (B.60) properly satisfies these boundary conditions.

From equation (B.59) we next obtain for the tangential velocity along the pressure side of a blade ($\Omega > 0$)

$$w_t^+(r) = w_t(r,\phi_o^j) = \frac{Q}{2\pi r \cos\beta} - \frac{2\pi\Omega r \cos\beta}{n} \quad \text{(B.63)}$$

and for the suction side

$$w_t^-(r) = w_t(r,\phi_o^{j+1}) = \frac{Q}{2\pi r\cos\beta} + \frac{2\pi\Omega r\cos\beta}{n} \qquad \text{(B.64)}$$

where we have used that $\phi_o^{j+1} - \phi_o^j = 2\pi/n$.

Equations (B.63) and (B.64) can be interpreted as if a relative eddy (see figure B.4) is generated between the impeller blades; this relative eddy basically originates from the irrotationality of the absolute flow field.

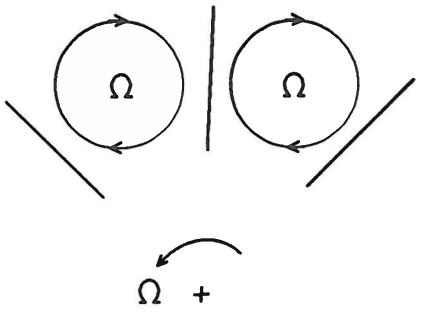

figure B.4 relative eddy

From the above, in particular from equation (B.63), it will be evident that back flow ($w_t < 0$) may occur along the pressure side of the blade, due to the existence of the relative eddy. To prevent this back flow we have by equation (B.63) as a sufficient condition

$$\frac{Q}{2\pi r\cos\beta} \geq \frac{2\pi\Omega r\cos\beta}{n} \qquad \text{(B.65)}$$

This condition clearly shows the positive effect of curving the blades. Taking for instance a 60 degree blade angle, we may settle for ¼ ($=\cos^2 60$) of the number of blades when comparing with straight radial blades ($\beta = 0$); or we may reduce the through flow by a factor 4 without running the risk of a back flow.

B.5 Pressure Distribution Along a Blade

In conclusion of this appendix we will briefly discuss the pressure distribution along a blade, following from the former solutions of the velocity distribution.

Recalling Bernoulli's theorem for steady two-dimensional flows relative to rotating axes, i.e.

$$\frac{p}{\rho} + \tfrac{1}{2}w^2 - \tfrac{1}{2}\Omega^2 r^2 = H \tag{B.66}$$

we obtain after substituting equations (B.63) and (B.64)

$$\frac{p^+}{\rho} = H - \frac{Q^2}{2\pi^2 r^2 \cos^2\beta} + \frac{Q\Omega}{n} + \tfrac{1}{2}\Omega^2 r^2\left[1 - \frac{4\pi^2\cos^2\beta}{n^2}\right] \tag{B.67}$$

$$\frac{p^-}{\rho} = H - \frac{Q^2}{2\pi^2 r^2 \cos^2\beta} - \frac{Q\Omega}{n} + \tfrac{1}{2}\Omega^2 r^2\left[1 - \frac{4\pi^2\cos^2\beta}{n^2}\right] \tag{B.68}$$

where the superscripts + and - denote the pressure and suction side respectively.

From equations (B.67) and (B.68) we readily obtain that the pressure difference over a blade simply equals (by the asymptotic solution!)

$$p^+ - p^- = \frac{2\rho Q\Omega}{n} \tag{B.69}$$

By this pressure difference the torque (τ_0) acting on the impeller would be

$$\tau_0 = n\int_{r_2}^{r_1} (p^+ - p^-)\, r\, dr = \rho Q\Omega(r_2^2 - r_1^2) \tag{B.70}$$

which is exactly the well-known Eulerian value for centrifugal impellers fitted with logarithmic spiral blades.

Finally we obtain from equations (B.67) and (B.68) that the mean (p^*) of the pressure distribution along a logarithmic spiral blade approximately reads

$$\frac{p^*}{\rho} = H - \frac{Q^2}{2\pi^2 r^2 \cos^2\beta} + \tfrac{1}{2}\Omega^2 r^2 \qquad \text{(B.71)}$$

Equation (B.71) tells us that for small radii the pressure distribution along a blade will show a $1/r^2$ behaviour, whereas large radii will give a r^2 behaviour. This effect is illustrated graphically in figure B.5 for the simple case of straight radial blades.

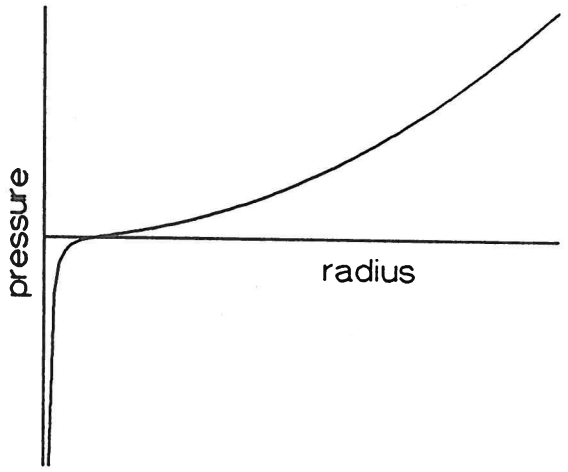

figure B.5 illustrative example of the asymptotic solution for the pressure distribution along a straight radial blade ($p^*(r) = r^2 - r^{-2}$)

REFERENCES

Abramowitz, M., and I.A. Stegun, *Handbook of Mathematical Functions with Formulas, Graphs, and Mathematical Tables*, John Wiley & Sons, New York (1972).

Acosta, A.J., "An Experimental and Theoretical Investigation of Two–Dimensional Centrifugal Pump Impellers", *Transactions of the ASME*, vol. 76 (1954), pp. 749–763.

Ahlfors, L.V., *Complex Analysis*, McGraw–Hill, New York (1953).

Atkinson, K.E., *An Introduction to Numerical Analysis*, John Wiley & Sons, New York (1989).

Ayyubi, S.B, and Y.V.N. Rao, "Theoretical Analysis of Flow Through Two–Dimensional Centrifugal Pump Impeller by Method of Singularities", *Journal of Basic Engineering*, (1971), pp.35–41.

Badie, R., "Analytische Berekenigen 2–D Incompressibele Rotatievrije Stroming in een Model voor een Radiale Waaier", M.Sc. Thesis, University of Twente, Enschede, The Netherlands (1988).

Badie, R., "Theoretical Considerations on some Aspects of the Flow Through a Radial Impeller", report no. WB–ThW/RS.89.004, University of Twente, Enschede, The Netherlands (1989).

Batchelor, G.K., *An Introduction to Fluid Dynamics*, Cambridge University Press, Cambrigde (1988).

Bateman,H., *Higher Transcendental Functions*, vol.1 (1953), McGraw–Hill, New York.

Bateman, H., *Partial Differential Equations of Mathematical Physics*, Cambridge University Press, Cambridge (1959).

Berkey, D.D., *Calculus of Several Variables*, Saunders College Publishing, New York (1988).

Betz, A., *Konforme Abbildung*, Springer–Verlag, Berlin (1964).

Betz, A., *Introduction to the Theory of Flow Machines*, Pergamon Press, Oxford (1966).

Bromwich, T.J., *An Introduction to the Theory of Infinite Series*, Macmillan & Co., London (1965).

Busemann, A., "Das Förderhöhenverhältnis radialer Kreiselpumpen mit logaritmisch–spiraligen Schaufeln", *Zeitschrift für angewandte Mathematik und Mechanik*, vol. 8 (1928), no. 5, pp. 372–384.

Courant, R., and D. Hilbert, *Methods of Mathematical Physics*, Interscience Publishers, New York (1953).

Csanady, G.T., "Head Correction Factors for Radial Impellers", *Engineering*, vol. 190 (1960), p. 195.

Cushing, J.T., *Applied Analytical Mathematics for Physical Scientists*, John Wiley & Sons, New York (1975).

Dettman, J.W., *Applied Complex Variables*, The Macmillan Company, New York (1965).

Dixon, S.L., *Fluid Mechanics, Thermodynamics of Turbomachinery*, Pergamon Press, Oxford (1986).

Eck, B., *Ventilatoren*, Springer–Verlag, Berlin (1972).

Elholm, T., "Experimental Study of Volute Flow in a Radial Pump", project report 1989–21, von Kármán Institute for Fluid Dynamics, Brussels (1989).

Elholm, T., E. Aydedr, and R. van den Braembussche, "Experimental Study of Swirling Flow in the Volute of a Centrifugal Pump", *American Society of Mechanical Engineers*, paper no. 90–GT–49 (1990).

Fox, R.W., and A.T. McDonald, *Introduction to Fluid Mechanics*, John Wiley & Sons, New York (1985).

Gradshteyn, I.S., and I.M. Ryzhik, *Table of Integrals, Series, and Products*, Academic Press, San Diego, (1980).

Greenspan, H.P., *The Theory of Rotating Fluids*, Cambridge University Press, Cambridge (1968).

Hamming, R.W., *Numerical Methods for Scientists and Engineers*, McGraw–Hill, New York (1973).

Henrici, P., *Applied and Computational Complex Analysis*, vol. 1 (1974), John Wiley & Sons, New York.

Henrici, P., *Applied and Computational Complex Analysis*, vol. 2 (1977), John Wiley & Sons, New York.

Henrici, P., *Applied and Computational Complex Analysis*, vol. 3 (1986), John Wiley & Sons, New York.

Jolley, L.B.W., *Summation of Series*, Dover Publications, New York (1961).

König, E., "Potential strömung durch Gitter", *Zeitschrift für angewandte Mathematik und Mechanik*, vol. 2 (1922), no. 6, pp. 422–429.

Koshlyakov, N.S., M.M. Smirnov, and E.B. Gliner, *Differential Equations of Mathematical Physics*, North–Holland Publishing Company, Amsterdam (1964).

Kucharski, W., *Strömung einer reibungsfreien Flüssigkeit*, München (1918).

Lamb, H., *Hydrodynamics*, Cambridge University Press, Cambridge (1957).

Leithold, L., *The Calculus with Analytic Geometry*, Harper & Row, New York (1986).

Lubkin, S., "A Method of Summing Infinite Series", *Journal of Research of the National Bureau of Standards*, vol. 48 (1952), no. 3, pp. 228–254.

Milne–Thomson, L.M., *Theoretical Aerodynamics*, Macmillan & Co., London (1958).

Milne–Thomson, L.M., *Theoretical Hydrodynamics*, Macmillan & Co., London (1968).

Mohann Kumar, T.C., and Y.V.N. Rao, "Theoretical Investigation of Pressure Distribution Along the Surfaces of a Thin Blade of Arbitrary Geometry of a Two–Dimensional Centrifugal Pump Impeller", *Journal of Fluids Engineering*, vol. 99 (1977), pp. 531–542.

Moretti, G., *Functions of a Complex Variable*, Prentice–Hall, Englewood Cliffs, N.J (1964).

Morse, P.M., and H. Feshbach, *Methods of Theoretical Physics*, McGraw–Hill, New York (1953).

Press, W.H., B.P. Flannery, S.A. Teukolsky, and W.T. Vetterling, *Numerical Recipes*, Cambridge University Press, Cambridge (1986).

Robinson, A., and J.A. Laurmann, *Wing Theory*, Cambridge University Press, Cambridge (1956).

Salzer, H.E., "A Simple Method for Summing Certain Slowly Convergent Series", *Journal of Mathematics and Physics*, vol. 33 (1954), pp. 356–359.

Scarborough, J.B., *Numerical Mathematical Analysis*, The John Hopkins Press, Baltimore (1962).

Schulz, W., "Das Förderhöhenverhältnis der Kreiselpumpen für die ideale und wirkliche Flüssigkeit", *Forschungsarbeiten auf dem Gebiete des Ingenieurswessens*, Heft 307, VDI–Verlag, Berlin (1928).

Schulz, W., "Das Förderhöhenverhältnis radialer Kreiselpumpen mit logaritmisch–spiraligen Schaufeln", *Zeitschrift für angewandte Mathematik und Mechanik*, vol. 8 (1928), no. 1, pp. 10–17.

Spannhake, W., "Die Leistungsaufnahme einer parallelkränzigen Zentrifugalpumpe", *Festschrift der Technische Hochschule Karlsruhe* (1925).

Spannhake, W., "Anwendung der Konforme Abbildung auf die Berechnung von Strömungen in Kreiselrädern", *Zeitschrift für angewandte Mathematik und Mechanik*, vol. 5 (1925), no 6.

Spannhake, W., "Eine strömungstechnische Aufgabe der Kreiselradforschung und ein Ansatz zu ihrer Lösung", *Mitteillungen des Instituts für Strömungsmaschinen der Technische Hochschule Karlsruhe*, (1930), pp. 4–38.

Sörensen, E., "Potentialströmungen durch rotierende Kreiselräder", *Zeitschrift für angewandte Mathematik und Mechanik*, vol. 7 (1927), no. 2, pp. 89–106.

Sörensen, E., "Potential Flow Through Centrifugal Pumps and Turbines", *NACA Technical Memorandum* 973 (1941).

Stanitz, J.D. "Some Theoretical Aerodynamic Investigations of Impellers in Radial and Mixed Flow Centrifugal Compressors", *Transactions of the ASME*, vol. 74 (1952), no. 4, pp. 473–493.

Thwaites, B., *Incompressible Aerodynamics*, Clarendon Press, Oxford (1960).

Uchimaru, S., "Experimental Research on the Distribution of Water Pressure in a Centrifugal Impeller", *The Journal of the Faculty of Engineering*, Tokyo Imperial University, Japan, vol. 16 (1925), no. 6, pp. 157 – 169.

Uchimaru, S., and S. Kito, "On Potential Flow of Water Trough a Centrifugal Impeller", *The Journal of the Faculty of Engineering*, Tokyo Imperial University, Japan, vol. 19 (1931), no. 8, pp. 191–223.

Van Essen, T.G., "Berekening van de twee dimensionale potential stroming in een draaiende waaier met rechte schoepen zonder dikte", M.Sc. Thesis, University of Twente, Enschede, The Netherlands (1989).

Vavra, M.H., *Aero – Thermodynamics and Flow in Turbo Machines*, John Wiley & Sons, New York (1960).

Weinig, F., *Die Strömung um die Schaufeln von Turbomaschinen*, John Ambrosius Barth, Leipzig (1935).

Wiesner, F.J., "A Review of Slip Factors for Centrifugal Impellers", *Journal of Engineering for Power*, vol. 89 (1967), no. 4, pp. 558–572.

Wislicenus, G.F., *Fluid Mechanics of Turbomachinery*, McGraw–Hill, New York (1947).